VIBRO-ACOUSTICS OF BEAMS UNDER VARIABLE AXIAL LOADS

Thesis

Submitted in partial fulfilment of the requirement for the degree of

DOCTOR OF PHILOSOPHY

by

NAIDU BALIREDDY S

DEPARTMENT OF MECHANICAL ENGINEERING

NATIONAL INSTITUTE OF TECHNOLOGY KARNATAKA

SURATHKAL, MANGALORE-575025, INDIA

March, 2024

Dedicated To

My Beloved
Parents, Wife & Son

DECLARATION

I hereby *declare* that the Research Thesis entitled **VIBRO-ACOUSTICS OF BEAMS UNDER VARIABLE AXIAL LOADS** which is being submitted to the **National Institute of Technology Karnataka, Surathkal** in partial fulfilment of the requirements for the award of the Degree of **Doctor of Philosophy** in **Mechanical Engineering** is a *bonafide report of the research work carried out by me.* The material contained in this Research Thesis has not been submitted to any University or Institution for the award of any degree.

Register No.: **177098ME502**
Name of the Research Scholar: **Naidu Balireddy S**
Signature of the Research Scholar: Naidu. B S.

Department of Mechanical Engineering.

Place: NITK – Surathkal
Date: 09/01/2024

CERTIFICATE

This is to *certify* that the Research Thesis entitled **VIBRO-ACOUSTICS OF BEAMS UNDER VARIABLE AXIAL LOADS**, submitted by **Naidu Balireddy S (Register Number: 177098ME502)** as the record of the research work carried out by him, is *accepted as the Research Thesis submission* in partial fulfilment of the requirements for the award of degree of **Doctor of Philosophy**.

Research Guide

Dr. P.Jeyaraj
Associate Professor
Department of Mechanical Engineering.
NITK Surathkal – 575025

11/3/2024

Chairman – DRPC
Department of Mechanical Engineering
National Institute of Technology, Karnataka
Surathkal, Mangalore–575025

ACKNOWLEDGEMENTS

I would like to express my deep gratitude to my research supervisor Dr. P. Jeyaraj, Professor, Department of Mechanical Engineering, National Institute of Technology Karnataka, Surathkal, Mangalore for his meritorious guidance, enthusiastic encouragement and useful critiques of this research work. Working under him has had a profound effect not only on how research should be carried out at its best, but also on how to develop humbleness and kindness towards students. With his support, suggestions, immense knowledge and abundant experience, he turned my dream into reality.

I sincerely thank the RPAC members, Dr. C P Devatha, Department of Civil Engineering and Dr. S C Kattimani, Department of Mechanical Engineering for providing valuable suggestions and also extending their support on all occasion.

I wish to express my sincere thanks to Prof. S.M Murigendrappa, Head of the Department, Department of Mechanical Engineering, National Institute of Technology Karnataka, Surathkal, Mangalore, for his kind help in providing the facilities.

I extend my sincere thanks to Dr. Vijay Gunasekaran for his un-wavering support during the dispirited time in research.

I wish to express my sincere thanks to my co-scholars Gouda Patil, Harsha Patil, Rakesh, Bakshi, Kurup Mithul and all the other students of ADL, NITK for their support during my research.

I sincerely acknowledge Dr. Ch V S Reddi, Vibro-Acoustics Lab of VIIT, for the help rendered to me during my earlier stages of research.

I am grateful to WSP consultancy India, for its un-conditional motivation and encouragement during my thesis submission and also to Dr.M K Naidu, Ramesh, and Dhanunjay Rao for their support during research work.

I always been grateful to my parents Sri. B. Naga Raju and Smt. Sanyasamma for imbibing the quest to pursue higher education. I would like to thank my brother, sisters, in-laws and whole family for their support throughout my life.

Important, despite being mentioned at the end, I would like to express my deepest gratitude to my wife, Dr. Asha Lakshmi, and my son, Naga Yashwin. They have been my rock, my inspiration, and my world. Without their unwavering support and love, achieving this goal would not have been possible.

I would like to thank God for giving me the strength, knowledge, ability and opportunity to understand this research study and to persevere and complete it satisfactorily.

Last but not least,
I want to thank me for believing in me.
"Do not be led by others,
awaken my own mind,
amass my own experience,
and decide for myself on my own path."
(-Veda's)

(Naidu Balireddy S)

ABSTRACT

KEYWORDS: Ritz method; Rayleigh's integral; variable axial load; buckling; free vibration; sound power levels; sound pressure levels; sound radiation; bi-directional grading; aspect ratio; lamination scheme; material composition

Stiffeners and beam like structural elements used in aircraft structures are subjected to variable axial loads. These structural elements are subjected to steady state mechanical excitations as well. The nature of variable axial load influences static stability and hence dynamic characteristics of the structural elements are also effected. Furthermore, the vibration and acoustic responses caused by steady state excitation need to be analyzed to take care of dynamic stress and human comfort. Numerical simulation studies carried out on a beam to analyze its vibro-acoustic response under the action of variable axial loads (VALs) is presented. Effects of six different types of VALs and three types of end conditions on buckling, free vibration and sound radiation characteristics of an isotropic beam is carried out initially. Static buckling and free vibration characteristics are analyzed using shear and normal deformable theorem and Ritz method. Forced vibration response is obtained using modal super-position method and the acoustic response parameters are obtained using Rayleigh integral. The nature of variation of VALs and end conditions are influencing buckling and free vibration characteristics remarkably. Results indicate that the acoustic response is highly sensitive to the nature of VAL and intensity of the VAL. In general, sound power at resonance decreases when the magnitude of VAL is increased.

In continuation, static stability and dynamic characteristics of a bi-directional functionally graded beams subjected to VALs using the Ritz method and Reddy's beam theory has been carried out. The material property is varied as a function of the gradation pattern along with the length and thickness directions. The influence of uniform, linear, and parabolically varying axial loads on buckling and free vibration frequencies is investigated. There is a remarkable variation observed in both the characteristics, by changing the material properties from isotropic to bi-direction functionally graded. Furthermore, the study reveals that higher stiffness is achieved by the material gradation index increment along the thickness direction compared to the lengthwise gradation index increment. Buckling and free vibration modes are also highly sensitive to the nature of variable axial loads and gradation index.

Similarly, a detailed investigation is carried out on the effects of bi-directional gradation, length-to-height ratio, and end conditions on the sound radiation behaviour of bi-directional functional graded beams subjected to quadratically decreasing axial load. The study reveals that the highest value in the gradation indexes in both directions significantly influences the sound power levels. The directivity pattern reveals that bi-directional functionally graded beams exhibits higher sound pressure levels around the critical buckling load. It is also observed that both structural and end conditions are influential factors in sound power levels (dB) and sound pressure levels (dB).

Finally, an investigation on the influence of bio-inspired laminate reinforced composite material on the static and dynamic responses of the beams, with a particular emphasis on the acoustic study is also done. The responses demonstrates the significance of variable axial loads, boundary stiffness, material composition, lay up pattern and aspect ratios highly influences the non-dimensional buckling loads of bio-inspired beams. The study further revealed that the vibration analysis are following the buckling trends, and the fundamental frequency is approaching minimum value at the critical buckling load. The study also includes the behaviour of the bio-inspired in comparison to vibrational responses at various modes and parameter variations. It is found that quasi isotropic-symmetric (QI) bio-inspired beam has poor buckling, vibration and acoustic behaviours, while uni-directional bio-inspired beams has better characteristics.

Contents

List of Figures

List of Tables

ABBREVIATIONS

VAL	: Variable Axial Load
FGM	: Functionally Graded Material
B-FGM	: Bi-Directional Functionally Graded Material
DQM	: Differential Quadrature Method
HSDT	: Higher Order Shear Deformation Theory
SNDBT	: Shear and Normal Deformation Beam Theory
BC	: Boundary Condition
SS	: Simply Supported
CC	: Clamped Clamped
CF	: Clamped Free
CS	: Clamped Supported
SWL	: Sound Power Level
SPL	: Sound Pressure Level
BL	: Buckling Load
dB	: Decibel
UD	: Uni Directional
CP	: Cross Ply
QI	: Quasi Isotropic
H	: Helicoidal
HE	: Helicoidal Exponential
GE	: Glass Epoxy
CE	: Carbon Epoxy

NOMENCLATURE

l	: Length of the beam
b	: Width of the beam
h	: Thickness of the beam
$\mathsf{F}^{\mathsf{e}}_{\mathsf{x}}(\mathsf{x})$	: Axially varying in-plane load
χ	: Load coefficient
E	: Young's modulus
G	: Shear modulus
μ	: Poissons's ratio
ρ	: Mass density
p_x	: Material property variation along Length (L)
p_z	: Material property variation along thickness (h)
u	: Axial displacement
w	: Transverse displacement
ϕ	: Rotation component
σ	: Stress component
$\varepsilon_{\mathsf{xx}}, \gamma_{\mathsf{xz}}$	: Strain displacements
V	: Volume of the beam
$[K]$	: Structural stiffness matrix
$[S]$	: Geometric stiffness matrix
$[M]$	: Mass matrix
Q_{ij}	: Material stiffness matrix
U	: Strain energy
K	: Kinetic energy
$\prod$	: Total potential energy
t	: time

$\mathsf{A}, \mathsf{B}, \mathsf{D}, \mathsf{C}, \mathsf{F}, \mathsf{H}, \mathsf{A_s}, \mathsf{D_s}, \mathsf{F_s}$	: Stiffness coefficients (Reddy's beam theory)
$\mathsf{A}, \mathsf{B}, \mathsf{B_s}, \mathsf{D}, \mathsf{D_s}, \mathsf{H}, \mathsf{Z}, \mathsf{X}, \mathsf{Y}, \mathsf{Y_s}, \mathsf{A_s}$	: Stiffness coefficients (SNDBT)
$I_0, I_1, I_2, J_1, J_2, K_1$	: Intertial coefficients(Reddy's beam theory)
$I_0, I_1, I_2, J_1, J_2, J_3, K_1, K_2$	: Intertial coefficients (SNDBT)
$\Theta_\mathsf{j}(\mathsf{x}),\ \varphi_\mathsf{j}(\mathsf{x})$ and $\psi_\mathsf{j}(\mathsf{x})$	: Trial functions
ω	: Natural Frequency
λ	: Dimensionless buckling load
ξ_i	: Modal damping ratio
F(t)	: Harmonic point load
$[\Phi]$	: Modal Matrix
p(r)	: Acoustic pressure radiated
$\omega(r)$	:Surface velocity
k	: Wave Number
ρ_0	: Fluid density
S	: Vibrating surface length
$\mathsf{I}(\mathsf{r})$	: Sound intensity
$\bar{\mathsf{W}}$	: Sound power radiated
SWL	: Sound power level
C_0	: Speed of sound in m/s
$\dot{W}_n$	: Normal velocity

Chapter 1

INTRODUCTION

Beam like thin-walled structural members are commonly used in automobile, aerospace, marine and nuclear industries. Elastic stability analysis of these thin-walled beams subjected to compression load is very important due to the risk and safety issues. Figure 1.1(a) and (b) depict the failure of various beams owing to buckling.

Generally, these kind of failures occur when the structures are subjected to the in-plane compressive load. Furthermore, the compressive load also influences dynamic characteristics of the beam. This motivated several researchers to investigate buckling and dynamic characteristics of beams under pre-stress. The changes in dynamic characteristics such as free vibrational frequencies and acoustic response can also be effectively used to analyze the stability of the pre-stressed structural members. Most of the buckling and vibration studies are performed under the influence of edge compressive load. However, in some structural applications the beam like structural elements are subjected to VAL in the process of load transfer. Studies on static stability and vibration response of beams subjected to VALs have proven to have more practical importance in the design of various structural elements. For example, in the aircraft wing the sandwich panels are connected through stiffeners which are subjected to VAL in the process of load transfer. Furthermore, the static pre-stress influences the vibration and sound radiation responses of the structures remarkably. Sound radiated from vibrating members is an important study in order to address the noise control issues. The amount of research work carried out on sound radiation characteristics of beam is very less compared to the plate and cylindrical panels.

In the context of selecting materials there is extensive research available with isotropic materials and in general, structure made of these materials are consid-

(a) Buckling failure near joint (b) Buckling failure of a bridge

Figure 1.1: Buckling failures of various beams (www.lusas.com)

ered first for any type of new investigation's. Furthermore, the study based on the isotropic materials gives great motivation for the analysis of structures made of alloys, fibre reinforced composites, functionally graded materials, and other advanced nano composites. With increase in requirements in the automobile for the light weight structural components, naval and aerospace sectors there is always a demand for the development of new materials. The new materials should meet the practical necessities of mechanical properties like high stiffness, low density and other essential functional requirement. These new materials are extensively used in various engineering applications like automotive, civil, aviation, defence sectors. Functionally graded materials (FGMs) caught the attention of researchers due to their enhancement of desired properties in the preferred directions compared to the traditional homogeneous materials. Desired mechanical properties can be achieved by tailoring material properties of FGM during manufacturing, which will sustain by exposing to extreme environmental conditions. Similarly, research on laminated composite beams inspired by nature has shown promising outcomes, leading to an increasing trend in their utilization. These bio-inspired beams offer the flexibility to customize lamination types and angles according to engineering requirements. Due to this, the researchers are keen on analysing the performance of FGM structures and bio-inspired materials under static and, dynamic load considerations.

Higher order theorems, such as the shear and normal deformation theory, Reddy's beam theory plays a crucial role in the analysis of structural behaviours. These approaches are essential for calculating static and dynamic responses of structures subjected to diverse loading conditions. Along with higher order theo-

rems, the Ritz method provides a powerful numerical approach that employs trial functions to approximate natural frequencies and mode shapes, enabling the investigation of complex systems with accurate results. Additionally, the Rayleigh integral serves as a fundamental link between structural vibrations and sound radiation, allowing engineers to quantify sound power level, sound pressure level characteristics of beams. By integrating these methodologies, researchers can conduct comprehensive studies, gaining deeper insights into the dynamic and acoustic behaviours of beams.

Sound radiation study is of significant importance in the field of vibration and acoustic analysis of beams, as it provides crucial information about the energy dissipation and transmission characteristics of the structures. Understanding the sound radiation behaviour of beams is essential for assessing their vibration responses and developing effective vibration reduction strategies. By investigating sound radiation from beams, engineers can gain insights into the structural integrity, identify potential sources of noise and vibration, and implement targeted measures to control and minimize undesirable acoustic emissions.

1.1 Literature Review

The next sections give a thorough literature assessment on the buckling, free vibration, and acoustic responses of beams made with various materials.

1.1.1 Studies on bi-directional functionally graded beams

Influence of material property variation along both the length and thickness directions on structural behaviour of FGM beams is investigated by some of the researchers. The dominant aspect for choosing bi-directional functional graded (B-FGM) beams by the researchers lies in the material enhancement in two different directions. This bi-directional material gradation in FGMs led researchers to design materials pertaining to failure methods. Below literature highlights the attention of the researchers capitalizing advantage in using B-FGM materials for beam designs.

Numerical study on static response of bidirectionally graded FGM beams using generalised differential quadrature method (DQM) is carried out by Nejad *et al.* (2016). The study highlighted the influence of inhomogeneity constant and material loading on static characteristics of B-FGM beams.

Nejad and Hadi (2016) numerically investigated the influence of small-scale effect, inhomogeneity parameter and material length variable on the natural frequency of B-GM nano beams. The analysis used Hamilton's principle and generalized DQM to obtain the results for various end conditions.

Wang *et al.* (2016) conducted analytical study on B-FGM beams for determining the free vibration characteristics. They reposrted that a non-homogeneous beam can be designed according to a particular frequency.

Nejad *et al.*(2017) carried out numerical study on Euler-Bernoulli nano B-FGM beams using GDQM method. The study highlighted the influence of small-scale effect, material gradation and end conditions on the natural frequencies of nano B-FGM beams.

An analytical model has been proposed by Nejad *et al.* (2018) to study the static response of B-FGM nano beams. The model was developed using Rayleigh-Ritz method and Eringen's non-local theory, and the effect of material loading on bending behaviour is highlighted.

Numerical investigation on natural frequencies of B-FGM beams using third order shear deformation theory was done by Karamanli (2018). The effect of bi-directional gradation index, length to thickness ratio and end conditions on free vibration frequencies are reported in the study.

Pradhan *et al.* (2019) provided a comprehensive state-of-the-art review on functionally graded materials and their analysis. The study covered various aspects of functionally graded materials, including their properties, fabrication methods, characterization techniques, and numerical and analytical analysis methods, offering a valuable resource for researchers in the field.

Influence of mechanical and magnetic loads on bending behaviour of a B-FGM nano beams is investigated by Khoram *et al.* (2020) using generalized DQM. The results were presented for different end conditions, slenderness ratios and material gradations.

Influence of magnetic field and bidirectional grading of material on the torsional behaviour of FGM tube is numerically studied by Barati *et al.* (2020). The studied employed generalized DQM in obtaining the solutions for the influence of heterogeneity constants and small scale effects.

Reza *et al.*(2020) developed FG nano-cone model for numerical analysis on torsional vibration of B-FGM beams using generalized DQM method. The proposed model behaved softer when analyzed with elasticity theory and harder when analyzed with strain gradient theory.

Selmi and Mustafa (2021) numerically investigated dynamic response of B-FGM beams using continuous elements method, the significance of the gradient indices and the aspect ratios are deeply analyzed.

Transverse vibrations of B-FGM nano beams subjected to longitudinal magnetic field is numerically studied by Barati *et al.*(2022). The study highlighted the significance of material gradation, magnetic field and size dependent variables on natural frequencies of B-FGM nano beams.

1.1.2 Studies on composite beams

The bio-inspired beams incorporate design principles observed in nature, such as hierarchical organization, lightweight construction, and optimized material distribution. Advancements in this field have led to the development of innovative materials and designs with improved strength-to-weight ratios, enhanced energy absorption capabilities, and reduced noise emissions. Understanding the evolution and advantages of these studies provides valuable insights into the design and optimization of bio-inspired structures for various applications, including aerospace, automotive, and civil engineering.

Cheng *et al.* (2011) conducted experimental and numerical investigations to determine the mechanical behaviour of bio-inspired laminated composites. They characterized the mechanical properties of laminated composites prepared through the inspiration by natural structures, providing valuable information for the development of lightweight and high-strength composite materials.

Vosoughi *et al.* (2012) investigated the thermal buckling and postbuckling behaviour of laminated composite beams with temperature-dependent properties. The study provides valuable insights into the mechanical response of composite beams under thermal loading conditions.

Mareishi *et al.* (2014) conducted thorough investigation on non-linear free vibration, post buckling, and non-linear static deflection of piezoelectric fiber-reinforced laminated composite beams. The investigation of these complex non-

linear behaviours in composite beams is crucial for designing and optimizing smart structures with enhanced vibration control capabilities.

Wang *et al.* (2015) presented an iso-geometric FE method for buckling responses of laminated composite beams with various end conditions. The buckling analysis provides accurate and efficient solutions for predicting the critical buckling loads and modes of composite beams.

Li *et al.* (2016) presented a unified higher-order shear deformation theory coupled with the dynamic stiffness method to investigate the free vibration characteristics of axially loaded laminated composite beams. The proposed approach offers a comprehensive and accurate analysis by considering the influence of shear deformation effects and allowing for more precise predictions of vibration responses and mode shapes.

Sabah *et al.* (2017) conducted a comparative study on the low-velocity impact behaviour of bio-inspired and conventional sandwich composite beams. The research findings provide insights into the performance and potential applications of bio-inspired composite structures in impact-resistant materials.

Liu *et al.* (2018) through experimental and numerical analyzes studied, the significance of inter-ply angles on the failure methods in bio-inspired composite helicoidal lay-up schemes. The study revealed the influence of inter-ply angles on the failure modes and mechanical properties of bio-inspired composite laminated composites, thereby providing insights for optimizing their structural performances.

In their study, Waddar *et al.* (2018) conducted experimental investigations to explore the stability and dynamic characteristics of a layered composite beam. The research provides valuable experimental data that enhance our understanding of the mechanical response of composite beams under various loading conditions.

George and Jeyaraj (2018) conducted experimental investigations on the buckling behaviour of a laminated composite beam under the influence of non uniform heat effects. The findings contribute to the advancement of thermal buckling analysis techniques, improving the reliability and safety of composite materials in engineering applications subjected to temperature gradients.

Waddar *et al.* (2019) investigated the buckling and vibration behaviour of a

syntactic foam core sandwich beam with natural fiber composite facings under axial compressive loads. Their research contributes to the understanding of the mechanical behaviour of sandwich beams with eco-friendly materials.

Talekar and Kotambkar (2020) carried out free vibration analysis of composite beams to analyze the influence of different lay-up configurations and end conditions on the natural frequencies and mode shapes of composite beams, providing valuable insights for design and optimization.

Melaibari *et al.* (2021) proposed a bio-inspired composite laminate design with improved out-of-plane strength and ductility. Their research focused on mimicking the hierarchical structure of natural materials to enhance the mechanical properties of composite laminates, offering potential applications in lightweight and resilient structures.

Chew *et al.* (2021) focused on enhancing the mechanical characteristics of natural fiber reinforced laminates composites through bio-mimicry. Their study explored bio-mimetic design strategies and fabrication techniques to enhance the strength and performance of natural fiber composites, offering potential solutions for sustainable and efficient material design.

Kanade *et al.* (2021) studied the buckling and natural frequencies of a composite beam subjected to VALs. Their research provides valuable insights into the structural response of composite beams under variable loading conditions, which is essential for designing and optimizing such structures in engineering applications.

Zhang *et al.* (2022) investigated the dynamic behaviours of bio-inspired structures by focusing on their design, mechanisms, and models. They explored the response of these structures under various loading conditions, providing insights for their practical applications.

Almitani *et al.* (2022) presented an exact solution for the non-linear behaviours of imperfect bio-inspired helicoidal composite beams resting on elastic foundations. Their study provided valuable insights into the structural response and stability of these beams, considering imperfections and the influence of elastic foundations.

Mohamed *et al.* (2022) investigated the non-linear static stability of imperfect

bio-inspired helicoidal composite beams. By considering the effects of imperfections, they analyzed the behaviour of these beams and provided insights into their stability under different loading conditions.

Mohamed *et al.* (2023) investigated the non linear stability of bio-inspired composite beams using a higher order shear theory. The study contributes to the understanding of the buckling behaviour of bio-inspired composite beams, providing valuable insights into their structural stability and performance under various loading conditions.

1.1.3 Studies using higher order theorems

For the effective design of a structural component, it is important to predict its static, buckling, and dynamic characteristics accurately. Studies implementing HSDT and Rayleigh-Ritz method in the formulations of governing equations predicting accurate results compared to other traditional theories. Relevant research articles are discussed.

Leissa (2005) provided an insightful overview of the historical development and underlying principles of the Rayleigh and Ritz methods for solving vibration problems. The review discusses the contributions of renowned scientists and engineers in formulating these methods and highlights their significance in structural dynamics.

Aydogdu (2005) employed the Ritz method to investigate the vibration analysis of cross-ply laminated beams with general boundary conditions. The study presented a systematic approach to obtain accurate natural frequencies and mode shapes for laminated beams, considering the effects of material anisotropy and boundary conditions.

Jaworski and Dowell (2008) conducted experimental and theoretical investigations on the natural frequencies of a CC beam with multiple steps. The study compared several theoretical methods, including the Rayleigh-Ritz method, with experimental data, highlighting the accuracy and limitations of each method in predicting the natural frequencies and mode shapes of the beam.

Influence of material gradient index on static behaviour of functionally graded metal–ceramic beam was studied by Kadoli *et al.* (2008) by using using FEM and higher order beam theory. The study depicted that there is a significant

variation in the static deflections and stresses when the material loading is varied from high ceramic composition to high metal composition.

Li *et al.* (2010) numerically investigated static and dynamic responses of FGM beams using various higher order beam theories. The computed deflection and stresses revealed that FG beams are sensitive to nature of variation of material property.

Zhu (2011) employed the Rayleigh-Ritz method to study the natural frequencies of pre-twisted rotating Timoshenko beams. The investigation presented a comprehensive analysis of the natural frequencies and mode shapes of rotating beams with different pre-twist angles, highlighting the influence of rpm and beam dimensions on the dynamic behaviour of such structures.

Thai and Thuc (2012) analytically studied the influence of higher order theories on the prediction of static and dynamic responses of FGM beam. Influence of the material gradient index and shear deformation effect is also highlighted.

Ghannadpour *et al.* (2013) applied the Ritz method to study bending, buckling, and vibration problems of non-local Euler beams. The study presented a comprehensive analysis of the structural behaviour, considering the effects of nonlocality on the bending, buckling, and vibration characteristics of Euler beams.

Larbi *et al.*(2013) proposed an efficient shear deformation beam theory based on neutral surface position for analyzing the bending and free vibration of functionally graded beams. The numerical findings showed that the theory was accurate in predicting the bending and vibration responses of FGM beams as it took into consideration the variation of material properties along the thickness of the beam.

Pradhan and Chakraverty (2014) investigated the effects of different shear deformation theories on the free vibration frequencies of FGM beams. The study compared the predictions of various shear deformation theories, highlighting their influence on the natural frequencies and mode shapes of FGM beams.

Ilanko *et al.*(2014) provided an in-depth exploration of the Rayleigh-Ritz method for solving structural analysis problems. The study covers the fundamental principles of the Rayleigh-Ritz method and its applications in various fields of structural engineering.

Chakraverty and Behera (2015) utilized the Rayleigh-Ritz method for investigating the free vibration of non-uniform nano beams. The work examined how geometric non-uniformity affected the free vibration and mode shapes of nano beams and offered important insights for the design and analysis of nano scale structures.

Nguyen *et al.*(2015) presented a new HSDT for vibration and buckling responses of FG sandwich beams. The theory accounted for the through-thickness variation of material properties and provided accurate predictions of the natural frequencies and buckling behaviour of functionally graded sandwich beams.

Nguyen *et al.*(2018) presented Ritz-based analytical solutions for bending, buckling, and natural frequency responses of laminated composite beams. The analytical approach provided efficient and accurate predictions of the structural responses, considering various boundary conditions and lay-up configurations.

Nguyen *et al.*(2020) proposed a novel unified model for laminated composite beams, considering the coupling effects between the bending and shear deformations. The unified model provided a comprehensive understanding of the structural behaviour and improved accuracy in predicting the response of laminated composite beams.

Zhang *et al.*(2020) investigated the effect of nature of material property variation on the deflection of micro-cantilever FGM beams induced by surface stress. The study analyzed the deflection behaviour of micro-cantilevers with varying material properties along the thickness, considering the influence of surface stress, and provided important findings for the design and application of functionally graded micro-structures.

Ozer *et al.*(2020) developed a shell based finite element model to analyze damped composite structures with multiple layers numerically. Their research provided an efficient numerical tool for analysing the dynamic behaviour of composite structures considering damping effect.

Li *et al.*(2020) focused on modelling the damping properties of fiber-reinforced composite structures. Their study presented a mathematical model to describe the damping behaviour of composite structure under varying vibration amplitudes, contributing to the accurate prediction and control of structural vibra-

tions.

Omidi Soroor *et al.* (2021) investigated the influence of an axially graded constraining layer on the free vibration properties of three-layered sandwich beams with a magnetorheological fluid core. The study explored the influence of the graded layer on the vibration behaviour of the beams, providing insights into the design and optimization of sandwich structures having magnetorheological fluid cores.

Priyanka and Pitchaimani (2022) analyzed the static stability and free vibration characteristics of a micro-laminated beam under varying axial load using the modified couple stress theory and Ritz method. The study focused on understanding the effect of axial load on the stability and vibration behaviour of micro-laminated beams, offering valuable insights into the design and analysis of such structures.

Alazwari *et al.*(2022) conducted vibration analysis on laminated composite beams using higher order beam theories subjected to VALs. Their study aimed to analyze the free vibration behaviour of beam under different loading scenarios, contributing to the design and optimization of composite structures.

Patil *et al.* (2023) investigated through a extensive study on the buckling and vibration of beams using the Ritz method, considering the effects of axial grading of GPL (graphene platelets) and axially varying loads.

1.1.4 Buckling studies

Beams exposed to axial loads are need to be analyzed for stability and dynamic characteristics, as the beams will experience buckling mode of failure. Since the current study is focused on the buckling and dynamic analysis of beam under variable axial load, the related research articles published recently are cited herein.

Aydogdu (2006) extended the application of the Ritz method to study the buckling behaviour of cross-ply laminated beams with general boundary conditions. They presented a comprehensive analysis of the buckling behaviours different beam geometries and boundary conditions, providing valuable insights for the design of laminated structures.

Heydari (2011) analytically investigated buckling capacity of FGM beams using

variational calculus approach. The study focused on analyzing the effects of material composition and geometrical parameters on the buckling load and mode shapes of the beams.

Akogz and Civalek (2013) using Bernoulli–Euler beam theory and modified strain gradient theory depicted the buckling response of functionally graded microbeams for various end conditions. The results are illustrated for influence of gradation pattern, aspect ratios and scale parameters on the buckling characteristics.

Sherafatnia *et al.* (2014) analytically analyzed static and dynamic responses of FGM beams using four different beam theories. On the buckling and free vibration responses, the impacts of crack location, aspect ratio, and material grading are discussed.

Li *et al.* (2016) estimated buckling loads and natural frequencies of laminated composite beams based on unified higher order shear deformation theory (HSDT). Through the effect of study the influence of shear deformation, VALs and end conditions on the static and dynamic responses were examined.

The free vibration properties of axially loaded composite beams were investigated using a four-unknown shear and normal deformation theory Vo *et al.*(2017). The governing equations of motion are derived using the Hamilton's principle, and the natural frequencies and mode shapes of the beams are determined through a numerical approach.

Sayyad and Ghugal (2017) conducted a review of literature on the bending, buckling, and free vibration of laminated composite and sandwich beams. Their review summarized the existing knowledge in this field, highlighting the key findings, challenges, and potential areas for future research.

Hadi *et al.*(2018) numerically analyzed buckling behaviour of a FG nano beam based on consistent couple-stress theorem with properties varying in three directions. Using generalised DQM method the study highlighted the influence of end conditions and material gradation on the static responses.

Karamanli and Aydogdu (2019) conducted numerical investigation on buckling responses of isotropic, laminated composite beams under different types of variable axial loads using Ritz method. The results depicted that the influence of

variable axial loads, aspect ratio and end conditions had significant effect on the buckling behaviours of laminated composite beams.

Buckling response and mode shapes of composite laminated beams are numerically analyzed using unified HSDT and DQM by Eltaher *et al.* (2020a). Where the effect of axial loads, fibre orientations, beam thickness and end conditions on the buckling characteristics is outlined in the study.

Using four HSDT and DQM Eltaher *et al.* (2020b) numerically investigated the effect of variable axial loads on static stability and corresponding mode shape of sandwich laminated composite beam. The significance of slenderness ratio, beam thickness, orthotropy ratio, axially varying loads, fiber orientation and end conditions on buckling stability are detailed.

Differential quadrature method is used in determining the critical buckling loads of composite laminated beam by Hamed *et al.*(2020). The parametric study was carried out for various elastic conditions, lamination thickness, axial loads and orthotropy ratios.

Melaibari *et al.*(2020a) numerically investigated buckling characteristics of FGM beams subjected to different types of VALs using DQM. The impact of the gradation patterns, axial loads, aspect ratios, and end conditions on buckling load characteristics is elaborated in the study.

Melaibari *et al.*(2020b) conducted numerical analysis on static buckling responses of sigmoid FGM beam under VALs using modified DQM. Where the study highlighted the influence of material gradation and nature of the VAL on the buckling load.

Hamed *et al.* (2020) performed optimisation study on a porous FG sandwich beam subjected to the VAL using DQM. They reported that nature of porosity variation, porosity coefficient and type of VAL affects the buckling load.

Abo-bakr *et al.* (2021), using DQM, studied the optimal weight of functionally graded (FG) beams in order to improve their buckling strength. The study revealed that the proposed optimal weight model will be effective in buckling strength design of isotropic and FGM beams subjected to VALs.

Harsha *et al.* (2021) investigated the effect of graded porosity and VALs for buck-

ling and dynamic behaviours of a FGM beam using Ritz method. They analyzed highly pointed the influence of distribution of porosity on the static buckling loads and free vibrations of FGM beams.

Dash *et al.*(2022) analyzed the buckling and free vibration characteristics of randomly distributed carbon nano tube (CNT) reinforced composite beams under thermo-mechanical loading. Their findings shed light on the structural performance of CNT-reinforced composites and their potential for various applications.

1.1.5 Vibration studies

The researchers are keen on analysing the free vibration characteristics of structural elements in order to avoid resonance and to analyze the dynamic response characteristics. A comprehensive literature on the free vibration studies on beams based on analytical and numerical approaches is presented in this section.

Ni and Adams (1984) investigated the damping and natural frequency of symmetrically layered composite beams, providing both conceptual and experimental responses. Their study contributed to the understanding of damping behaviour in composite materials and offered valuable insights for predicting the vibration responses of laminated composite structures.

Liao *et al.*(1994) investigated the vibration and damping characteristics of interlayered carbon fibre epoxy composite beams. They examined how interleaved layers affected the composite beams damping properties, providing valuable information for designing composite structures with enhanced damping capabilities.

Chandra *et al.*(1999) conducted a comprehensive review on damping studies in fibre reinforced composites. Their analysis covered various damping mechanisms, including visco-elastic, interfacial, and structural damping to provide a comprehensive understanding of the factors in influencing damping behaviour of composite materials.

Aydogdu and Taskin (2007) investigated on natural frequencies of FG beams using various beam theories. The effect of through thickness material gradation and slenderness ratio on the natural frequencies is highlighted in the study.

Simsek and Kocatürk (2009) based on the Euler-Bernoulli beam theory, exam-

ined the free vibration characteristics of a simply supported FGM beam. They carried out detailed parametric studies to analyze the effect of varying load on the natural frequencies, mode shapes, and dynamic responses of the beam.

In their analytical work, Sina *et al.* (2009) used first-order shear deformation theory to examine the free vibration response of FG beams. The study illustrated the effect of end conditions, shear deformation and material gradation on the free vibration characteristics. The study also established a comparison between the natural frequencies predicted using various beam theories.

Huang and Li (2010) used Fredholm integral equations to predict free vibration frequencies of tapered FGM beams with various end support conditions.

Huang and Fang (2010) used Freholm integral equations in their numerical investigation on dynamic responses of FG tapered beams. They reported that the material gradation and boundary conditions have considerable influence on the natural frequencies of the non-homogeneous tapered FG beam.

Simsek (2010) numerically investigated fundamental frequency of FGM beams using classical and various higher order beam theories. The study examined the influence of aspect ratios, gradation index and different numerical formulations on the fundamental frequency of the FGM beams.

Giunta *et al.* (2011) proposed a one-dimensional beam element to predict the natural frequencies of FGM beams. They demonstrated the accuracy of the proposed model and influence of material distribution on the free vibration.

Wattanasakulpong *et al.* (2012) performed free vibration analysis of FGM beams through numerical method and validated their findings through experimental measurements.

Vo *et al.*(2014) investigated the static and vibration behaviour of functionally graded beams using an improved shear deformation theory. Through their approach, they obtained accurate results for the deflection, natural frequencies, and mode shapes of the beams.

Nguyen and Nguyen (2015) introduced a new higher-order shear deformation theory for analyzing the statics, buckling, and free vibration of functionally graded sandwich beams. In contrast to conventional theories, their method took into

account the impact of transverse shear deformation and produced more precise predictions of the structural response.

Hadi *et al.*(2018) carried out numerical simulation studies to analyze free vibration frequencies of nano beams under the influence of three-dimensional grading of material. From the study significance of small scale variables and material gradation on the dynamic characteristics is demonstrated.

Banerjee and Ananthapuvirajah (2018) used the Wittrick-Williams algorithm and the dynamic stiffness matrix in their analytical approach to investigate the inherent frequencies and mode shapes of FGM beams. When analysing the natural frequencies of FG beams with uniform and non-uniform cross sections, the proposed model is determined to be accurate.

Karamanli and Aydogdu (2019) investigated the vibration behaviour of rotating laminated composite and sandwich microbeams considering size dependency. They proposed a transverse shear-normal deformation theory and demonstrated its effectiveness in capturing the size-dependent effects on the free vibration and mode shapes of microbeams.

Dangi *et al.*(2020) developed a size-dependent finite element model to analyze static and dynamic characteristics of bi-directional functionally graded nanobeams. Their study considered the influence of material composition and beam size and presented results providing valuable insights for the design and analysis of such structures.

Sharma and Singh (2021) carried out a numerical investigation on axial functionally graded material (FGM) beams to determine natural frequencies. Using finite element method, they investigated the influence of various parameters, such as gradient index and beam length, on the natural frequencies and mode shapes of FGM beams.

Sharma *et al.* (2022) conducted numerical study on free vibration frequencies of axially functionally graded beam using generalized DQM. The influence of grading patterns, volume indices, and geometry patterns is reported.

Kumar (2022) analytically studied dynamic responses of functionally graded beam subjected to non-uniform axial loading. Rayleigh-Ritz method is used in computing the results, which predicts that the effect of varying the material

gradation index, thickness, and layers stiffness significantly influence the fundamental frequencies of the beam.

1.1.6 Acoustic response studies

The sound radiation from vibrating structures, offer valuable insights into the dynamic characteristics of a structure aiding in the identification and recognition of dynamic related issues. This enables engineers to diagnose potential mechanical faults leading to improved design optimization and enhanced structural integrity.

Zheng and Cai (2004) focused on the minimization of sound radiation from baffled beams through the optimization of partial constrained layer damping treatment. Their research aimed to improve the acoustic performance of beams by optimizing the location of damping treatments, contributing to the reduction of noise and vibration in engineering structures.

Ruzzene (2004) investigated the natural frequencies and sound radiation characteristics of honeycomb truss core sandwich beam. Through experimental and numerical analyzes, the study examined the structural and acoustic behaviour of sandwich beams.

Spadoni and Ruzzene(2006) explored the structural and acoustic behaviour of chiral truss-core beams. Their research focused on characterizing the vibration and sound radiation properties of chiral truss-core beams, offering potential applications in lightweight and efficient structural designs.

Majkut (2006) investigated the cracks in beam-like structures and their acoustical diagnostics. The study focused on the analysis of acoustic responses to detect and characterize cracks in beams, providing insights into the application of acoustical methods for structural health monitoring.

Denli and Sun (2007) focused on the structural-acoustic optimization of cellular core sandwich structures to minimize sound radiation. Their study employed optimization techniques to determine the optimal design parameters of sandwich structures, leading to reduced sound radiation and improved acoustic performance.

Alshabatat and Naghshineh (2014) explored the optimization of natural frequen-

cies and sound power amplitude of FGM beams. Their study utilized optimization algorithms to determine the optimal material distribution in beams, leading to improved vibrational and acoustic performance.

Tang and Xu (2014) developed a vibro-acoustic model to investigate the behaviour of a flexible beam subjected to low subsonic flows characterized by average velocities. Their research aimed to investigate the interaction between flow-induced vibrations and acoustics in beams subjected to low-speed airflow.

Arunkumar *et al.*(2016) investigated the acoustic response of a sandwich panel constructed with composite facings and a honeycomb core, focusing on its sound radiation and the level of transmission loss. They specifically investigated the effect of inherent material damping on the acoustic performance of the panel, providing valuable insights for noise control and mitigation strategies in composite structures.

Torres-Romero *et al.*(2018) conducted an experimental approach to the vibro-acoustic study of beam-type structures. The study involved measurements and analyzes of the vibration and acoustic responses of beam structures, providing valuable experimental data and insights into their dynamic behaviour.

Li and Yang (2020) explored the design and vibro-acoustic properties of annular cellular structures using graded auxetic mechanical meta materials. Their study examined the sound transmission characteristics of annular cellular structures, revealing the potential of graded auxetic materials in enhancing the vibro-acoustic properties of such structures.

1.2 Closure

It is clear from the literature review that research on buckling and free vibration response of traditional FGM beams using higher order theories is abundantly available, but very few studies have been conducted on bi-directional functionally graded beams and bio-inspired beams. It is also observed from the literature that acoustic response study motivated several researchers while analysing the dynamic behaviour of structures. The dynamic responses are proven to be more accurate when the the numerical investigation is based on higher order beam theories. The literature also clearly highlighted the significance of considering variable axial loads while designing the beam with dynamic response consider-

ation. The earlier literatures also highlighted the implications of variation in material property along both the length and thickness directions for functionally graded beams and variation in lamination types, angle schemes for bio-inspired beams. While there have been extensive studies on the vibration characteristics of functionally graded beams and composite laminate beams, there is a lack of research regarding the acoustic response exhibited by structure made of these materials.

It is obvious that there is a clear void in investigating static and dynamic behaviours of B-FGM and bio-inspired beams subjected to VAL. The present study initiates the investigation on buckling, vibration and acoustic response characteristics of an isotropic, bi-directional functionally graded and bio-inspired laminated composite beams, subjected to VAL under the action of a steady state mechanical excitation.

1.3 Research objectives

The application of higher-order theories significantly enhances the accuracy of predicting structural failures, particularly in the fields like aerospace and civil engineering. As demonstrated from the works such as Karamanli and Aydogdu (2019), these theories offer improved precision in portraying structural failures. The Ritz method, known for its superiority in analyzing static buckling and vibration responses of beams, is a key focus in this context. Understanding the unique static buckling and dynamic behaviors of beams under Variable Axial Loads (VALs) is essential for the design of structures such as tall buildings and bridges, where axial loads vary due to environmental conditions. This distinction in static buckling and dynamic performance between beams subjected to VALs and those under end compression, as highlighted by Eltaher and Mohamed (2020), underlines the need for a detailed investigation. Investigating harmonic responses due to steady-state excitation is vital for aerospace applications. The constant vibrations experienced by critical components, such as wing elements and fuselage parts, can lead to fatigue and structural damage. This understanding is crucial for predicting and mitigating potential failures in these aerospace components, ensuring overall structural integrity and the safety of aircraft. Additionally, exploring the acoustic radiation resulting from structural vibrations is essential for noise control. This has direct implications for the aerospace industry, where minimizing the acoustic impact of vibrating components, such as wing

elements, fuselage sections, and engine parts, is critical for both environmental considerations and the prevention of critical component failures. This targeted approach contributes to safer and more durable aerospace structures, ensuring the prolonged reliability of crucial components in aircraft design.
The main objectives of the proposed work are:

- To investigate the vibro-acoustic behavior of isotropic beams under Variable Axial Loads (VALs.
- To analyze the influence of bi-directional grading on the buckling and vibration behavior of beams subjected to VALs.
- To explore the acoustic behavior of beams with bi-directional grading under VALs.
- To investigate the vibro-acoustic characteristics of bio-inspired beams under VALs.

The thesis highlights the calculations of buckling, natural frequency and acoustic behaviours of isotropic, B-FGM and bio-inspired beams from the conceptual 2D continuum model. Hence, the introduction section of each chapter in the thesis highlights the mathematical model of the material followed by results and discussion and at the end of the chapter conclusive observations were presented.

Various investigations in the present study is detailed in the below chapters.

Chapter 2, Chapter 2 presents the solution methodology for analyzing the buckling, natural frequency, and acoustic radiation of isotropic, B-FGM, and bio-inspired beams. The chapter also includes validation studies to ensure the accuracy and reliability of the proposed methods.

Chapter 3 presents a comprehensive investigation into the buckling and vibro-acoustic responses of an isotropic beam subjected to variable axial loads. The study explores these responses while considering various parameters, including an aspect ratio of '50' and three different boundary conditions.

Chapter 4, investigates the buckling and natural frequency behaviours of bi-directional functionally graded beams under various in-plane axial loads. The investigation also includes for two material gradation indexes, four boundary conditions and two aspect ratios.

Chapter 5, presents the acoustic radiation characteristics of bi-directional functionally graded beams subjected to a type of in-plane axial load along with two

aspect ratios and two material gradation indexes.

Chapter 6, presents investigation on buckling and vibro-acoustic behaviours of bio-inspired laminated composite beams under variable axial loads. The responses are determined additionally for nine layup schemes, three boundary conditions and two aspect ratios.

Chapter 7, salient observations and conclusions from the investigations on vibro-acoustic responses of isotropic, B-FGM and bio-inspired composite beams are detailed.

Chapter 2

METHODOLOGY AND VALIDATION STUDIES

2.1 Introduction

This chapter details the method used to forecast buckling, free vibration and acoustic response characteristics of isotropic, bi-directional functionally graded and bio-inspired laminated composite beams under the influence of VALs with the help of numerical simulation. Additionally, validation studies are provided to show how well the suggested technique predicts the aforementioned characteristics.

2.2 Methodology for numerical studies

Fig.2.1 represents the flow chart of the analysis methodology followed in the current work. For a given material, boundary condition, and axially variable load, it is possible to determine the initially critical buckling load and the basic buckling mode of the beam. Then, the pre-stressed modal analysis is carried out for a given intensity of the VAL as a function of critical buckling to obtain the free vibration characteristics. Followed by this pre-stressed harmonic response analysis of the beam excited by a concentrated mechanical load is performed similar to the free vibration study. In order to forecast sound radiation characteristics including sound pressure/power level, radiation efficiency, and directivity pattern, the steady state harmonic response is fed to the Rayleigh integral. It should be noted here that the vibration and acoustic parameters are analyzed as a function of the critical buckling load for a given VAL. The beam with $l\ x\ b\ x\ h$ as shown in

Fig. 2.2 under different types of VAL is considered for the detailed investigation. The schematic diagram of the problem studied is given in Fig. 2.2(a). Fig.2.2(a)

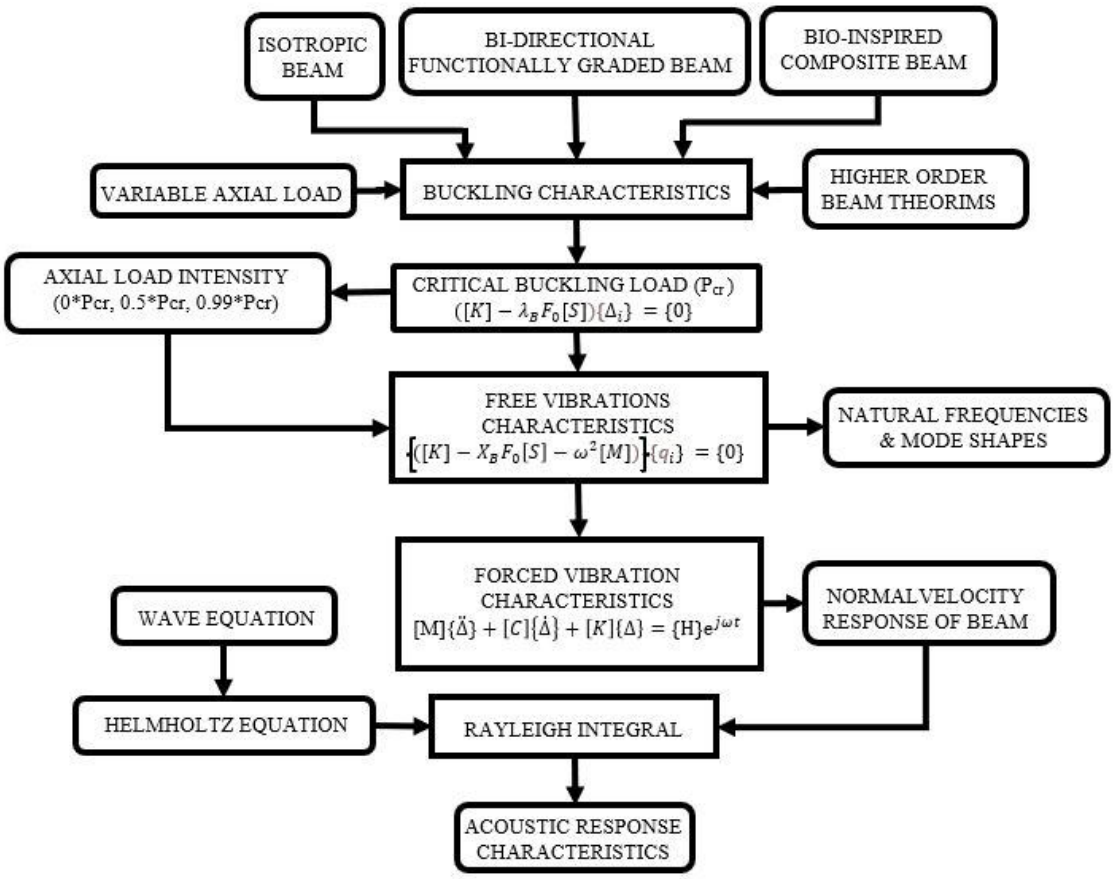

Figure 2.1: Analysis approach followed in the present work

is representing isotropic beam, Fig.2.2(b) is representing bi-directional functional graded beam and Fig.2.2 (c) is representing bio-inspired composite beams. The beam is studied for simply supported (SS), clamped clamped (CC), clamped simple (CS) and clamped free (CF) boundary conditions. As shown in Fig.2.3, six different types of VAL's are considered to analyze the effect of nature of axial load variation along the length for the buckling, natural frequencies and sound radiation characteristics of the beam. The variation of VAL for the different cases analyzed along the length is defined as,

$$F_x^e(x) = F_0\left\{\chi_1\left(x + \frac{L}{2}\right)^2 + \chi_2\left(x + \frac{L}{2}\right) + \chi_3\right\} \tag{2.1}$$

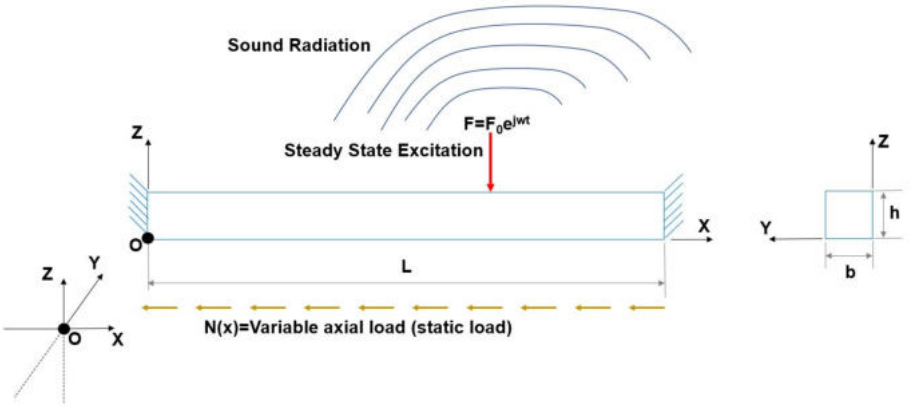

(a) Schematic diagram representation of geometry, co-ordinates, loads and excitation

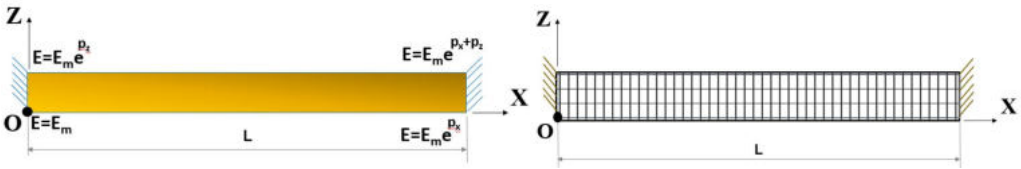

(b) B-FGM beam

(c) Bio-inspired composite beam

Figure 2.2: Geometry with co-ordinates of the beam considered for analysis

The coefficients χ_1, χ_2 and χ_3 are varied as shown in Table 2.1 [Karamanli and Aydogdu (2019)] in order to obtain different types of VALs shown in Fig. 2.3. Fig. 2.2(a) demonstrates how the axial loads are distributed along the length of the beam.

Table 2.1: The load coefficients for different VALs

Notation	Category of loading	χ_1	χ_2	χ_3
F_x^1	Uniformly distributed load	0	0	1
F_x^2	Gradually increasing load	0	2	0
F_x^3	Gradually decreasing load	0	-2	2
F_x^4	Exponentially increasing load	3	0	0
F_x^5	Exponentially decreasing load	3	-6	3
F_x^6	Parabolic load	-6	6	0

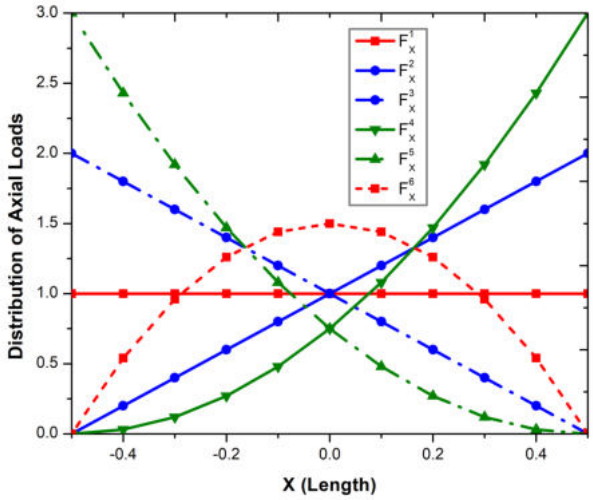

(a) Variations of VALs

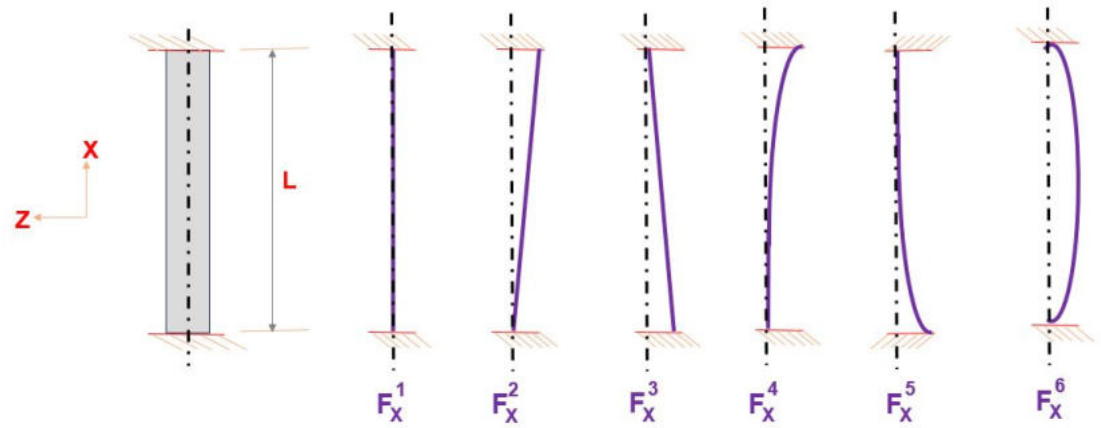

(b) Distribution of VALs

Figure 2.3: VALs variation and distribution along the length of the beam

2.2.1 Numerical model based on Reddy's beam theorem

In the investigation on B-FGM beams, the displacement field based on Reddy's higher order theory is considered [Aydogdu and Taskin (2007), Trung and Ba (2015)]. Young's modulus (E), shear modulus (G), Poissons's ratio (μ) and mass density (ρ) vary according to the following expressions,

$$\mathsf{E}(\mathsf{x},\mathsf{z}) = \mathsf{E}_{\mathsf{m}}\mathsf{e}^{\left\{\mathsf{p}_{\mathsf{x}}\left(\frac{\mathsf{x}}{\mathsf{L}}+\frac{1}{2}\right)+\mathsf{p}_{\mathsf{z}}\left(\frac{\mathsf{z}}{\mathsf{h}}+\frac{1}{2}\right)\right\}} \tag{2.2a}$$

$$\mathsf{G}(\mathsf{x},\mathsf{z}) = \frac{\mathsf{E}(\mathsf{x},\mathsf{z})}{2(1+\mu_{\mathsf{m}})} \tag{2.2b}$$

$$\rho(\mathsf{x},\mathsf{z}) = \rho_{\mathsf{m}}\mathsf{e}^{\left\{\mathsf{p}_{\mathsf{x}}\left(\frac{\mathsf{x}}{\mathsf{L}}+\frac{1}{2}\right)+\mathsf{p}_{\mathsf{z}}\left(\frac{\mathsf{z}}{\mathsf{h}}+\frac{1}{2}\right)\right\}} \tag{2.2c}$$

where E_m, μ_m *and* ρ_m are the respective properties defined at point $(\frac{-L}{2}, \frac{-h}{2})$ and the gradient indexes p_x and p_z are used to represent the variation of the material property along the length (L) and thickness (h) respectively. For the isotropic beam and bio-inspired beams, p_x and p_z are set to zero with the change in their respective elastic modulus, Poisson's ratio and density. According to the Reddy's beam theory, the displacement field is define as

$$\mathsf{U}(\mathsf{x},\mathsf{z},\mathsf{t}) = \mathsf{u}(\mathsf{x},\mathsf{t}) + \mathsf{z}\phi(\mathsf{x},\mathsf{t}) - \alpha\mathsf{z}^3\left(\phi(\mathsf{x},\mathsf{t}) + \frac{\partial \mathsf{w}(\mathsf{x},\mathsf{t})}{\partial \mathsf{x}}\right) \tag{2.3}$$

$$\mathsf{W}(\mathsf{x},\mathsf{z},\mathsf{t}) = \mathsf{w}(\mathsf{x},\mathsf{t}) \tag{2.4}$$

where u and w are axial and transverse displacements, ϕ is rotation component for the cross sections and $\alpha = \frac{4}{3h^2}$. From Eq.(2.3) and Eq.(2.4), the strain displacement relation can be written as

$$\varepsilon_{\mathsf{xx}} = \frac{\partial \mathsf{U}}{\partial \mathsf{x}} = \frac{\partial \mathsf{u}}{\partial \mathsf{x}} + \mathsf{Z}\frac{\partial \phi}{\partial \mathsf{x}} - \alpha\mathsf{Z}^3\left(\frac{\partial \phi}{\partial \mathsf{x}} + \frac{\partial^2 \mathsf{w}}{\partial \mathsf{x}^2}\right) \tag{2.5}$$

$$\gamma_{\mathsf{xz}} = \frac{\partial \mathsf{U}}{\partial \mathsf{z}} + \frac{\partial \mathsf{W}}{\partial \mathsf{x}} = \phi + \frac{\partial \mathsf{w}}{\partial \mathsf{x}} - \beta\mathsf{Z}^2\left(\phi + \frac{\partial \mathsf{w}}{\partial \mathsf{x}}\right) \tag{2.6}$$

where $\beta = 3\alpha$, The stress-strain relation is given by

$$\begin{Bmatrix} \sigma_{\mathsf{xx}} \\ \sigma_{\mathsf{xz}} \end{Bmatrix} = \begin{bmatrix} \mathsf{E}(\mathsf{x}.\mathsf{z}) & 0 \\ 0 & \mathsf{G}(\mathsf{x},\mathsf{z}) \end{bmatrix} \begin{Bmatrix} \epsilon_{\mathsf{xx}} \\ \gamma_{\mathsf{xz}} \end{Bmatrix} \tag{2.7}$$

The strain energy is,

$$\mathsf{U} = \frac{1}{2}\int_{\mathsf{v}} (\sigma_{\mathsf{xx}}\epsilon_{\mathsf{xx}} + \sigma_{\mathsf{xz}}\gamma_{\mathsf{xz}})\mathsf{dV} \tag{2.8}$$

Here, V is the volume of the analyzed beam. Strain energy is obtained by substituting Eq.(2.5) and Eq.(2.6) into Eq.(2.7).

$$\begin{aligned} U = \frac{1}{2}\int_v \Bigg[E(x,z)\Bigg\{ \Big(\frac{\partial u}{\partial x}\Big)^2 + (z^2 - 2\alpha z^4 + \alpha^2 z^6)\Big(\frac{\partial \phi}{\partial x}\Big)^2 + \\ \alpha^2 z^6 \Big(\frac{\partial^2 w}{\partial x^2}\Big)^2 + 2(z - \alpha z^3)\frac{\partial u}{\partial x}\frac{\partial \phi}{\partial x} - 2\alpha z^3 \frac{\partial u}{\partial x}\frac{d^2 w}{dx^2} + \\ 2(\alpha^2 z^6 - \alpha z^4)\frac{\partial \phi}{\partial x}\frac{d^2 w}{dx^2}\Bigg\} + G(x,z)\Bigg\{ (1 - 2\beta z^2 + \beta^2 z^4)\phi^2 + \\ (1 - 2\beta z^2 + \beta^2 z^4)\Big(\frac{\partial w}{\partial x}\Big)^2 + (1 - 2\beta z^2 + \beta^2 z^4)\phi\Big(\frac{\partial w}{\partial x}\Big)\Bigg\}\Bigg] dV \end{aligned} \tag{2.9}$$

The stiffness coefficients are defined as,

$$(A, B, D, C, F, H) = b\int_{\frac{-h}{2}}^{\frac{h}{2}} E_m e^{p_z(\frac{z}{h}+\frac{1}{2})}(1, z, z^2, z^3, z^4, z^6)dz \tag{2.10a}$$

$$(A_s, D_s, F_s) = b\int_{\frac{-h}{2}}^{\frac{h}{2}} G_m e^{p_z(\frac{z}{h}+\frac{1}{2})}(1, z^2, z^4)dz \tag{2.10b}$$

. The strain energy can be written as,

$$\begin{aligned} U = \frac{1}{2}\int_{\frac{-L}{2}}^{\frac{L}{2}} e^{p_x(\frac{x}{L}+\frac{1}{2})}\Bigg[A\Big(\frac{\partial u}{\partial x}\Big)^2 + (D + \alpha^2 H - 2\alpha F)\Big(\frac{\partial \phi}{\partial x}\Big)^2 + \\ \alpha^2 H\Big(\frac{\partial^2 w}{\partial x^2}\Big)^2 + 2(B - \alpha C)\frac{\partial u}{\partial x}\frac{\partial \phi}{\partial x} - 2\alpha C\frac{\partial u}{\partial x}\frac{d^2 w}{dx^2} + \\ 2(\alpha^2 H - \alpha F)\frac{\partial \phi}{\partial x}\frac{d^2 w}{dx^2} + (A_s + \beta^2 F_s - 2\beta D_s)\left(\phi^2 + \Big(\frac{\partial w}{\partial x}\Big)^2 + 2\phi\frac{\partial w}{\partial x}\right)\Bigg] dx \end{aligned} \tag{2.11}$$

Similarly, the kinetic energy can be expressed as

$$K = \frac{1}{2}\int_v \rho(\dot{u}_i \delta \dot{u}_i)dv \tag{2.12}$$

$$\begin{aligned} = \frac{1}{2}\int_{\frac{-L}{2}}^{\frac{L}{2}} e^{p_x(\frac{x}{L}+\frac{1}{2})}\Bigg[I_0\Big(\frac{\partial u}{\partial t}\Big)^2 + (I_2 + \alpha^2 K_1 - 2\alpha J_2)\Big(\frac{\partial \phi}{\partial t}\Big)^2 \\ + I_0\Big(\frac{\partial w}{\partial t}\Big)^2 + 2(I_1 - \alpha J_1)\frac{\partial u}{\partial t}\frac{\partial \phi}{\partial t} + 2(\alpha^2 K_1 - \alpha J_2)\frac{\partial \phi}{\partial t}\frac{\partial^2 w}{\partial x \partial t} - \\ 2\alpha J_1 \frac{\partial u}{\partial t}\frac{\partial^2 w}{\partial x \partial t} + \alpha^2 K_1\Big(\frac{\partial^2 w}{\partial x \partial t}\Big)^2\Bigg] dx \end{aligned}$$

where t is the time and the inertial coefficients are expressed as follows,

$$\left(\mathsf{I}_0, \mathsf{I}_1, \mathsf{I}_2, \mathsf{J}_1, \mathsf{J}_2, \mathsf{K}_1\right) = b \int_{\frac{-h}{2}}^{\frac{h}{2}} \rho_m e^{p_z(\frac{z}{h}+\frac{1}{2})}(1, z, z^2, z^3, z^4, z^6)dz \tag{2.13}$$

and the work done by VAL can be expressed as ,

$$\mathsf{V} = -\frac{1}{2}\int_{-\frac{\mathsf{L}}{2}}^{\frac{\mathsf{L}}{2}} \mathsf{F}_{\mathsf{x}}^{\mathsf{e}}(\mathsf{x})\left[\int_{-\frac{\mathsf{L}}{2}}^{\mathsf{x}} \left\{\left(\frac{\partial\phi}{\partial\mathsf{x}}\right)^2 + 2\frac{\partial\phi}{\partial\mathsf{x}}\frac{\partial\mathsf{w}}{\partial\mathsf{x}} + \left(\frac{\partial\mathsf{w}}{\partial\mathsf{x}}\right)^2\right\}\mathsf{dx}\right]\mathsf{dx} \tag{2.14}$$

Total potential energy can be expressed as,

$$\prod = \mathsf{U} + \mathsf{V} - \mathsf{K} \tag{2.15}$$

then,

$$0 = \int_{\mathsf{t}_1}^{\mathsf{t}_2} (\mathsf{K} - \mathsf{U} - \mathsf{V})\mathsf{dt}$$

$$\begin{aligned}
0 = \Bigg[\int_{\mathsf{t}_1}^{\mathsf{t}_2}\int_0^{\mathsf{L}} \Big[\frac{1}{2}\int_{\frac{-\mathsf{L}}{2}}^{\frac{\mathsf{L}}{2}} e^{\mathsf{p}_\mathsf{x}(\frac{\mathsf{x}}{\mathsf{L}}+\frac{1}{2})}\Bigg[\mathsf{A}\Big(\frac{\partial\mathsf{u}}{\partial\mathsf{x}}\Big)^2 + (\mathsf{D} + \alpha^2\mathsf{H} - 2\alpha\mathsf{F})\Big(\frac{\partial\phi}{\partial\mathsf{x}}\Big)^2 + \alpha^2\mathsf{H}\Big(\frac{\partial^2\mathsf{w}}{\partial\mathsf{x}^2}\Big)^2 + \\
2(\mathsf{B} - \alpha\mathsf{C})\frac{\partial\mathsf{u}}{\partial\mathsf{x}}\frac{\partial\phi}{\partial\mathsf{x}} - 2\alpha\mathsf{C}\frac{\partial\mathsf{u}}{\partial\mathsf{x}}\frac{\mathsf{d}^2\mathsf{w}}{\mathsf{dx}^2} + 2(\alpha^2\mathsf{H} - \alpha\mathsf{F})\frac{\partial\phi}{\partial\mathsf{x}}\frac{\mathsf{d}^2\mathsf{w}}{\mathsf{dx}^2} + \\
(\mathsf{A}_\mathsf{s} + \beta^2\mathsf{F}_\mathsf{s} - 2\beta\mathsf{D}_\mathsf{s})\left(\phi^2 + \Big(\frac{\partial\mathsf{w}}{\partial\mathsf{x}}\Big)^2 + 2\phi\frac{\partial\mathsf{w}}{\partial\mathsf{x}}\right)\Bigg]\mathsf{dx} - \\
\frac{1}{2}\int_{\frac{-\mathsf{L}}{2}}^{\frac{\mathsf{L}}{2}} e^{\mathsf{p}_\mathsf{x}(\frac{\mathsf{x}}{\mathsf{L}}+\frac{1}{2})}\Bigg[\mathsf{I}_0\Big(\frac{\partial\mathsf{u}}{\partial\mathsf{t}}\Big)^2 + (\mathsf{I}_2 + \alpha^2\mathsf{K}_1 - 2\alpha\mathsf{J}_2)\Big(\frac{\partial\phi}{\partial\mathsf{t}}\Big)^2 \\
+\mathsf{I}_0\Big(\frac{\partial\mathsf{w}}{\partial\mathsf{t}}\Big)^2 + 2(\mathsf{I}_1 - \alpha\mathsf{J}_1)\frac{\partial\mathsf{u}}{\partial\mathsf{t}}\frac{\partial\phi}{\partial\mathsf{t}} + 2(\alpha^2\mathsf{K}_1 - \alpha\mathsf{J}_2)\frac{\partial\phi}{\partial\mathsf{t}}\frac{\partial^2\mathsf{w}}{\partial\mathsf{x}\partial\mathsf{t}} - \\
2\alpha\mathsf{J}_1\frac{\partial\mathsf{u}}{\partial\mathsf{t}}\frac{\partial^2\mathsf{w}}{\partial\mathsf{x}\partial\mathsf{t}} + \alpha^2\mathsf{K}_1\Big(\frac{\partial^2\mathsf{w}}{\partial\mathsf{x}\partial\mathsf{t}}\Big)^2\Bigg]\mathsf{dx} - \\
-\frac{1}{2}\int_{-\frac{\mathsf{L}}{2}}^{\frac{\mathsf{L}}{2}} \mathsf{F}_{\mathsf{x}}^{\mathsf{e}}(\mathsf{x})\left[\int_{-\frac{\mathsf{L}}{2}}^{\mathsf{x}} \left\{\left(\frac{\partial\phi}{\partial\mathsf{x}}\right)^2 + 2\frac{\partial\phi}{\partial\mathsf{x}}\frac{\partial\mathsf{w}}{\partial\mathsf{x}} + \left(\frac{\partial\mathsf{w}}{\partial\mathsf{x}}\right)^2\right\}\mathsf{dx}\right]\mathsf{dx}
\end{aligned} \tag{2.16}$$

The kinematic relations associated with all the four end conditions are shown in Table 2.2. The displacement functions $\mathsf{u}(\mathsf{x},\mathsf{t})$, $\mathsf{w}(\mathsf{x},\mathsf{t})$ and rotation function $\phi(x,t)$ are defined as follows

Table 2.2: Boundary exponents for different end conditions

BC	Left end			Right end		
	p_u	p_w	p_ϕ	q_u	q_w	q_ϕ
SS	1	1	0	0	1	0
CS	1	2	1	0	1	0
CC	1	2	1	1	2	1
CF	1	2	1	0	0	0

$$\mathsf{u}(\mathsf{x},\mathsf{t}) = \sum_{\mathsf{i}=1}^{\mathsf{m}} \mathsf{A_i}\Theta_\mathsf{i}(\mathsf{x})\mathsf{e}^{\mathsf{i}\omega\mathsf{t}}, \quad \Theta_\mathsf{i}(\mathsf{x}) = \left(\mathsf{x}+\frac{\mathsf{L}}{2}\right)^{\mathsf{p_u}}\left(\mathsf{x}-\frac{\mathsf{L}}{2}\right)^{\mathsf{q_u}}\mathsf{x}^{\mathsf{m}-1} \tag{2.17a}$$

$$\mathsf{w}(\mathsf{x},\mathsf{t}) = \sum_{\mathsf{i}=1}^{\mathsf{m}} \mathsf{B_i}\varphi_\mathsf{i}(\mathsf{x})\mathsf{e}^{\mathsf{i}\omega\mathsf{t}}, \quad \varphi_\mathsf{i}(\mathsf{x}) = \left(\mathsf{x}+\frac{\mathsf{L}}{2}\right)^{\mathsf{p_w}}\left(\mathsf{x}-\frac{\mathsf{L}}{2}\right)^{\mathsf{q_w}}\mathsf{x}^{\mathsf{m}-1} \tag{2.17b}$$

$$\phi(\mathsf{x},\mathsf{t}) = \sum_{\mathsf{i}=1}^{\mathsf{m}} \mathsf{C_i}\psi_\mathsf{i}(\mathsf{x})\mathsf{e}^{\mathsf{i}\omega\mathsf{t}}, \quad \psi_\mathsf{i}(\mathsf{x}) = \left(\mathsf{x}+\frac{\mathsf{L}}{2}\right)^{\mathsf{p}_\phi}\left(\mathsf{x}-\frac{\mathsf{L}}{2}\right)^{\mathsf{q}_\phi}\mathsf{x}^{\mathsf{m}-1} \tag{2.17c}$$

In Eq.(2.17), $\mathsf{A_j}$, $\mathsf{B_j}$ and $\mathsf{C_j}$ are unknown coefficients and $\Theta_\mathsf{j}(\mathsf{x})$, $\varphi_\mathsf{j}(\mathsf{x})$ and $\psi_\mathsf{j}(\mathsf{x})$ are the trial functions and p_ζ and q_ζ are the end exponents in which $\zeta = u,\ w,\ \phi$. The governing differential equations of motion are determined by substituting Eq.(2.17) into Eq.(2.16). Using Lagrange equations

$$\frac{\partial \prod}{\partial \mathsf{q_i}} - \frac{\partial}{\partial \mathsf{t}}\left[\frac{\partial \prod}{\partial \dot{\mathsf{q}}_\mathsf{i}}\right] = 0 \tag{2.18}$$

Where q_j represents A_i, B_i and C_i, and the governing equations of motion are derived as

$$\left\{ \begin{bmatrix} [\mathsf{K}_{11}] & [\mathsf{K}_{12}] & [\mathsf{K}_{13}] \\ [\mathsf{K}_{12}]^T & [\mathsf{K}_{22}] & [\mathsf{K}_{23}] \\ [\mathsf{K}_{13}]^T & [\mathsf{K}_{23}]^T & [\mathsf{K}_{33}] \end{bmatrix} - \lambda_B F_0 \begin{bmatrix} [0] & [0] & [0] \\ [0] & [\mathsf{S}_{22}] & [0] \\ [0] & [0] & [0] \end{bmatrix} \right.$$

$$-\omega^2 \begin{bmatrix} [\mathsf{M}_{11}] & [\mathsf{M}_{12}] & [\mathsf{M}_{13}] \\ [\mathsf{M}_{21}]^T & [\mathsf{M}_{22}] & [\mathsf{M}_{23}] \\ [\mathsf{M}_{13}]^T & [\mathsf{M}_{23}]^T & [\mathsf{M}_{33}] \end{bmatrix} \begin{Bmatrix} \{A\} \\ \{B\} \\ \{C\} \end{Bmatrix} = \begin{Bmatrix} \{0\} \\ \{0\} \\ \{0\} \end{Bmatrix} \tag{2.19}$$

Where [K] represents structural stiffness matrix, [S] represents geometric stiffness matrices and [M] represents mass matrix. The elements of all these matrices are presented in Appendix A.

2.2.2 Numerical model based on shear and normal deformation beam theorem

The displacement field is defined based on the shear and normal deformation theory proposed by Karamanli and Aydogdu (2019). In accordance with shear and normal deformation theory (SNDBT), hypothesis on beams,

$$\mathsf{U}(\mathsf{x},\mathsf{z},\mathsf{t}) = \mathsf{u}(\mathsf{x},\mathsf{t}) - \mathsf{z}\frac{\partial \mathsf{w_b}(\mathsf{x},\mathsf{t})}{\partial \mathsf{x}} - \mathsf{f}(\mathsf{z})\frac{\partial \mathsf{w_s}(\mathsf{x},\mathsf{t})}{\partial \mathsf{x}} \tag{2.20}$$

$$\mathsf{W}(\mathsf{x},\mathsf{z},\mathsf{t}) = \mathsf{w_b}(\mathsf{x},\mathsf{t}) + \mathsf{w_s}(\mathsf{x},\mathsf{t}) + \mathsf{g}(\mathsf{z})\mathsf{w_z}(\mathsf{x},\mathsf{t}) \tag{2.21}$$

Where, u represents axial displacement, $\mathsf{w_b}$ and $\mathsf{w_s}$ correspond to the bending and shear displacements components, and w_z captures the effect of rotation and, $\mathsf{f}(\mathsf{z}) = \frac{4\mathsf{z}^3}{3\mathsf{h}^2}$, $\mathsf{g}(\mathsf{z}) = \left(1 - \frac{4\mathsf{z}^2}{\mathsf{h}^2}\right)$. The axial, normal and shear strain components are determined by:-

$$\varepsilon_{\mathsf{x}} = \frac{\partial \mathsf{U}}{\partial \mathsf{x}} = \mathsf{u}^{'} - \mathsf{z}\mathsf{w}_{\mathsf{b}}'' - \mathsf{f}\mathsf{w}_{\mathsf{s}}'' \tag{2.22a}$$

$$\varepsilon_{\mathsf{z}} = \frac{\partial \mathsf{W}}{\partial \mathsf{z}} = \mathsf{g}^{'}\mathsf{w}_{\mathsf{z}} \tag{2.22b}$$

$$\gamma_{\mathsf{xz}} = \frac{\partial \mathsf{W}}{\partial \mathsf{x}} + \frac{\partial \mathsf{U}}{\partial \mathsf{z}} = \mathsf{g}(\mathsf{w}_{\mathsf{b}}^{'} + \mathsf{w}_{\mathsf{z}}^{'}) \tag{2.22c}$$

The stress-strain relationship for the K^{th} layer is expressed as,

$$\begin{Bmatrix} \sigma_x \\ \sigma_x \\ \sigma_{xz} \end{Bmatrix}^k = \begin{bmatrix} \mathsf{Q}_{11} & \mathsf{Q}_{13} & 0 \\ \mathsf{Q}_{31} & \mathsf{Q}_{33} & 0 \\ 0 & 0 & \mathsf{Q}_{55} \end{bmatrix}^k \begin{Bmatrix} \epsilon_x \\ \epsilon_z \\ \gamma_{xz} \end{Bmatrix}^k \tag{2.23}$$

In Eq.(2.23) $(\sigma_x, \sigma_z, \sigma_{xz})$ and $\epsilon_x, \epsilon_z, \gamma_{xz}$ are stress-strain components, while, the material stiffness Q_{ij} can be mentioned as,

$$Q_{11} = C_{11}\cos^4\theta + 2(C_{12} + 2C_{66})\cos^2\theta\sin^2\theta + C_{22}\sin^4\theta \tag{2.24a}$$

$$Q_{13} = C_{23}\sin^2\theta + C_{13}\cos^2\theta \tag{2.24b}$$

$$Q_{33} = C_{33} \tag{2.24c}$$

$$Q_{55} = C_{55}\sin^2\theta + C_{44}\cos^2\theta \tag{2.24d}$$

Where,

$$C_{11} = \frac{E_1}{\Delta}; C_{12} = \frac{E_1\nu_{21}}{\Delta}; C_{22} = \frac{E_2(1-\nu_{13}\nu_{31})}{\Delta}; C_{13} = \frac{E_1\nu_{31}}{\Delta};$$
$$C_{23} = \frac{E_2\nu_{12}\nu_{31}}{\Delta}; C_{33} = \frac{E_3(1-\nu_{12}\nu_{21})}{\Delta}; C_{66} = G_{12}; C_{44} = G_{13}; C_{55} = G_{23};$$
$$\Delta = 1 - \nu_{12}\nu_{21} - \nu_{13}\nu_{31}$$

$E_1, E_2, G_{12}, G_{13}, G_{23}, \nu_{12}$ and ν_{21} are material properties of the bio-inspired composite beam.

In the current study, the investigation on isotropic beams was carried out by assuming equal values for the Young's modulus along all principal material axes, i.e., $E_1 = E_2 = E_3$. Additionally, the shear moduli $G_{12} = G_{13} = G_{23}$ and the Poisson's ratios $\nu_{12} = \nu_{23} = \nu_{13}$ were also considered equal to maintain isotropic material behaviour. These assumptions were made to model the isotropic beam responses accurately, and they allow for a more focused investigation on the buckling, vibration and acoustic characteristics of isotropic beams within the broader context of the research on both composite and isotropic beams.

The strain energy is expressed as,

$$U = \int_v \left(\sigma_x\epsilon_x + \sigma_z\epsilon_z + \sigma_{xz}\gamma_{xz}\right)dv \tag{2.25}$$

The kinetic energy is expressed as,

$$T = \frac{1}{2}\int_v \rho(z)\left(\dot{U}^2 + \dot{W}^2\right)dv \tag{2.26}$$

The work done by VAL is expressed as,

$$K = -\frac{1}{2}\int_0^L \left\{F_x^e(x)\int_0^L \left[w_b'^2 + 2w_b'w_s' + w_s'^2\right]dx\right\}dx \tag{2.27}$$

The total potential energy is given by

$$\prod = U + V - K \tag{2.28}$$

$$\begin{aligned}\prod = \frac{1}{2}\int_0^L \Big[& Au'' + Dw_b''^2 + Hw_s''^2 - 2D_s w_b'' w_s'' - 2Bu' w_b'' + 2B_s u' w_s'' \\ & + 2Xu' w_z - 2Yw_b'' w_z + 2Y_s w_s'' w_z + z w_z^2 + A_s\{w_s'^2 + w_z'^2 + 2w_s' w_z'\} \\ & - I_0\{\dot{u}^2 + \dot{w_b}^2 + \dot{w_s}^2 + 2\dot{w_b}\dot{w_s}\} + 2I_1\dot{u}\dot{w_b}' + I_2\dot{w_b}'^2 - 2J_1\dot{u}\dot{w_s}' \\ & - 2J_2\{\dot{w_b}\dot{w_z} + \dot{w_s}\dot{w_z}\} + 2J_3\dot{w_b}'\dot{w_s}' - K_1\dot{w_s}'^2 - K_2\dot{w_z}^2 \\ & - F_x^e(x)\{w_b'^2 + 2w_b' w_s' + w_s'^2\}\Big] dx\end{aligned}$$

The stiffness coefficients are defined as follows,

$$(A, B, B_s, D, D_s, H, Z) = \int_{-\frac{h}{2}}^{\frac{h}{2}} Q_{11}(1, z, -f, z^2, fz, f^2, g'^2) b dz \tag{2.29}$$

$$(X, Y, Y_s) = \int_{-\frac{h}{2}}^{\frac{h}{2}} Q_{13}(1, z, -f) g' b dz \tag{2.30}$$

$$A_s, Z = \int_{-\frac{h}{2}}^{\frac{h}{2}} (Q_{55} g^2, Q_{33} g'^2) b dz \tag{2.31}$$

The inertial coefficients are defined as,

$$(I_0, I_1, I_2, J_1, J_2, J_3, K_1, K_2) = \int_{\frac{-h}{2}}^{\frac{h}{2}} \rho(z)(1, z, z^2, -f, g, -fz, f^2, g^2) b dz \tag{2.32}$$

In present work, Ritz method is adopted to solve the problem. The displacement functions are chosen in such a way that they satisfy the end conditions given in Table 2.3, as follows

$$u(x,t) = \sum_{j=1}^{m} A_j \Theta_j(x) e^{i\omega t}, \Theta_j(x) = \left(x + \frac{L}{2}\right)^{p_u} \left(x - \frac{L}{2}\right)^{q_u} x^{j-1} \tag{2.33a}$$

$$w_b(x,t) = \sum_{j=1}^{m} B_j \varphi_j(x) e^{i\omega t}, \varphi_j(x) = \left(x + \frac{L}{2}\right)^{p_{w_b}} \left(x - \frac{L}{2}\right)^{q_{w_b}} x^{j-1} \tag{2.33b}$$

$$w_s(x,t) = \sum_{j=1}^{m} C_j \zeta_j(x) e^{i\omega t}, \zeta_j(x) = \left(x + \frac{L}{2}\right)^{p_{w_s}} \left(x - \frac{L}{2}\right)^{q_{w_s}} x^{j-1} \tag{2.33c}$$

$$w_z(x,t) = \sum_{j=1}^{m} D_j \psi_j(x) e^{i\omega t}, \psi_j(x) = \left(x + \frac{L}{2}\right)^{p_{w_z}} \left(x - \frac{L}{2}\right)^{q_{w_z}} x^{j-1} \tag{2.33d}$$

The functions $u(x,t)$, $w_b(x,t)$, $w_s(x,t)$, and $w_z(x)$ represent the displacement

Table 2.3: Boundary conditions

BC	Left end	Right end
SS	$u_0 = 0, w_b = 0, w_s = 0, w_z = 0$	$w_b = 0, w_s = 0, w_z = 0$
CS	$u_0 = 0, w_b = 0, w_s = 0, w_z = 0, w_b' = 0, w_s' = 0$	$w_b = 0, w_s = 0, w_z = 0$
CC	$u_0 = 0, w_b = 0, w_s = 0, w_z = 0, w_b' = 0, w_s' = 0$	$u_0 = 0, w_b = 0, w_s = 0,$ $w_z = 0, w_b' = 0, w_s' = 0$
CF	$u_0 = 0, w_b = 0, w_s = 0, w_z = 0, w_b' = 0, w_s' = 0$	

fields for different modes of vibration and buckling in the structural system, as defined by Karamanli and Aydogdu (2019). These displacement functions are used in the Ritz method, the Ritz method facilitates the determination of approximate solutions and enables the construction of the stiffness matrix [K], mass matrix [M], and geometric stiffness matrix [S] for buckling and vibration analyzes. Subsequently, eigenvalue analysis on these matrices provides critical buckling loads and natural frequencies, while eigenvectors offer mode shapes. In Eq.2.33, A_j, B_j, C_j and D_j are unknown coefficients, $\Theta_j(x)$, $\varphi(x)$, $\zeta_j(x)$ and $\psi_j(x)$ are trial functions and p_ξ and q_ξ are the boundary exponents. The boundary exponents are ($\xi = u, w_b, w_s, w_z$).

By substituting Eq. (2.33) into Eq. (2.28), the governing differential equations for the motions can be derived. Using Lagrange equations

$$\frac{\partial \prod}{\partial q_i} - \frac{\partial}{\partial t}\left[\frac{\partial \prod}{\partial \dot{q}_j}\right] = 0 \tag{2.34}$$

Where q_j represents A_j, B_j and C_j, and the governing equations of motion are derived as

$$\left\{ \begin{bmatrix} [K_{11}] & [K_{12}] & [K_{13}] & [K_{14}] \\ [K_{12}]^T & [K_{22}] & [K_{23}] & [K_{24}] \\ [K_{13}]^T & [K_{23}]^T & [K_{33}] & [K_{34}] \\ [K_{14}]^T & [K_{24}]^T & [K_{34}]^T & [K_{44}] \end{bmatrix} - \lambda_B F_0 \begin{bmatrix} [0] & [0] & [0] & [0] \\ [0] & [S_{22}] & [S_{23}] & [0] \\ [0] & [S_{23}] & [S_{33}] & [0] \\ [0] & [0] & [0] & [0] \end{bmatrix} \right.$$

$$-\omega^2 \begin{bmatrix} [\mathsf{M}_{11}] & [\mathsf{M}_{12}] & [\mathsf{M}_{13}] & [\mathsf{M}_{14}] \\ [\mathsf{M}_{21}]^T & [\mathsf{M}_{22}] & [\mathsf{M}_{23}] & [\mathsf{M}_{24}] \\ [\mathsf{M}_{13}]^T & [\mathsf{M}_{23}]^T & [\mathsf{M}_{33}] & [\mathsf{M}_{34}] \\ [\mathsf{M}_{14}]^T & [\mathsf{M}_{24}]^T & [\mathsf{M}_{34}]^T & [\mathsf{M}_{44}] \end{bmatrix} \Bigg\} \begin{Bmatrix} \{A\} \\ \{B\} \\ \{C\} \\ \{D\} \end{Bmatrix} = \begin{Bmatrix} \{0\} \\ \{0\} \\ \{0\} \\ \{0\} \end{Bmatrix} \tag{2.35}$$

The elements of the [K], [S] and [M] matrices are presented in Appendix B.

2.2.3 Buckling load calculation

The relation for buckling load is obtained from the structural stiffness matrix [K] and geometric stiffness matrix [S] considered from Eq.(2.19) of B-FGM beam and from Eq.(2.35) of isotropic and bio-inspired composite beam's can be written as,

$$\Big([\mathsf{K}] - \lambda_{\mathsf{B}}\mathsf{F}_0[\mathsf{S}]\Big)\{\Delta_{\mathsf{B}}\} = \{0\} \tag{2.36}$$

$'\lambda'$ is dimensionless critical buckling load, The dimensionless critical buckling load can be defined by:

$$\lambda = \frac{F_0 L^2}{E_1 b h^3} \tag{2.37}$$

Critical buckling load of the beam under six different VALs is obtained first. Then, free vibration frequencies of beam subjected to VALs are calculated considering the pre-stress effect caused by the in-plane load. The fundamental buckling mode is analyzed in order to quantify the influence of nature of variation of VAL on the buckling modes. The eigenvector associated with lowest eigenvalue is used for this purpose.

2.2.4 Free Vibration study

Similarly, ω, the natural frequencies are calculated from the below relation

$$\Big\{[\mathsf{K}] - \lambda_{\mathsf{B}}\mathsf{F}_0[\mathsf{S}] - \omega^2[\mathsf{M}]\Big\}\{\mathsf{q_i}\} = \{0\} \tag{2.38}$$

While, the dimensionless natural frequency is obtained by,

$$\Omega = \frac{\omega \mathsf{L}^2 \rho}{\mathsf{h}\sqrt{\mathsf{E}_1}} \tag{2.39}$$

Modal damping is the dissipation of energy in each mode of vibration. It is represented by the modal damping ratio ξ_i for mode i. The modal damping ratio

relates the imaginary part (damping) to the real part (frequency) of the complex modal frequency $\widetilde{\omega}_i = \omega + j\widetilde{\xi}_i$. The modal damping ratio ξ_i can be calculated using the formula:

$$\xi_i = \frac{\mathrm{Im}(\widetilde{\omega}_i)}{\mathrm{Re}(\widetilde{\omega}_i)} \tag{2.40}$$

where $\mathrm{Im}(\widetilde{\omega}_i)$ represents the imaginary part of the complex modal frequency and $\mathrm{Re}(\widetilde{\omega}_i)$ represents the real part.

2.2.5 Acoustic response study

In forced vibration analysis, the response of the beam to a time-varying harmonic point load ($F(t) = Fe^{i\omega t}$) is determined using modal superposition analysis. The eigenvalues obtained from the free vibration analysis are utilized as input in the modal superposition analysis. The resulting general equation of motion for the forced vibration response is derived as follows:

$$\mathsf{M}\ddot{\mathsf{X}} + \mathsf{C}\dot{\mathsf{X}} + (\mathsf{F_0}\mathsf{K^g})\mathsf{X} = \mathsf{F(t)} \tag{2.41}$$

Where, $\ddot{X}$ is acceleration, $\dot{X}$ is velocity and X is the displacement vector of the vibrating beam. By employing modal coordinates $\mathsf{y_k}$, where k=1,2,...,n, with n representing the total number of degrees of freedom, the axial compressive load F_0 is varied as a function of the critical buckling load (Pcr) specific to the analyzed case. The transformation from physical coordinates to modal coordinates is expressed as:

$$\{U\} = \sum_{\mathsf{k=1}}^{\mathsf{n}} \mathsf{\Phi_k y_k} = \mathsf{[\Phi]y} \tag{2.42}$$

In the above equation Φ_k is modal displacement with respect to eigenvalues ω_k and $[\Phi]$ is modal matrix. Hence, Eq.(2.42) can be written as,

$$\mathsf{M[\Phi]\ddot{y} + C[\Phi]\dot{y} + (F_0K^g)[\Phi]y = F(t)} \tag{2.43}$$

With orthogonality relations and pre multiplying Eq.(2.41) with $[\Phi]^T$, the Eq.(2.41) will be,

$$\ddot{\mathsf{y}}_\mathsf{k} + 2\omega\dot{\mathsf{y}}_\mathsf{k} + \omega_\mathsf{i}^2\mathsf{y}_\mathsf{k} = \mathsf{F}_\mathsf{k} \tag{2.44}$$

From Eq.(2.44), the forced vibration velocity response of the vibrating beam is determined. In continuation, the beam is assumed to be surrounded by an infinite baffle, as illustrated in Fig. 2.4. According to Rayleigh Integral, the

acoustic pressure radiated by the beam is given by:

$$p(r) = \frac{j\omega\rho_0}{2\pi}\int_S \dot{W}(r_s)\frac{e^{-jk|r-r_s|}}{|r-r_s|}dx \tag{2.45}$$

Here p(r) is pressure, $\omega(r)$ is surface velocity, k wave number, ρ_0 is fluid density and $|r-r_s|$ represents for the distance among the surface and field and S represents vibrating surface length. The sound intensity at a location r is,

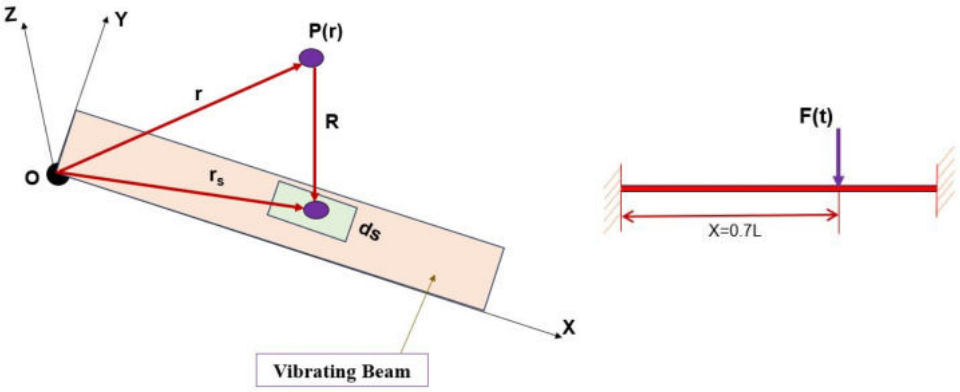

(a) Co-ordinates reference (b) Excitation location

Figure 2.4: Schematic diagram representing radiator co-ordinates and location

$$I(r) = \frac{1}{2}Re\big(p(r)\dot{w}^*(r_s)\big) \tag{2.46}$$

and the sound power radiated is

$$\bar{W} = \oint I(r)\, n(r_s)dx \tag{2.47}$$

here $n(r_s)$ is surface normal

$$\bar{W} = \frac{1}{2}Re\left(\oint p(r)\dot{W}^*(r)dx\right) \tag{2.48}$$

From the above equation, the sound power level can be determined by solving Eq.(2.49)

$$SWL = 10\log\frac{\bar{W}}{W_{ref}} \tag{2.49}$$

W_{ref} is reference sound power level, which is 10^{-12} Watts and the sound radiation efficiency (σ) can be obtained from,

$$\sigma = \frac{\bar{\mathsf{W}}}{\rho_0 \mathsf{C}_0 \mathsf{S} \left\langle \bar{\dot{\mathsf{W}}}^2 \right\rangle} \tag{2.50}$$

In the above equation, C_0 is speed of sound in m/s, $\left\langle \bar{\dot{W}}^2 \right\rangle = \dot{W}_n^H N \dot{W}_n$ and N=(1/2)NI. 'I' a unit matrix will be in respective size, N elements number used in discretization. $\dot{W}_n$ and $\dot{W}_n^H$ represents normal velocity with its conjugate velocity.

2.3 Validation studies

2.3.1 Validation of buckling load calculation

The buckling load calculation approach followed in the present work is validated by considering the work done by Karamanli *et al.* (2019a). As the results are not available for the B-FGM beam. The results of Karamanli *et al.* (2019a) for the isotropic beams under different boundary conditions simply supported (SS), clamped clamped (CC), clamped simply supported (CS) and clamped free (CF) and VALs are considered for this comparison study. An isotropic beam of length 1 m, with square cross section and L/h ratio of 50 is considered. The results of non-dimensional buckling load obtained using present study are presented along with results of Karamanli *et al.* (2019a) in Table 2.4. The percentage in error in Table 2.4 is found to be considerably less. While Karamanli *et al.* (2019a) focused on the buckling characteristics of isotropic and laminated composite beams, the present study advances this research by conducting a detailed analysis of buckling characteristics of isotropic, B-FGM and bio-inspired beams. These characteristics are analysed for variations in VALs, aspect ratios and boundary conditions.

2.3.2 Validation of natural frequency

B-FGM beam studied by Karamanli (2018) for the free vibration behaviour is considered for the validation of natural frequencies calculation method used present approach. Comparison of first three non-dimensionless frequencies of SS B-FGM beam obtained using present approach with the results reported by Karamanli (2018) is given in Table 2.5. For this comparison purpose P_x is kept constant at

Table 2.4: Comparison of buckling loads calculated using present method with Karmanli *et al.* (2019a) results

BC		F_x^1	F_x^2	F_x^3	F_x^4	F_x^5	F_x^6
	Karmanli *et al.* (2019)	18.55	15.34	23.21	14.14	26.64	18.33
SS	Present study	18.76	15.51	23.47	14.30	26.94	18.53
	Karmanli *et al.* (2019)	74.59	56.23	107.78	50.21	139.50	72.68
CC	Present study	75.42	56.86	108.97	50.77	141.04	73.51
	Karmanli *et al.* (2019)	7.85	5.13	16.14	4.23	27.35	8.73
CF	Present study	7.92	5.18	16.27	4.27	27.55	8.80

0.4 and P_z is varied from 0 to 1. The results from Table 2.5 illustrates that the present study results are in good agreement with the results reported by Karamanli (2018) study.

From the validation study of the natural frequency, it is clear that the methodology followed in present work can be extended for further studies on B-FGM beam. The current study further enhances with the Karamanli (2018) study by determining the effect of natural frequencies due to change in the material, aspect ratio, boundary condition and VAL.

Table 2.5: Comparison of dimensionless frequencies with Karamanli (2018) results.

		P_x					
Mode		0	0.2	0.4	0.6	0.8	1
	Karamanli (2018)	2.67	2.67	2.66	2.65	2.63	2.61
Ω_1	Present	2.69	2.68	2.68	2.67	2.65	2.63
	Karamanli (2018)	7.23	7.22	7.21	7.19	7.15	7.11
Ω_2	Present	7.23	7.23	7.22	7.21	7.19	7.16
	Karamanli (2018)	9.29	9.29	9.27	9.25	9.22	9.18
Ω_3	Present	9.46	9.45	9.44	9.42	9.39	9.35

2.3.3 Sound radiation validation

For validating the current investigation, the sound power level investigation by Zheng and Cai (2004) on an isotropic beam using Rayleigh's integral is considered. An aluminium beam subjected to SS boundary condition and having dimensions of $0.4 \times 0.03 \times 0.004$ m^3 is numerically analyzed. Fig.2.5 corresponds to the calculated sound power levels with the current and Zheng and Cai (2004) studies. From Fig.2.5 it is evident that the sound power levels determined with present approach is having a good agreement with that of Zheng and Cai (2004) results. With the validation it is obvious that current research could employed for further investigations. Building upon the validated isotropic beam study by Zheng and Cai (2004), the current investigation delves deeper into the acoustic characteristics. This includes a thorough analysis of parameters such as sound power level, radiation efficiency, and sound pressure level. The study specifically explores how variations in material properties, end conditions, VALs, and aspect ratios of beams influence these acoustic responses.

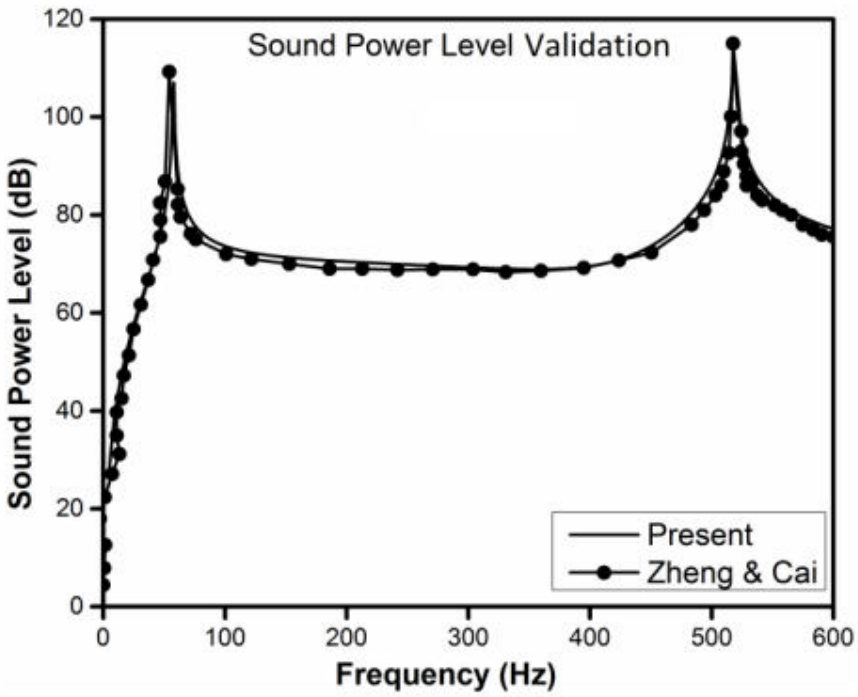

Figure 2.5: Comparison of sound power level with Zheng and Cai study

2.4 Closure

The procedural steps for evaluating the buckling, vibration, and acoustic responses of bi-directional functionally graded beam are elucidated in the flow chart presented in Fig. 2.6. The process initiates with the selection of the Variable Axial Load category, accomplished by adjusting the coefficients specified in Table 2.1 and referenced in Eq. 2.1. Subsequently, the application of Reddy's beam theorem, along with the incorporation of various coefficients pertaining to stiffness, inertia, and boundary conditions, forms the foundation for defining the Lagrange equations. In the context of determining the static and dynamic responses of B-FGM beams for variation in the material composition is carried out by increasing the length-wise (p_x) and thickness-wise (p_z) gradation indexes. The critical buckling loads are then determined by utilizing the structural stiffness matrix [K], the geometrical stiffness matrix [S], and the formulation presented in Eq. 2.36. To comprehensively explore the beam's behaviour, the buckling load intensity is varied as 0Pcr, 0.5Pcr, and 0.99*Pcr. Following this, careful examination on how the beam vibrates and produces sound is carried out. By using forced vibrations and Rayleigh integral, acoustic responses are calculated accurately. It helps in assessing on how the isotropic beam behaves when subjected to VALs and various end conditions.

In the determination of static and dynamic characteristics of isotropic beams, a similar procedure as described for B-FGM beams is adopted. Where, Reddy's beam theory is replaced with shear and normal deformation beam theory and the material composition is chosen isotropic instead of variations along length(p_x) and thickness (p_z) directions.

Similarly, with the methodology shown in Fig,2.6 and change in the material properties, lamination scheme from B-FGM to composite scheme the static bucking and dynamic characteristics of bio-inspired composite beams were also determined. The bio-inspired beams are chosen based on the lamination scheme unlike the B-FGM beams which are chosen based on gradation indexes. Each category of lamination scheme consists of unique scheme's for the 32 lay-ups. While, the effect of orientation of each lamination scheme on the static and dynamic responses is outlined in the overall study.

This chapter presented the methodology followed to depict the buckling, natural frequency and acoustic responses of various material beams. From there upon presented validation studies to demonstrate the accuracy of present approach in predicting various parameters. It is evident from the validation studies that the

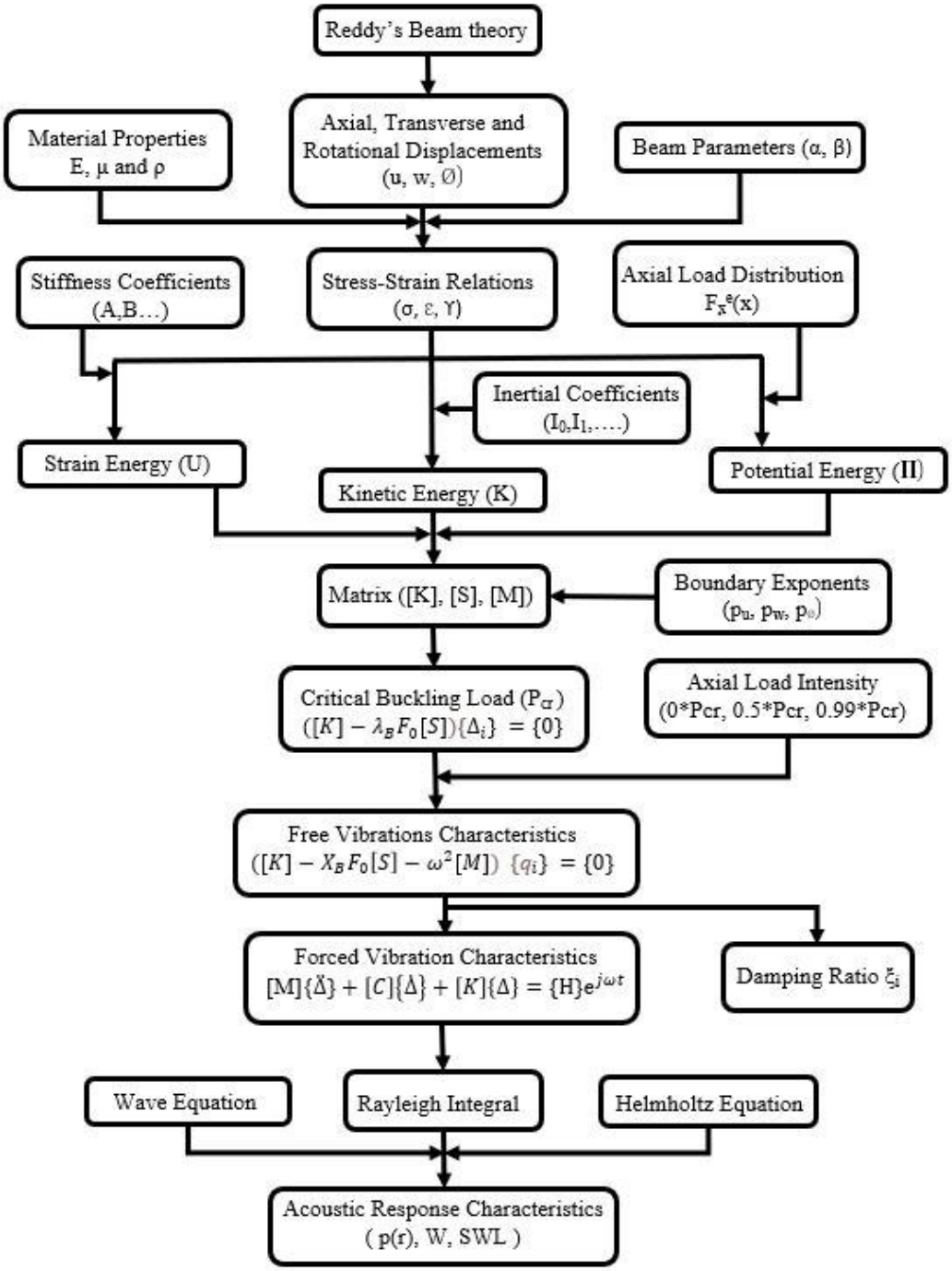

Figure 2.6: Detailed methodology for an isotropic beam

results obtained using present approach are in good agreement with the results reported in literature. Hence, from all the comparison studies it is very clear that the present study can be extended for analysing the buckling, vibration and acoustic characteristics of various material beams.

Chapter 3

STUDIES ON AN ISOTROPIC BEAM

3.1 Introduction

Vibro-acoustic response characteristics of an isotropic beam under various VALs, and boundary conditions is presented in this chapter. The study is presented for six types of VALs and under SS,CC and CF end conditions. To start with, the buckling loads are calculated first for each boundary condition under different VALs and the same are tabulated in Table 3.1. Then vibration and acoustic response studies are carried out at different intensities of the VAL by considering the pre-stress effect. An isotropic beam made of aluminium with cross section $b \times h$ and length(L) of 1 m is used in the study. The beam is having square cross section and aspect ratio (L/h=50) defines thickness of the beam and E=70 GPa; ν=0.3; ρ=2700 $\frac{kg}{m^3}$ are its material properties.

Table 3.1: Buckling loads (N) for various VALs

BC	F_x^1	F_x^2	F_x^3	F_x^4	F_x^5	F_x^6
SS	19050.38	15751.79	23842.64	14522.32	27368.42	18821.46
CC	77144.71	58115.54	111650.02	51881.54	144745.89	75190.83
CF	8083.92	5279.79	16639.04	4350.24	28221.40	8990.26

3.2 Buckling characteristics of isotropic beam

Table 3.1 depicts the effects on critical buckling loads with change in boundary conditions and VALs. As anticipated stiffness of the beams due to boundary condition is influencing the buckling strength. The difference between the critical buckling load values of SS and CF beams is marginal with SS beams having higher magnitudes than CF beams except for F_x^5 loading. The trend in the variation of critical buckling loads across VALs is same for all the three boundary conditions and is also depicting same with earlier reported studies (Karamanli 2019a) as well. The magnitude of buckling load from Table 3.1, highly influenced to the end conditions and type of VAL. As, high stiffness CC beams are dominating in buckling loads than compared with SS and CF beams. It can also be predicted from the results, that the variation in the buckling loads with end conditions is also stiffness dependent as, the variation is low between SS and CF beams and is high between CC and CF beams. The lowest and highest values

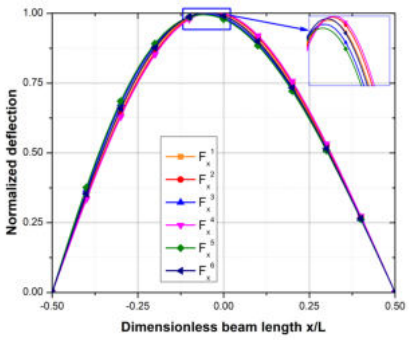

(a) SS

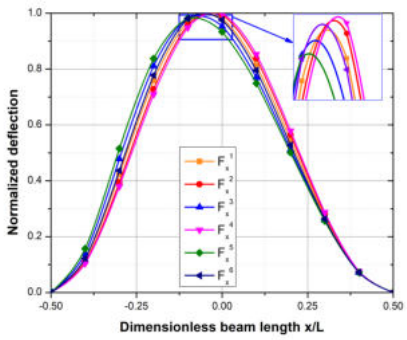

(b) CC

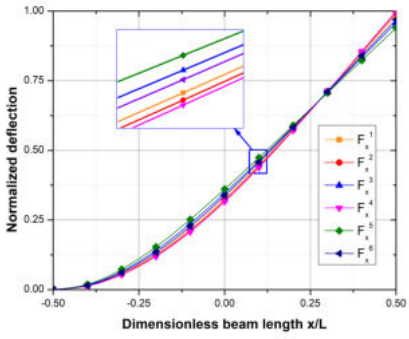

(c) CF

Figure 3.1: Effect of nature of VAL on fundamental buckling mode shape of various beams

in buckling load across each boundary condition is reporting to be for F_x^4 and F_x^5 axial loads respectively. In comparison to uniformly distributed load (F_x^1), the bell shaped (F_x^6) axially variable in-plane load is having lower critical buckling load value. From Table 3.1 it is evident that F_x^3 and F_x^5 load distribution reports higher critical buckling loads and F_x^2, F_x^4 and F_x^6 loads reporting relatively lower critical buckling loads. Hence, the nature of variation of VAL highly influences the buckling behaviour of the beam. F_x^4 loading is considered for Case-2 studies as the least critical buckling load is observed for this loading. Influence of nature of variation of VAL on the fundamental buckling mode shapes of the beam under different boundary conditions is not much seen as shown in Fig. 3.1.

3.3 Free vibration characteristics

Free vibration and acoustic response studies are carried out at different magnitudes of the axial load for the given type of VAL . This study is done in two different ways: in Case 1, the magnitude of the applied load is changed according to buckling load associated with the corresponding VAL load. In case 2, the applied load is changed according to least critical buckling load out of all the VALs. The case studies on the effect of varying critical buckling loads on natural frequency for the three different boundary conditions are plotted from Fig. 3.2 to Fig. 3.4. Each figure consists of two case study plots, variation of fundamental frequency under Case-1 loading as shown in plot (a), and variation of fundamental frequency under Case-2 loading as shown in plot (b).

Plots in Fig. 3.2 presents the effect on the fundamental frequency of SS beam due to increase in axial load intensity under different VALs. For Case 1, as the respective critical buckling load of each axial load is considered for the analysis, the variation of natural frequency under the given VAL is observed to be zero at their associated critical buckling load. This trend in natural frequency is also observed by other researchers in earlier studies. The difference in the trends of fundamental frequency for the two cases can be easily depicted from Fig. 3.2. As Fig. 3.3(b) is plotted by taking P_{cr} of F_x^4 load its corresponding fundamental frequency is observed to be zero at the P_{cr} and for the remaining load cases the natural frequencies are following a reducing trend with increase in the load without approaching to zero. Similarly, influence of type of VAL on fundamental mode of CC beam subjected to F_x^4 load case is presented in Fig. 3.5. The plots in Fig. 3.5 depicts marginal variation across the first three mode shapes with

variation in axial compression load.

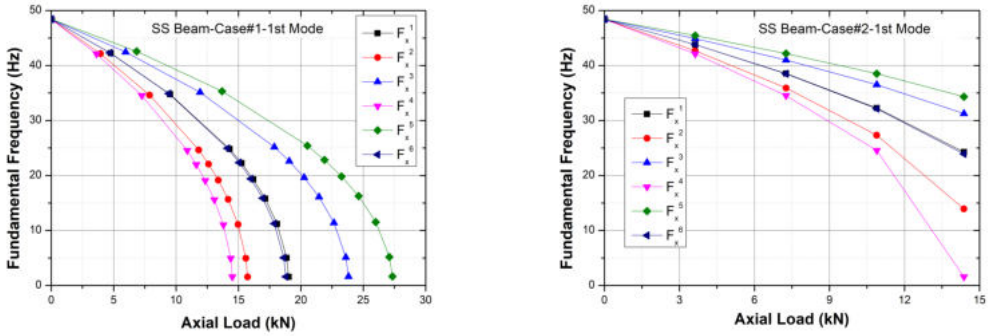

(a) Case 1 (b) Case 2

Figure 3.2: Influence of increase in axial load intensity on the fundamental frequency of SS beam

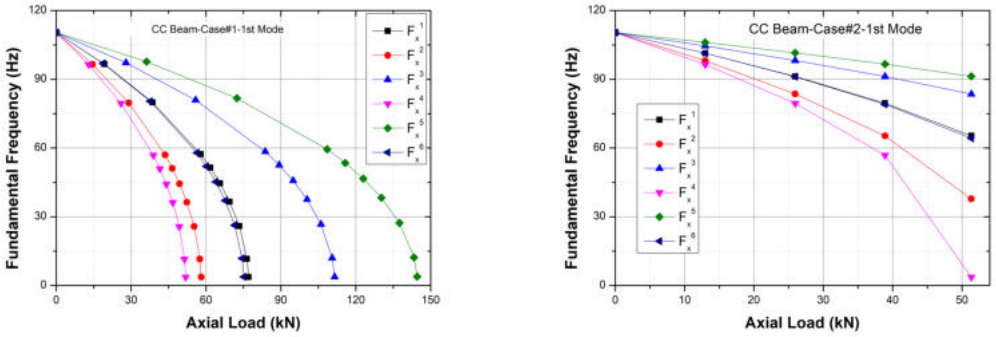

(a) Case 1 (b) Case 2

Figure 3.3: Influence of increase in axial load intensity on the fundamental frequency of CC beam

3.4 Acoustic response characteristics

3.4.1 Sound power level

Effect of variation in VAL intensity on acoustic response characteristics is investigated in this section. The beam is excited with 1 N of harmonic force in 0 to 1500 Hz frequency range. The acoustic response analysis in the present study is carried for the least critical buckling load (P_{cr}), which is observed for F_x^4 axial load. The effect of variation in VAL is determined by considering respective loadings

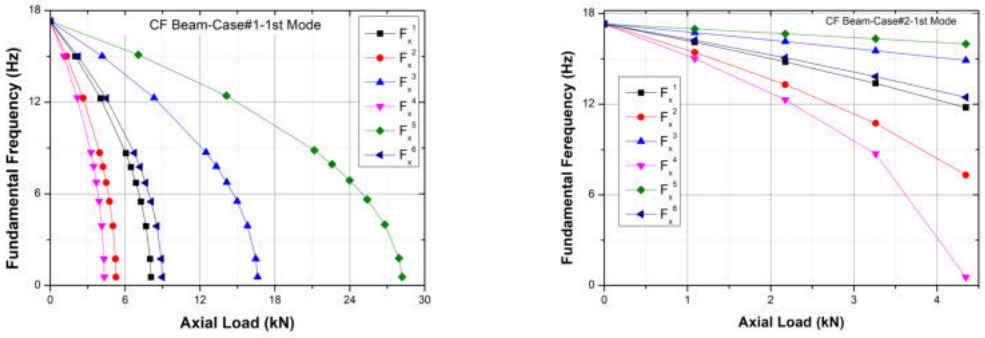

(a) Case 1 (b) Case 2

Figure 3.4: Influence of increase in axial load intensity on the fundamental frequency of CF beam

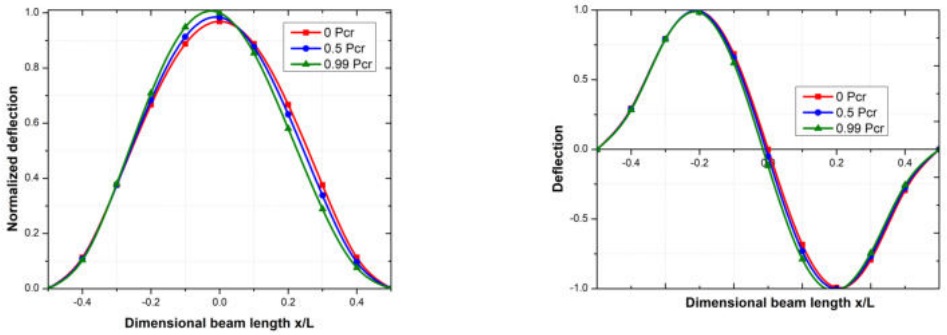

(a) 1^{st} Mode (b) 2^{nd} Mode

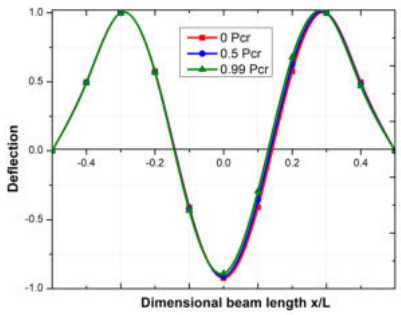

(c) 3^{rd} Mode

Figure 3.5: Influence of increase in axial load intensity on free vibration modes of CC beams under F_x^4 loading

in fraction of $0P_{cr}$, $0.5P_{cr}$ and $0.99P_{cr}$. The beam is excited at 0.7 m from the left extreme end of the beam so that the response of first few modes can be analyzed. Sound power level of the SS, CC and CF beams under F_x^4 and F_x^5 cases

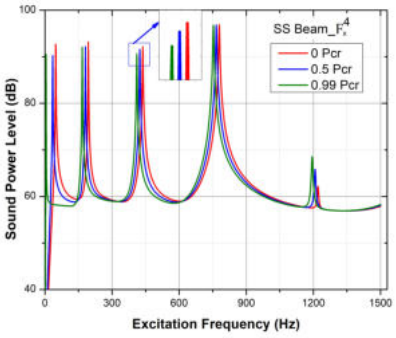

(a) SS Beam under F_x^4 loading

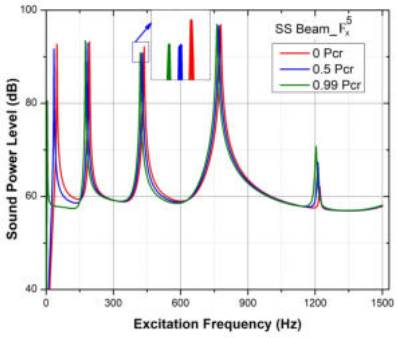

(b) SS Beam under F_x^5 loading

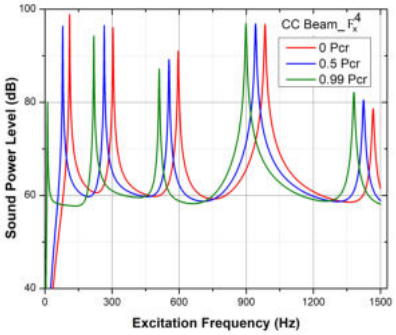

(c) CC Beam under F_x^4 loading

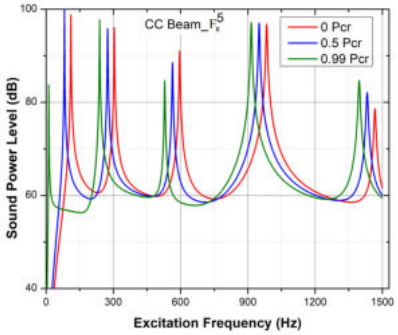

(d) CC Beam under F_x^5 loading

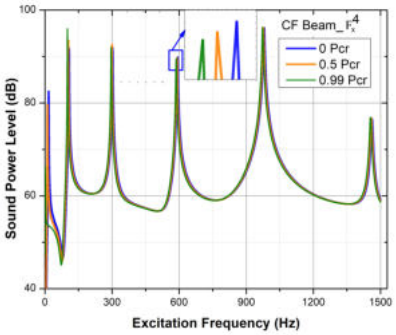

(e) CF Beam under F_x^4 loading

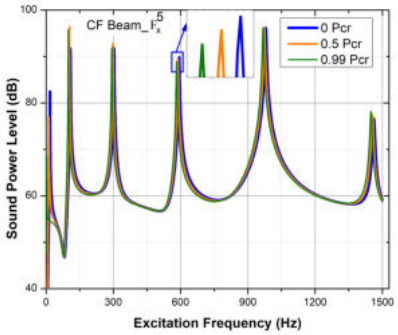

(f) CF Beam under F_x^5 loading

Figure 3.6: Effect of magnitude of VAL on sound power response

at different intensities of applied load, in terms of fractions of P_{cr} of the corresponding load case, is shown in Fig. 3.6. Due to the reduction in beam stiffness with rise in magnitude of applied load there is a decrease in natural frequencies of each mode. This shift in natural frequencies can be clearly seen for the CC beam compared to the other cases. Similarly, in most of the cases the resonant amplitudes of each mode reduces with rise in magnitude of VAL. This trend can

be clearly seen for the peak amplitudes of the fundamental mode. Basically, the reduction in beam stiffness should lead to increase in response amplitudes, but reverse trend is observed here. The sound power is a function of normal velocity which is a function of displacement amplitude and frequency. The reduction in natural frequency in turn reduced the velocity, which resulted in reduction of sound power radiated. However, the trend in variation of resonant amplitudes with rise in magnitude of VAL is reverse for the fifth mode which can be clearly seen for the CC beam. The shift in natural frequencies and variation in peaks with rise in the intensity of applied VAL are not clearly seen for SS beams (Fig. 3.6(a) and 3.6(b)) and CF beams (Fig. 3.6(e) and 3.6(f)). However, the variations in natural frequency and peaks are similar to the CC beams as seen in the sub-figures. The variation seems to be insignificant in the actual figure due to very low stiffness associated with the SS and CF beams. The resonant amplitude increases with rise in magnitude of the load for the fifth mode. Influence of rise in magnitude of the load and boundary condition is negligible on sound radiation efficiency of the beams as shown in Fig. 3.7. This indicates that the radiation efficiency is not sensitive to increase in axial load intensity. The results of SS, CC and CF beams under F_x^4 loading of Fig. 3.6 are presented as constant octave bands in Fig. 3.8. Fig. 3.8 charts depicts the effect of increase in axial load is following non-uniformity trend for increase in octave band frequencies. Increase in the amplitude is due to the association of natural frequency in that respective loading fraction. From the charts, it is evident that more the stiffness of the beam more will be the variation in the natural frequency and more is the variation in the SWL in the octave bands. The overall SWL for increase in loading fraction for SS, CC and CF beams is plotted in Fig. 3.9. Fig. 3.9 depicts that with increase in axial load there is a decrease in the overall SWL amplitudes for SS and CC beams. For CF beams the trend is uniform from $0P_{cr}$ to $0.5P_{cr}$ axial load and response increases marginally when the axial load varied from $0.5P_{cr}$ to $0.99P_{cr}$ axial load.

3.4.2 Directivity pattern

The sound pressure level (SPL) radiated from the beams is represented as contour plots in Table 3.2 upto a distance of 1.5m above the beam. Contour plots shown in Table 3.2 are plotted across the distances along length and thickness directions of the beam. For the cases when the beam is excited at the fundamental frequency corresponds to the axial load intensity. Plots in Table 3.2 are plotted for funda-

Table 3.2: Contour representation of effect of increase in axial load intensity on sound pressure level for fundamental mode of SS and CF boundary conditions

P_{cr}	SS	CF
0	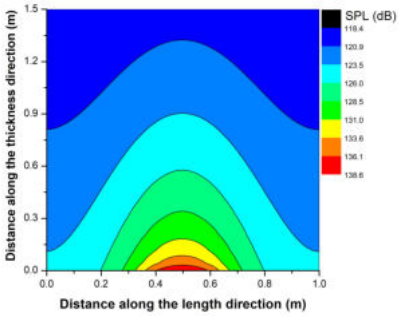	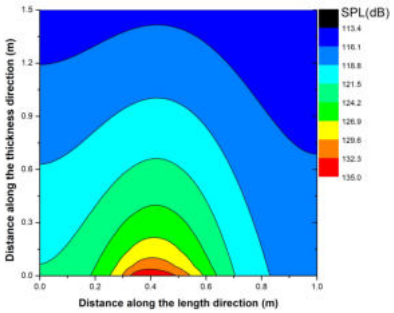
0.5	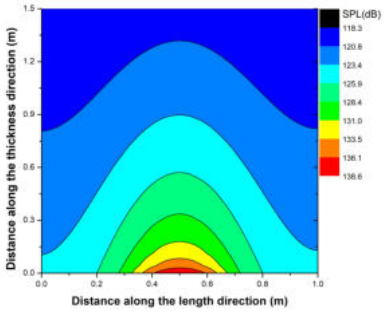	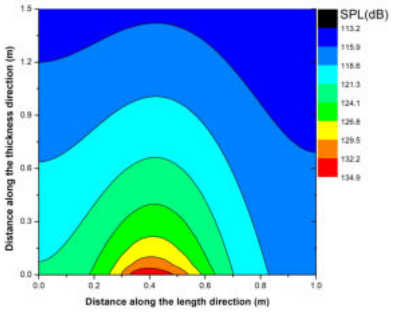
0.99	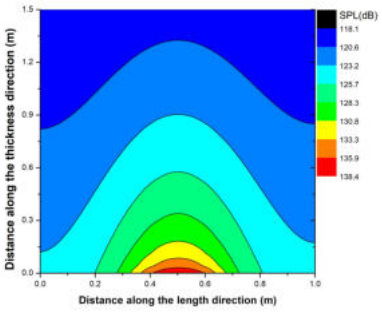	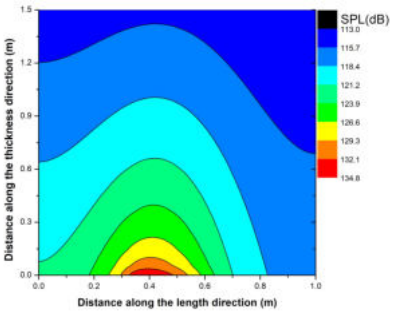

mental mode of SS and CF beams for increase in axial load intensity. Similarly, contour plots for fundamental mode of CC beams are represented in Table 3.3. As anticipated, the structural stiffness influenced the SPL, which is observed to be significant for CC beams than compared to SS and CF beams. The shift of sound radiation pattern in CF beams is due to the variation in edge stiffness of the beam. For SS and CC beams sound radiation is observed to be symmetric about the center due to their equal edge stiffness. Effect of axial load intensity on SPL is found to be less significant for all the beams for the fundamental frequency excitation. From the plots, it is evident that with increase in compression

Table 3.3: Contour representation of effect of increase in axial load intensity on sound pressure level for first and fifth mode of CC boundary condition

P_{cr}	1^{st}Mode	5^{th}Mode
0	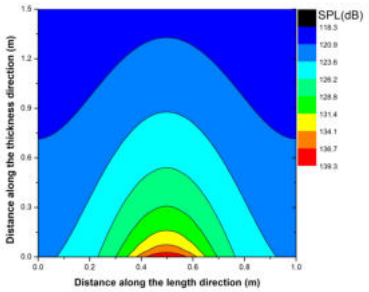	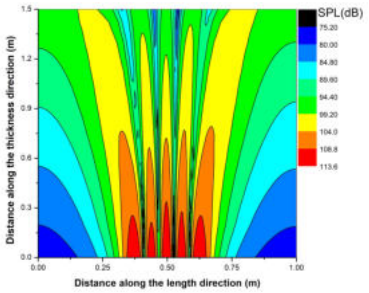
0.5	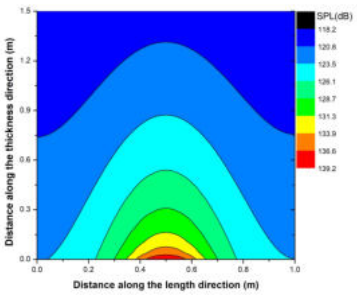	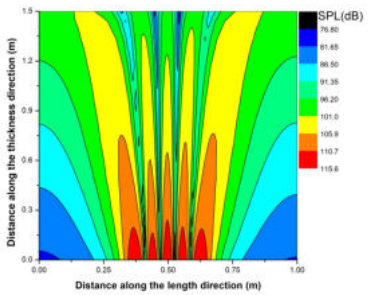
0.99	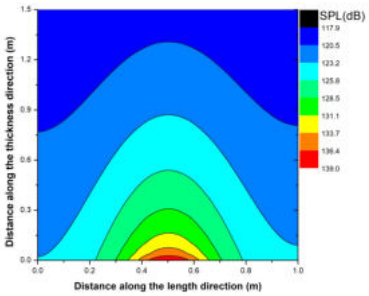	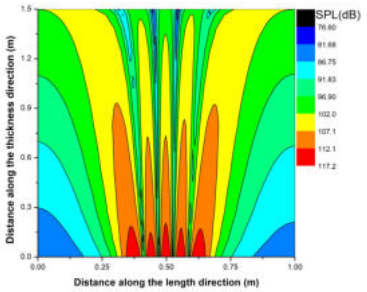

load there is marginal decrement in intensity of sound radiation. The marginal decrement is found to be of the same trend of SWL plotted in Fig. 3.6. To have better understanding in the behaviour of the beams for higher order modes, CC beam under F_x^4 axial loading is analyzed for varying loading fraction. From the contour plots of fifth mode (Table 3.3) SWL plots in Fig.3.6, it is evident that with increase in axial load intensity there is a increase in sound radiation. The SPL directivity pattern at a distance of 1 m from the beam is studied for the three beams and is presented in Fig. 3.10. Fig. 3.10(a), Fig. 3.10(c) and Fig. 3.10(e) for fundamental mode of SS, CC and CF beams respectively. The variation in SPL with increase in loading fraction is marginal for the fundamental

mode of the three beams. From these plots it is evident that with increase in axial compression load the SPL is partially reducing. The plots in Fig. 3.10(b), Fig. 3.10(d) and Fig. 3.10(f) depicts the effect of loading fraction on third mode. The effect of loading fraction in directivity pattern is more significant in third modes of SS and CC beams compared to CF beams.

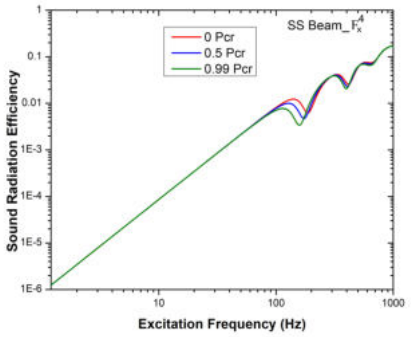

(a) SS Beam under F_x^4 loading

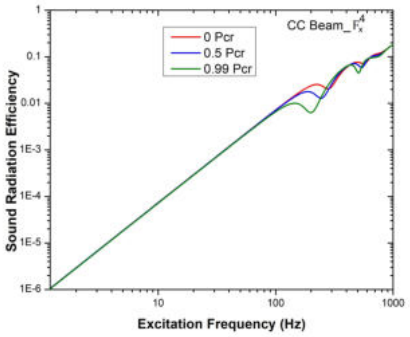

(b) CC Beam under F_x^4 loading

Figure 3.7: Effect of axial load intensity on sound radiation efficiency

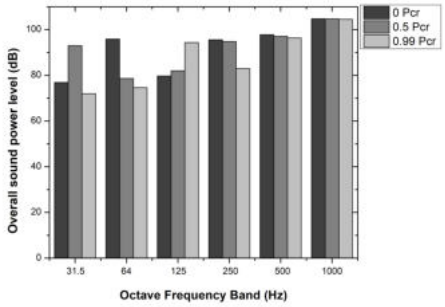

(a) SS Beam under F_x^4 loading

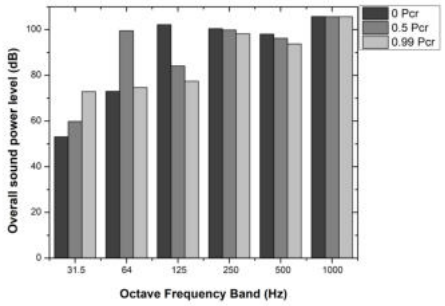

(b) CC Beam under F_x^4 loading

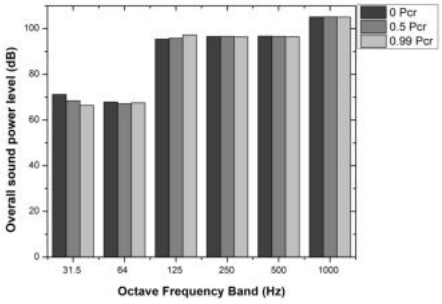

(c) CF Beam under F_x^5 loading

Figure 3.8: Effect of axial load intensity on band wise sound power level

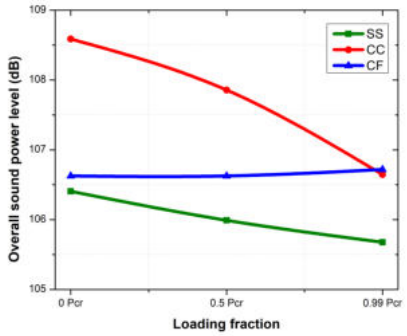

Figure 3.9: Effect of increase in F_x^4 axial load intensity on overall sound power

3.5 Closure

An aluminium beam subjected to various boundary conditions and different types of variable axial loads is investigated for static buckling and dynamic responses. The overall study highlights the influence of variable axial loads for different beams (SS, CC, & CF) on the buckling, vibration and acoustic responses. Buckling load values for variation in the nature of VALs across the three boundary conditions are tabulated. Natural frequencies for different types of VALs and boundary conditions are calculated. A distinctive study in predicting the natural frequencies is carried out by varying the axial load intensity from 0 to its critical value. Sound power levels are presented in the selected frequency band and in octave bands as well. Sound pressure levels are presented as directivity pattern and in contour plot representation. The detailed analysis highly correlates with earlier studies, as the nature of variation in the buckling load for various beams subjected to VALs found to be coincidental in trend. The critical buckling load is higher for exponentially decreasing load, lower for exponentially increasing type of VAL. The trend in the variation of natural frequency for an increase in the axial load intensity from 0 to buckling load is analyzed. It is also observed that the acoustic responses are greatly affected by the nature of VAL. The variation in the sound power level is found to be more in lower frequency bands. From the sound radiation efficiency plots one can depict that the effect of type of VAL and boundary conditions does not have any significant influence.

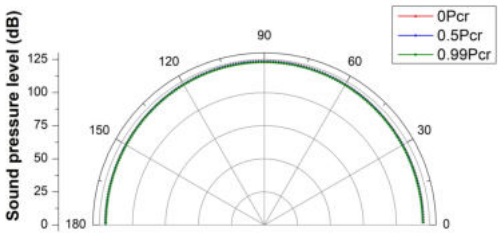

(a) For SS Beam under F_x^4 loading

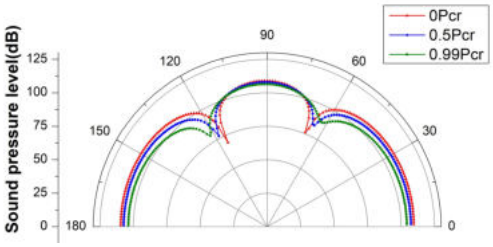

(b) Third mode of SS Beam under F_x^4 loading

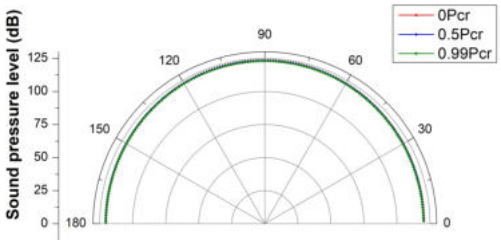

(c) For CC Beam under F_x^4 loading

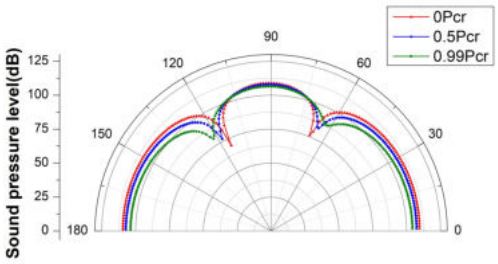

(d) Third mode of CC Beam under F_x^4 loading

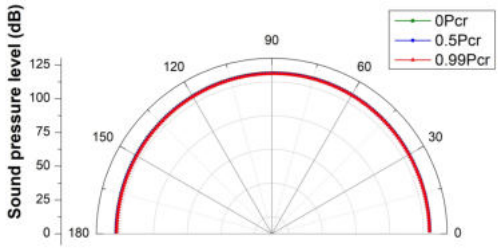

(e) For CF Beam under F_x^4 loading

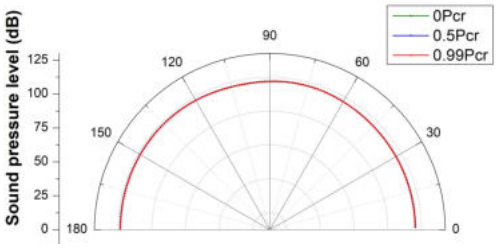

(f) Third mode of CF Beam under F_x^4 loading

Figure 3.10: Effect of increase in axial load intensity on directivity pattern

Chapter 4

BUCKLING AND FREE VIBRATION STUDIES ON B-FGM BEAM

4.1 Introduction

Numerical simulation studies carried out on the bi-directional functionally graded material (B-FGM) beam to analyze the buckling and free vibration behaviour under the influence of variable axial load is presented in this chapter. Detailed parameter study is carried out to analyze the effect of material gradation indexes as, end conditions, aspect ratios (L/h), and type of variable axial load. For this purpose, six different types of VALs, four different end conditions (SS, CC, CS, and CF), two aspect ratios thick (L/h=5) & thin(L/h=20), and gradation indexes to account for material property variation along x and z directions were considered. Fig. 2.3 illustrates the different types of VALs namely, F_x^1-uniformly distributed, F_x^2-linearly increasing, F_x^3-linearly decreasing, F_x^4-quadratically increasing, F_x^5-quadratically decreasing and F_x^6-parabolic in nature. The non-dimensional form of buckling loads and natural frequencies as per Eq.2.37 and Eq.2.39 respectively are used in the following sections. A B-FGM beam of length 1 m with square cross-section are $b \times h$ is used in the study and the height of the beam is defined with respect to the given aspect ratio L/h. The material properties of the B-FGM beam are $E_m = 210\ GPa$; μ_m=0.3; ρ_m=2700 $\frac{kg}{m^3}$. Detailed investigation carried out on various outlined parameters is presented in below individual sections.

4.2 Buckling behaviour of B-FGM beam

The current section details the influence of various parameters on dimensionless buckling load (BL, λ) and buckling mode shape.

4.2.1 Influence of type of VAL

Tables 4.1 & 4.2 along with Fig.4.1 illustrates the influence of type of VALs on the buckling strength of the B-FGM beam with different gradation indexes along with the length and thickness directions of the beam. The same phenomenon as noted in the homogenous beam condition is also opined in the B-FGM as well. The highest and least dimensionless BLs are observed for F_x^5 *and* F_x^4 axial loads respectively. Decreasing nature (F_x^3 *and* F_x^5) axial loads are depicting higher buckling loads compared to other types of axial loads (F_x^1, F_x^2, F_x^4, *and* F_x^6). It is also observed that the parabolic loading (F_x^6) is showing less influence on dimensionless BLs compared to uniformly distributed loading ($\mathsf{F}_{\mathsf{x}}^{\mathsf{1}}$). For the cases other than CF, the beam has less stiffness as its center. In F_x^6 load case, the maximum load also acts at the center of the beam which leads to least buckling load for F_x^6 load case. The nature of VAL on the buckling load is more influential when there is a change in aspect ratio and end condition as well. Due to the significant variation in the stiffness of the B-FGM beam due to the variation in the gradation indexes there is a considerable variation in the dimensionless buckling loads. From Fig.4.1, it is observed that for all the axial load cases there is a proportional increment in the dimensionless buckling loads with an increase in the gradation index P_z. Furthermore, F_x^3 *and* F_x^5 VALs are showing quadratically increasing in nature of buckling strength compared to the other VALs.

4.2.2 Influence of gradation indexes

Based on the study carried out in the previous section, four types of VALs such as F_x^1, F_x^4, F_x^5 and F_x^6 are chosen for the study on the influence of gradation indexes on the dimensionless BLs of B-FGM beams. The results are shown in Fig.4.2. The beam with both the gradation index coefficients set at '0' is an isotropic beam and set at the highest value '1' is a rich B-FGM beam. It is evident that with a linear increase in the gradation index there is a linear increase in the buckling strength of the structure as presented in Tables 4.1 & 4.2. Hence, the study depicts that the buckling strength of a B-FGM beam is higher compared to an isotropic beam. The linear increment in dimensionless BLs was observed for both the gradation indexes

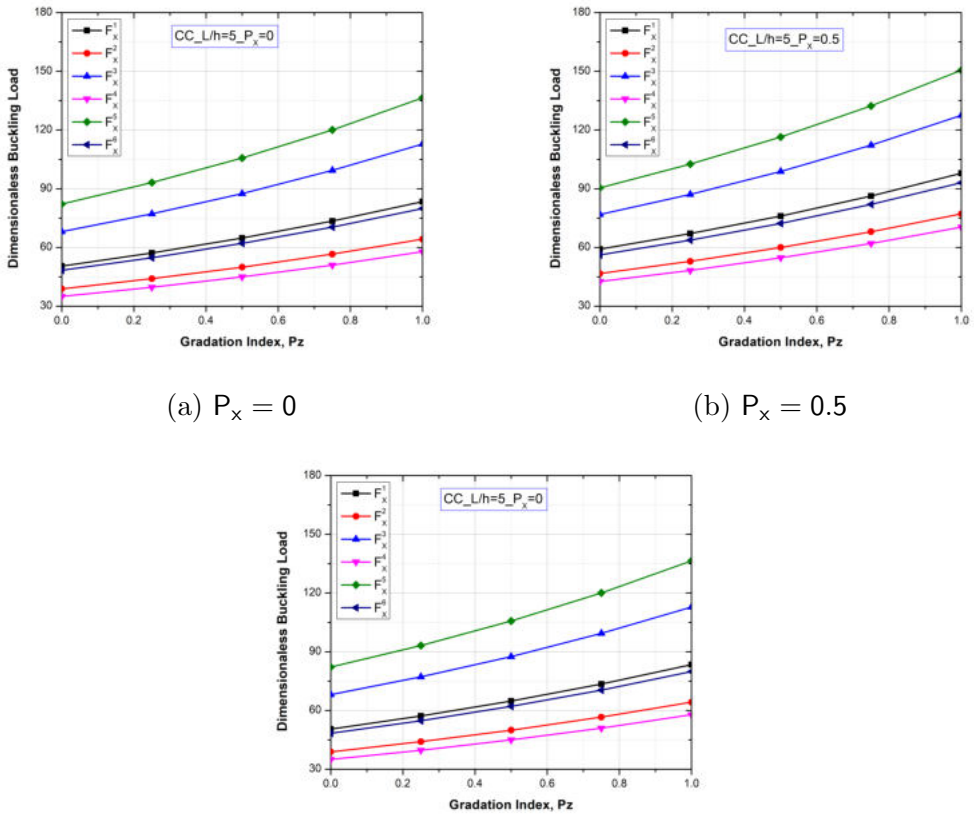

(a) $\mathsf{P_x} = 0$ (b) $\mathsf{P_x} = 0.5$

(c) $\mathsf{P_x} = 1$

Figure 4.1: Influence of VALs on dimensionless BL of CC B-FGM beam for L/h=5 and for various gradation indexes of $\mathsf{P_x}$

across all VALs. In comparison, the thickness-wise increment in the gradation index (P_z) predicted higher dimensionless BLs compared to the increment in the lengthwise gradation index (P_x). It is due to the predominant increase in the bending stiffness along the thickness direction, enhancing the B-FGM beam's buckling strength. As presented in Fig.4.2, the influence of gradation indexes on dimensionless buckling loads of B-FGM beams shows the same trend irrespective of the type of VAL. F_x^5 type of VAL yields a higher dimensionless buckling load than other types of VALs. The plots also ensures the earliest observation about the effect of gradation index on the dimensionless buckling load i.e., the effect is significant for gradation along the thickness direction compared to the length direction.

Table 4.1: Influences of VALs, gradation indexes and aspect ratios on dimensionless BLs of CC & SS B-FGM beams

BC	VAL	P_z	L/h=5					L/h=20				
			P_x					P_x				
			0	0.25	0.5	0.75	1	0	0.25	0.5	0.75	1
CC	F_x^1	0	50.45	54.74	59.17	63.72	68.35	72.53	79.75	87.56	95.98	105.04
		0.25	57.17	62.04	67.06	72.22	77.48	82.14	90.33	99.17	108.70	118.97
		0.5	64.82	70.34	76.05	81.91	87.88	92.95	102.21	112.21	123.00	134.62
		0.75	73.52	79.79	86.28	92.94	99.74	105.07	115.55	126.86	139.06	152.19
		1	83.41	90.54	97.93	105.52	113.28	118.69	130.52	143.30	157.08	171.92
	F_x^2	0	38.86	42.67	46.68	50.87	55.23	54.76	60.68	67.13	74.13	81.73
		0.25	44.04	48.36	52.90	57.66	62.60	62.02	68.72	76.03	83.96	92.56
		0.5	49.93	54.82	59.98	65.37	70.98	70.17	77.76	86.02	95.00	104.74
		0.75	56.61	62.17	68.02	74.15	80.53	79.33	87.91	97.25	107.40	118.41
		1	64.21	70.52	77.18	84.15	91.41	89.61	99.30	109.85	121.32	133.75
	F_x^3	0	68.09	72.45	76.84	81.23	85.57	104.30	113.16	122.63	132.75	143.54
		0.25	77.18	82.13	87.11	92.09	97.02	118.14	128.17	138.90	150.35	162.58
		0.5	87.54	93.16	98.83	104.49	110.11	133.68	145.03	157.17	170.14	183.97
		0.75	99.35	105.76	112.22	118.68	125.10	151.13	163.97	177.69	192.36	208.00
		1	112.82	120.14	127.52	134.92	142.27	170.72	185.22	200.74	217.31	234.99
SS	F_x^1	0	16.48	18.10	19.82	21.62	23.50	18.42	20.35	22.41	24.62	26.97
		0.25	18.66	20.51	22.45	24.49	26.62	20.87	23.05	25.38	27.88	30.55
		0.5	21.13	23.22	25.42	27.73	30.14	23.61	26.07	28.72	31.55	34.56
		0.75	23.91	26.27	28.76	31.38	34.12	26.68	29.47	32.46	35.66	39.07
		1	27.04	29.71	32.53	35.50	38.60	30.13	33.28	36.65	40.27	44.12
	F_x^2	0	13.71	15.15	16.68	18.30	20.01	15.24	16.91	18.71	20.64	22.71
		0.25	15.53	17.16	18.90	20.73	22.67	17.26	19.15	21.19	23.38	25.73
		0.5	17.58	19.43	21.40	23.48	25.67	19.53	21.67	23.97	26.45	29.11
		0.75	19.89	21.99	24.21	26.56	29.04	22.07	24.49	27.09	29.90	32.90
		1	22.49	24.86	27.38	30.05	32.85	24.92	27.65	30.60	33.76	37.15
	F_x^3	0	20.30	22.12	24.02	26.00	28.05	23.03	25.27	27.66	30.20	32.89
		0.25	23.00	25.06	27.21	29.46	31.78	26.09	28.62	31.33	34.20	37.25
		0.5	26.04	28.37	30.82	33.36	35.99	29.51	32.38	35.44	38.69	42.14
		0.75	29.46	32.11	34.88	37.76	40.74	33.36	36.60	40.06	43.74	47.63
		1	33.33	36.33	39.46	42.73	46.11	37.67	41.33	45.24	49.39	53.79

4.2.3 Influence of aspect ratios

In connection to the above sections, the influence of aspect ratios, i.e., for thin beam (L/h=5) and thick beam (L/h=20) on dimensionless BLs is studied for three distinctive gradation indexes of P_x. As seen in Fig.4.3, it is observed that with an increase in the gradation index, there is a substantial increase in the dimensionless BLs of the B-FGM beams. It is also found that the buckling strength is marginally varying for aspect ratio L/h=20 as compared to thick

Table 4.2: Influences of VALs, gradation indexes and aspect ratios on dimensionless BLs of CS & CF B-FGM beams

BC	VAL	P_z	L/h=5					L/h=20				
			P_x					P_x				
			0	0.25	0.5	0.75	1	0	0.25	0.5	0.75	1
CS	F_x^4	0	26.62	29.29	32.11	35.08	38.19	33.53	37.07	40.89	45.00	49.43
		0.25	30.16	33.18	36.38	39.75	43.28	37.98	41.98	46.31	50.97	55.98
		0.5	34.17	37.59	41.22	45.04	49.04	42.97	47.50	52.39	57.67	63.34
		0.75	38.71	42.59	46.70	51.03	55.56	48.57	53.69	59.22	65.19	71.60
		1	43.85	48.25	52.91	57.82	62.97	54.86	60.64	66.89	73.63	80.87
	F_x^5	0	70.03	73.67	77.30	80.92	84.49	101.30	108.34	115.74	123.52	131.66
		0.25	79.38	83.50	87.62	91.72	95.78	114.73	122.70	131.09	139.90	149.12
		0.5	90.01	94.70	99.38	104.05	108.67	129.82	138.84	148.33	158.30	168.74
		0.75	102.12	107.46	112.80	118.12	123.40	146.75	156.96	167.69	178.96	190.76
		1	115.92	122.01	128.11	134.20	140.24	165.76	177.29	189.42	202.15	215.49
	F_x^6	0	39.01	42.07	45.23	48.50	51.86	51.27	55.79	60.60	65.73	71.17
		0.25	44.21	47.67	51.26	54.97	58.77	58.07	63.18	68.64	74.44	80.61
		0.5	50.10	54.02	58.10	62.30	66.62	65.71	71.49	77.66	84.23	91.20
		0.75	56.78	61.23	65.85	70.63	75.54	74.27	80.81	87.79	95.21	103.10
		1	64.35	69.41	74.66	80.09	85.67	83.89	91.27	99.15	107.54	116.45
CF	F_x^4	0	4.09	4.34	4.61	4.87	5.14	4.21	4.47	4.73	5.00	5.27
		0.25	4.63	4.92	5.22	5.52	5.82	4.77	5.06	5.36	5.66	5.96
		0.5	5.24	5.57	5.90	6.24	6.59	5.40	5.73	6.06	6.40	6.75
		0.75	5.92	6.29	6.67	7.06	7.45	6.10	6.47	6.85	7.23	7.62
		1	6.69	7.11	7.54	7.97	8.41	6.89	7.31	7.73	8.17	8.61
	F_x^5	0	24.87	25.73	26.59	27.45	28.32	27.10	28.00	28.91	29.83	30.74
		0.25	28.17	29.14	30.11	31.09	32.08	30.69	31.72	32.75	33.78	34.82
		0.5	31.89	32.99	34.09	35.20	36.31	34.72	35.88	37.05	38.22	39.39
		0.75	36.07	37.31	38.56	39.81	41.07	39.25	40.56	41.87	43.19	44.52
		1	40.78	42.19	43.60	45.01	46.43	44.32	45.80	47.28	48.78	50.27
	F_x^6	0	8.29	8.70	9.10	9.51	9.93	8.68	9.09	9.50	9.91	10.33
		0.25	9.39	9.85	10.31	10.77	11.24	9.83	10.29	10.76	11.23	11.70
		0.5	10.63	11.15	11.67	12.19	12.72	11.12	11.64	12.17	12.70	13.24
		0.75	12.02	12.60	13.19	13.78	14.39	12.57	13.16	13.75	14.36	14.96
		1	13.58	14.24	14.90	15.57	16.25	14.20	14.86	15.53	16.21	16.90

beam for an increment in gradation index P_x. Calculated values of buckling strength for both the aspect ratios are quadratically increasing with an increase in the gradation index P_z. Dimensionless buckling loads presented in Tables 4.1 & 4.2 also illustrate the difference between thick (L/h=5) and thin (L/h=20) B-FGM beams because of the non-dimension form representation. The calculated values are showing that the effect of aspect ratio on dimensionless BLs is high for F_x^5 VAL, medium for F_x^1 VAL, and less for F_x^4 VAL. As anticipated thin beams

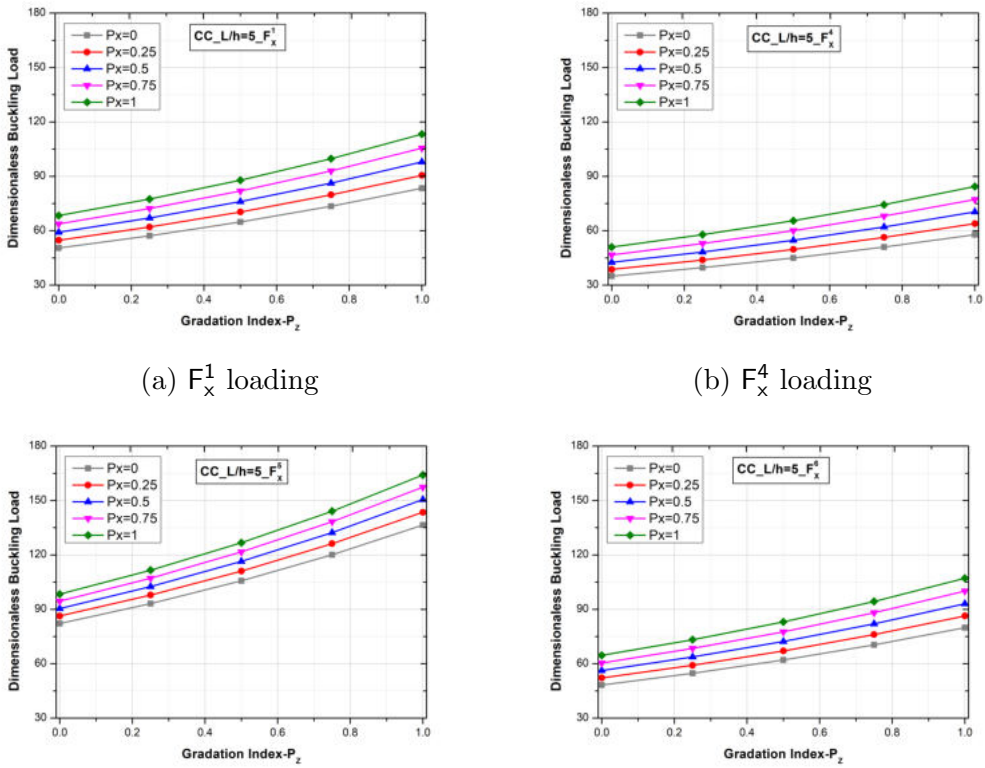

(a) $\mathsf{F}_{\mathsf{x}}^{\mathsf{1}}$ loading

(b) $\mathsf{F}_{\mathsf{x}}^{\mathsf{4}}$ loading

(c) $\mathsf{F}_{\mathsf{x}}^{\mathsf{5}}$ loading

(d) $\mathsf{F}_{\mathsf{x}}^{\mathsf{6}}$ loading

Figure 4.2: Influence of gradation index on dimensionless BL of CC B-FGM beam with aspect ratio L/h=5

are predicted higher dimensionless buckling loads than thick beams because of the non-dimension from representation.

4.2.4 Influence of end conditions

In continuation with earlier studies, the effect of end conditions on dimensionless BLs is carried out for three specific cases of gradation coefficient P_x along with an increment in the gradation index P_z. The dominance of the end conditions over other parameters is due to the influence of end stiffness on the B-FGM beams. In the current study, the different types of end conditions used are fixed, simply supported, and the free end. The degree of constraint is high for fixed support followed by simply support and negligible at the free end, since the stiffness provided by the support will be higher for the fixed end followed for simply supported-end and negligible at the free end. Due to this reason, the B-FGM beams with changed edges will have higher dimensionless BLs. Among the four end conditions analyzed the dimensionless buckling loads are higher for CC and

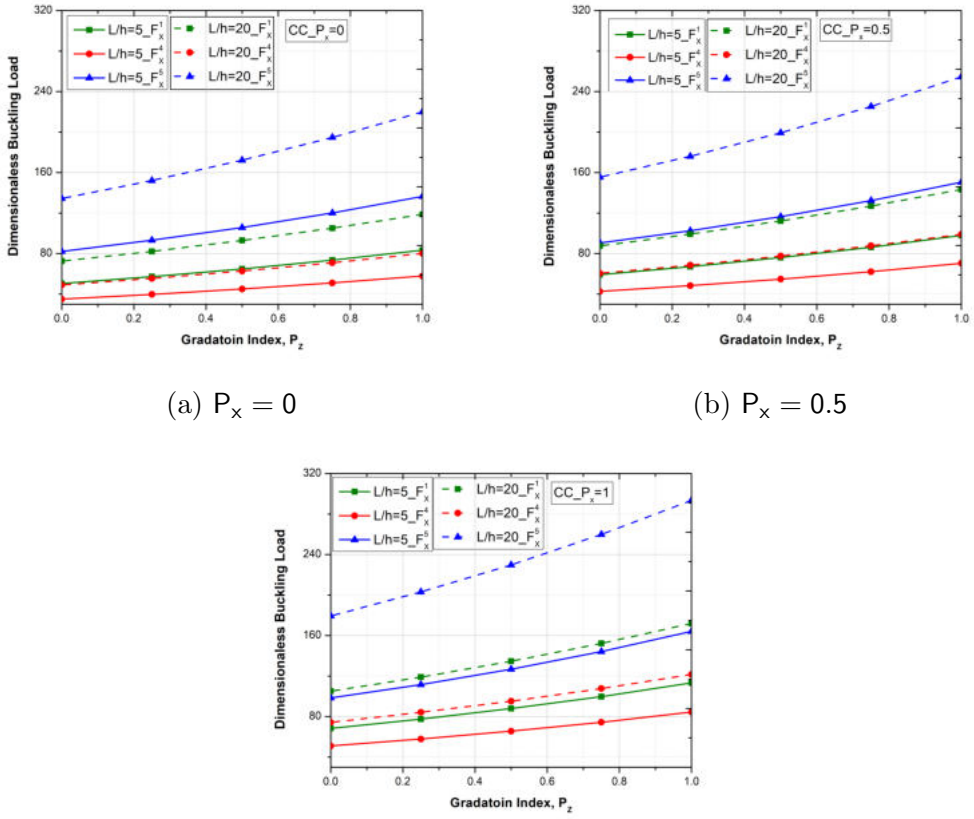

(a) $\mathsf{P_x} = 0$ (b) $\mathsf{P_x} = 0.5$

(c) $\mathsf{P_x} = 1$

Figure 4.3: Influence of aspect ratio on dimensionless BL of CC B-FGM beam subjected to various VALs and for various gradation indexes of $\mathsf{P_x}$

less for CF B-FGM beams. Even the curves for the four end conditions presented in Fig.4.4 reveal that B-FGM beams with higher-end stiffness are having quadratic increment while low stiffness beams are having linear increment linearly. Sub-plots from Fig.4.4 reveal that there is a distinctive characteristic for SS and CF beams. For P_x=0, dimensionless BLs of CF B-FGM beams are higher than SS B-FGM beams, but for the remaining two cases (P_x=0.5 & 1) the values of SS B-FGM beams are of higher than CF B-FGM beams. This particular case reveals the significance of variation of stiffness on the gradation of metals on the end conditions of the B-FGM beams. As the richness of gradation is improving in P_x=0.5 and P_x=1 cases, SS beams which are less influential than CF beams are having higher dimensionless BLs. From Tables 4.1 & 4.2 one can observe that dimensionless buckling loads are highly sensitive to end conditions compared to other parameters in the study.

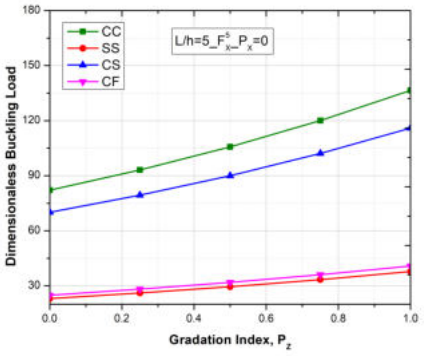

(a) $P_x = 0$

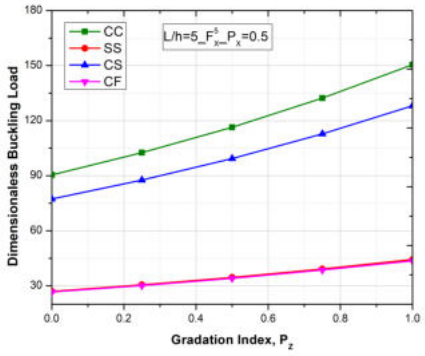

(b) $P_x = 0.5$

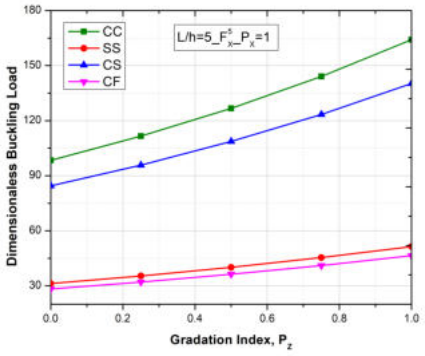

(c) $P_x = 1$

Figure 4.4: Influence of end conditions on dimensionless BL subjected to F_x^5 VAL and for various gradation indexes of P_x

4.2.5 Analysis on buckling mode shape

Influences of nature of VALs, aspect ratios, gradation indexes, and end conditions on the fundamental buckling mode shape are detailed in this section. The corresponding results are shown in Fig.4.5 & 4.6. There is a noticeable variation in the buckling mode shape of B-FGM beams due to the effect of the nature of VALs as seen in Fig.4.5(a) & 4.5(b). The effect of VALs on buckling mode shape is observed to be more for thick CC B-FGM beams. However, from Fig.4.5(c) & 4.5(d), the effect of end conditions and aspect ratios on the buckling mode of B-FGM beams is found to be negligible when they are subjected to the same type of VAL. Hence, from Fig.4.5, one can depict that the buckling mode shape is sensitive to the nature of VALs compared to end conditions and aspect ratios. Similarly, to comprehend the effect of gradation index on the buckling mode shape of B-FGM beams three case studies were carried out and results are shown

in Fig.4.6. Fig.4.6(a) & 4.6(b) are plotted for variation in the buckling mode shape with variation in gradation index along z and x directions respectively. From these two plots, it is apparent that the influence of gradation index on buckling mode shape is significant for P_z compared to P_x. From Fig.4.6, one can predict that the isotropic beams are having highest deflection in buckling mode compared to B-FGM beams.

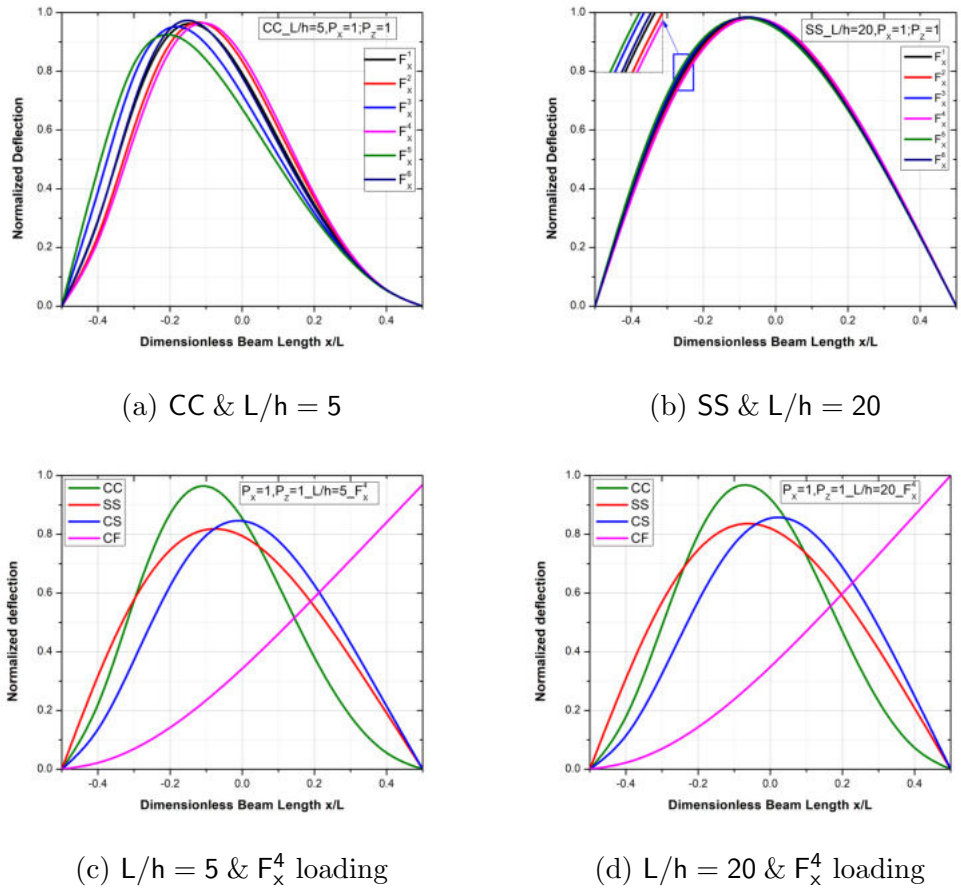

(a) CC & L/h = 5

(b) SS & L/h = 20

(c) L/h = 5 & F_x^4 loading

(d) L/h = 20 & F_x^4 loading

Figure 4.5: Influence of VAL, end conditions and aspect ratios on buckling mode shape

4.3 Free vibration behaviour of B-FGM beams

Investigation on the free vibration characteristics of B-FGM beam under VALs for variation in gradation indexes, aspect ratios, and end conditions is detailed in this section.

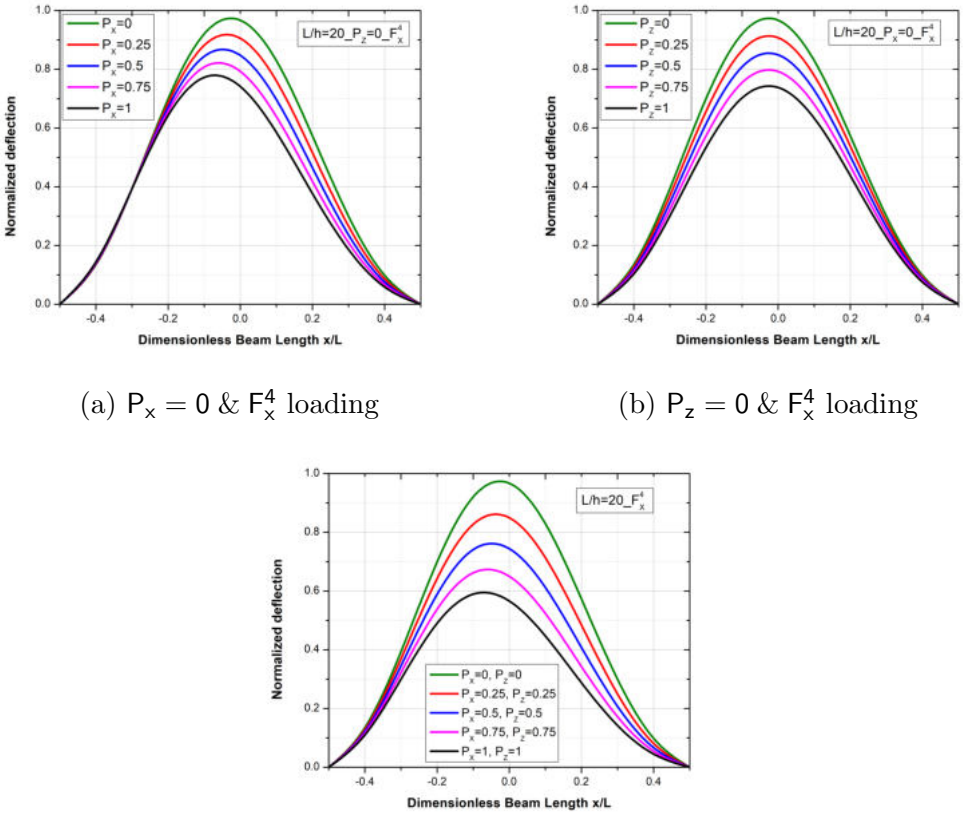

(a) $P_x = 0$ & F_x^4 loading

(b) $P_z = 0$ & F_x^4 loading

(c) F_x^4 loading

Figure 4.6: Influence of gradation index on buckling mode shape of CC B-FGM beam with L/h=20 and subjected to F_x^4 loading

4.3.1 Influence of type of VAL

Influence of nature of variation of VAL on the non-dimensional fundamental frequency for given gradation indexes is discussed in this section. Variation of the non-dimensional fundamental frequency with respect to the variation in VAL for metal and B-FGM beams is shown in Fig.4.7. The variation in the frequency follows the same trend of variation of P_{cr} with respect to the type of VAL. For all types of VALs, the dimensionless frequency decreases with an increase in the axial load intensity as mentioned earlier for the isotropic beam. Similarly, the fundamental frequency reaches zero value when the axial load intensity is equal to the P_{cr} of the given VAL. Furthermore, the frequency variation trend with respect to the axial load intensity is not sensitive to the variation in the gradation indexes. However, there is a considerable increase in the P_{cr} with respect to the increase in gradation indexes. Hence, one can expect similar kind of variation in

the fundamental frequency with increase in the axial load intensity with respect to the end conditions, aspect ratio and gradation indexes.

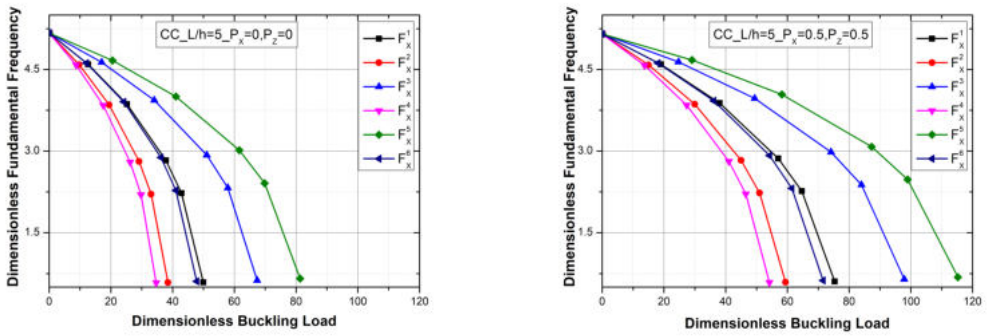

(a) $P_x = 0$ & $P_z = 0$ (b) $P_x = 0.5$ & $P_z = 0.5$

Figure 4.7: Influence of VALs on fundamental frequency of CC B-FGM beam with L/h=5 and for various gradation indexes

4.3.2 Influence of gradation indexes

Influence of certain gradation indexes and two types of VAL on the dimensionless frequency of CC B-FGM beam is shown in Fig.4.8. From the plots in Fig.4.8, it is evident that an increase in the gradation index increases the fundamental frequency, as anticipated, due to the enhancement in bending stiffness caused by improvement in elastic property. The influence of gradation indexes on the first three natural frequencies of B-FGM beams is presented in Table 4.3 and Table 4.4. From Table 4.3, for CC B-FGM beam and for the aspect ratio L/h=5, it is observed that with an increase in the gradation index along length direction (P_x), there is an increment in the first and third natural frequencies and decrement in the second natural frequency. The incremental nature of the first and third dimensionless frequencies is due to the enhancement of structural stiffness due to the increase in the gradation index (P_x). However, for the increase in gradation indexes along the thickness direction (P_z), there is a decrement in all the three natural frequencies. The dominance of mass over stiffness enhances the decremental nature of dimensionless frequency with an increase in the gradation index P_z. For the same CC B-FGM beam and aspect ratio L/h=20, all the first three natural frequencies are increasing with an increase in the gradation index P_x and decreasing with an increase in gradation index P_z. With an increase in the gradation index in both directions, SS B-FGM beams for both aspect ratios

Table 4.3: Influences of gradation indexes and aspect ratios on first three dimensionless frequencies of CC and SS B-FGM beams

BC	P_z	Ω	L/h=5					L/h=20				
			P_x					P_x				
			0	0.25	0.5	0.75	1	0	0.25	0.5	0.75	1
CC	0	Ω_1	5.17	5.17	5.18	5.19	5.20	6.36	6.36	6.37	6.38	6.39
		Ω_2	7.18	7.17	7.16	7.13	7.11	17.16	17.16	17.17	17.19	17.21
		Ω_3	7.37	7.38	7.40	7.42	7.46	32.65	32.65	32.66	32.68	32.70
	0.25	Ω_1	5.17	5.17	5.17	5.18	5.19	6.35	6.35	6.36	6.37	6.38
		Ω_2	7.17	7.16	7.15	7.12	7.09	17.14	17.14	17.15	17.16	17.19
		Ω_3	7.36	7.36	7.38	7.41	7.44	32.60	32.60	32.61	32.63	32.65
	0.5	Ω_1	5.15	5.15	5.15	5.16	5.17	6.32	6.32	6.33	6.34	6.36
		Ω_2	7.14	7.13	7.11	7.09	7.06	17.06	17.06	17.07	17.09	17.11
		Ω_3	7.32	7.33	7.35	7.38	7.41	32.46	32.46	32.47	32.49	32.51
	0.75	Ω_1	5.12	5.12	5.12	5.13	5.14	6.27	6.27	6.28	6.29	6.31
		Ω_2	7.09	7.08	7.06	7.04	7.01	16.94	16.94	16.95	16.96	16.99
		Ω_3	7.26	7.27	7.29	7.32	7.35	32.23	32.23	32.24	32.26	32.28
	1	Ω_1	5.08	5.08	5.08	5.09	5.10	6.20	6.21	6.21	6.23	6.24
		Ω_2	7.02	7.01	7.00	6.97	6.94	16.77	16.77	16.78	16.79	16.81
		Ω_3	7.18	7.19	7.21	7.24	7.27	31.92	31.92	31.93	31.94	31.97
SS	0	Ω_1	2.69	2.69	2.68	2.67	2.66	2.84	2.84	2.83	2.82	2.81
		Ω_2	5.44	5.42	5.40	5.38	5.37	11.23	11.23	11.23	11.24	11.25
		Ω_3	7.85	7.46	7.08	6.70	6.34	24.80	24.80	24.81	24.82	24.84
	0.25	Ω_1	2.69	2.68	2.68	2.67	2.65	2.83	2.83	2.83	2.82	2.81
		Ω_2	5.43	5.41	5.40	5.38	5.36	11.21	11.21	11.22	11.22	11.23
		Ω_3	7.84	7.45	7.07	6.70	6.34	24.76	24.76	24.77	24.77	24.75
	0.5	Ω_1	2.67	2.67	2.67	2.65	2.64	2.82	2.82	2.81	2.80	2.79
		Ω_2	5.41	5.39	5.37	5.35	5.34	11.16	11.16	11.16	11.17	11.18
		Ω_3	7.82	7.43	7.05	6.68	6.32	24.64	24.63	24.63	24.61	24.52
	0.75	Ω_1	2.65	2.65	2.64	2.63	2.62	2.80	2.80	2.79	2.78	2.77
		Ω_2	5.37	5.35	5.34	5.32	5.30	11.07	11.07	11.08	11.08	11.09
		Ω_3	7.77	7.39	7.02	6.65	6.29	24.44	24.43	24.41	24.37	24.22
	1	Ω_1	2.63	2.62	2.62	2.61	2.59	2.77	2.77	2.76	2.75	2.74
		Ω_2	5.32	5.30	5.29	5.27	5.25	10.95	10.95	10.96	10.96	10.97
		Ω_3	7.71	7.34	6.97	6.60	6.25	24.16	24.14	24.11	24.05	23.87

Table 4.4: Influences of gradation indexes and aspect ratios on first three dimensionless frequencies of CS and CF B-FGM beams

BC	P_z	Ω	L/h=5					L/h=20				
			P_x					P_x				
			0	0.25	0.5	0.75	1	0	0.25	0.5	0.75	1
CS	0	Ω_1	3.90	3.84	3.77	3.70	3.63	4.41	4.33	4.26	4.19	4.11
		Ω_2	5.15	5.14	5.13	5.11	5.10	14.07	14.00	13.94	13.88	13.83
		Ω_3	7.83	7.46	7.08	6.70	6.34	28.63	28.57	28.31	26.82	25.37
	0.25	Ω_1	3.90	3.83	3.76	3.70	3.63	4.40	4.33	4.25	4.18	4.11
		Ω_2	5.15	5.13	5.12	5.11	5.09	14.05	13.98	13.92	13.86	13.81
		Ω_3	7.82	7.46	7.08	6.70	6.34	28.59	28.52	28.31	26.82	25.37
	0.5	Ω_1	3.88	3.82	3.75	3.68	3.61	4.38	4.31	4.23	4.16	4.09
		Ω_2	5.13	5.11	5.10	5.09	5.07	13.98	13.92	13.85	13.80	13.74
		Ω_3	7.78	7.46	7.08	6.70	6.34	28.46	28.40	28.31	26.82	25.37
	0.75	Ω_1	3.86	3.79	3.73	3.66	3.59	4.35	4.28	4.20	4.13	4.06
		Ω_2	5.10	5.08	5.07	5.06	5.04	13.88	13.81	13.75	13.70	13.64
		Ω_3	7.72	7.46	7.08	6.70	6.34	28.26	28.20	28.14	26.82	25.37
	1	Ω_1	3.83	3.76	3.69	3.63	3.56	4.30	4.23	4.16	4.09	4.01
		Ω_2	5.05	5.04	5.03	5.01	5.00	13.74	13.67	13.61	13.56	13.50
		Ω_3	7.64	7.46	7.08	6.70	6.34	27.98	27.92	27.86	26.82	25.37
CF	0	Ω_1	0.99	0.91	0.85	0.78	0.72	1.01	0.94	0.87	0.80	0.74
		Ω_2	5.25	5.13	5.00	4.88	4.76	6.27	6.12	5.98	5.84	5.70
		Ω_3	7.85	7.46	7.08	6.70	6.34	17.20	17.06	16.93	16.81	16.69
	0.25	Ω_1	0.98	0.91	0.84	0.78	0.72	1.01	0.94	0.87	0.80	0.74
		Ω_2	5.24	5.12	5.00	4.87	4.75	6.26	6.12	5.97	5.83	5.69
		Ω_3	7.85	7.46	7.08	6.70	6.34	17.17	17.04	16.91	16.78	16.66
	0.5	Ω_1	0.98	0.91	0.84	0.78	0.72	1.01	0.93	0.86	0.80	0.73
		Ω_2	5.23	5.10	4.98	4.86	4.73	6.23	6.09	5.94	5.80	5.67
		Ω_3	7.85	7.46	7.08	6.70	6.34	17.09	16.96	16.83	16.71	16.59
	0.75	Ω_1	0.97	0.90	0.83	0.77	0.71	1.00	0.92	0.86	0.79	0.73
		Ω_2	5.19	5.07	4.95	4.83	4.71	6.19	6.04	5.90	5.76	5.62
		Ω_3	7.85	7.46	7.08	6.70	6.34	16.97	16.83	16.71	16.58	16.47
	1	Ω_1	0.96	0.89	0.83	0.76	0.71	0.99	0.92	0.85	0.78	0.72
		Ω_2	5.15	5.03	4.91	4.79	4.67	6.12	5.98	5.84	5.70	5.57
		Ω_3	7.85	7.46	7.08	6.70	6.34	16.79	16.66	16.53	16.41	16.30

depict decrement in all the three dimensionless frequencies except for the second natural frequency. The second natural frequency of the thin beam shows increasing trend with increase in the gradation index P_x. The effect of gradation

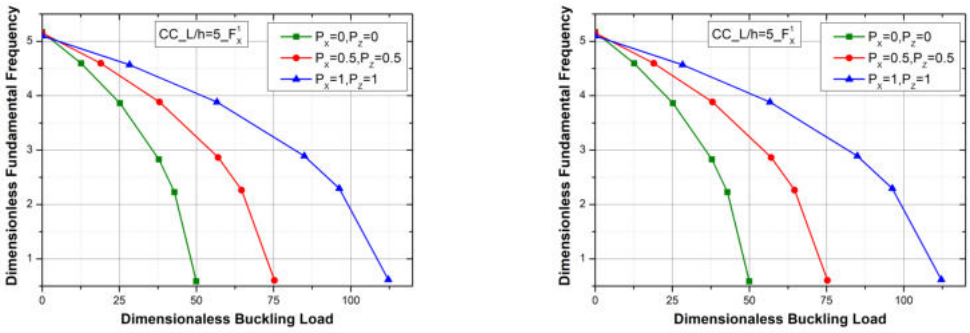

(a) F^1_x loading (b) F^4_x loading

Figure 4.8: Influence of gradation index on fundamental frequency of CC B-FGM beam with L/h=5 and for various VALs

indexes on the first three natural frequencies is studied for CS B-FGM beam, and the results are tabulated in Table 4.4. From the results, it is observed that the natural frequencies decrease with the increase in both the gradation indexes P_x and P_z except for a few cases. Noticeable variation in the first two dimensionless frequencies was observed for every incremental value of gradation index P_z and for a set of given gradation indexes P_x. However, there is no change in the third natural frequency for certain values of gradation index P_z. It can be noted that the dimensionless frequencies of CS B-FGM beams are influenced by the density of the material than the structural stiffness of the beams. The influence of gradation indexes on the first three frequencies of CF B-FGM beams presented in Table 4.4 is also showing the similar behaviour. However, the third natural frequency of the CF B-FGM beams having aspect ratio L/h=5 is not influenced by the gradation index P_z. The depiction in the natural frequencies reveals that CF B-FGM beams are more sensitive to the material mass of the beams than to their structural stiffness.

4.3.3 Influence of aspect ratios

Influence of aspect ratio of the B-FGM beam on the first three dimensionless frequencies is presented in Table 4.3 and Table 4.4. From the results it is observed that the effect of the aspect ratio is significant on the dimensionless frequencies

of B-FGM beams compared to the influence of gradation indexes and end conditions. This can be attributed to the higher flexural stiffness associated with the shorter beam compared to the longer beam. The natural frequencies are increasing with an increase in the aspect ratio from L/h=5 and L/h=20. As the natural frequencies are presented in the dimensionless form the increment in the natural frequencies with increase in the aspect ratio is observed. The natural frequency increment is observed to be higher with increase in the mode number. Predictably, B-FGM beams with high-end stiffness are having higher increments in the natural frequencies with an increase in the aspect ratio. Similarly, B-FGM beams with low-end stiffness are having lesser increments in the natural frequency with an increase in the aspect ratio.

4.3.4 Analysis on the free vibration mode shapes

Influence of increase in applied load intensity on the first two free vibration mode shapes is shown in Fig.4.9. The mode shapes are plotted with an increase in the intensity of the applied VAL in fractions of the Pcr. From both the plots, it is observed that the mode shapes are sensitive to the applied load intensity. Furthermore, the changes in the first mode shape with increase in applied load intensity end up with the fundamental buckling mode shape of the beam with same conditions. Significant change in terms if peak and zero amplitude can be observed for the second mode.

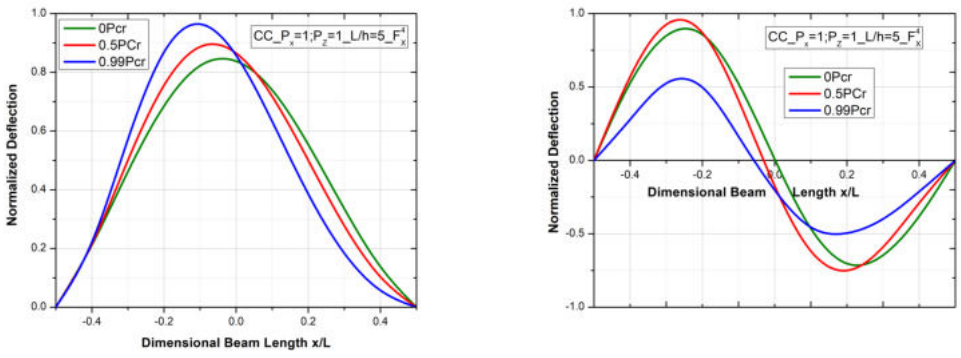

(a) First Mode (b) Second Mode

Figure 4.9: Influence of load intensity on first two mode shapes of CC B-FGM beam with L/h=5

4.4 Closure

Buckling and free vibration behaviour of a B-FGM beam subjected to different types of axial loads, aspect ratios and boundary conditions is investigated along with varying material property. The buckling loads are calculated and tabulated for six different types of VALs and for four boundary conditions. Free vibration analysis are carried out distinctively for increase in the buckling load intensity from 0 to its maximum value. The nature of variation in the buckling load for change in the VALs is coinciding with earlier literature investigations. Stiffness of the beam due to variation in the boundary condition and aspect ratio is found to be significantly effecting the buckling load responses. Gradation index increment along both the directions shown significant influence in the postulated buckling load values. But, an increment of gradation index along thickness direction is depicting higher buckling loads compared to lengthwise gradation index increment. Buckling mode shapes for the change in the aspect ratio, boundary condition, and increment in the gradation indexes concretes the nature of variation in the buckling load. Natural frequencies of the B-FGM beam is influenced by the variation of material gradation indexes along the directions.

Chapter 5

SOUND RADIATION BEHAVIOUR OF B-FGM BEAMS

5.1 Introduction

Influence of various aspect ratios (L/h), end conditions, and gradation indexes on sound radiation characteristics of B-FGM beam is presented. Sound power radiated, directivity pattern, radiation efficiency and sound pressure variation as a contour plot are analyzed for the B-FGM subjected to a steady state harmonic excitation. The study has been carried out for two aspect ratios i.e., for thick beam ($\frac{L}{h}$=5) and for thin beam ($\frac{L}{h}$=20), three different boundary conditions, and for specific gradation indexes varied along (x) and (z) directions. The quadratically decreasing type of VAL as shown in Fig.2.3 is considered for the analysis. Similar to the isotropic beam study, the sound radiation characteristics of the B-FGM beam are analyzed for different intensity values of VAL as a function of the P_{cr}. A bi-directional functionally graded beam with length 1m, and having square cross-section is used in the analysis. The thickness of the beam can be determined based on the aspect ratio L/h. The B-FGM beam has the material properties as E_m=210 GPa ; μ_m=0.3; ρ_m=2700 $\frac{kg}{m^3}$. The beam is excited at a location 0.7 m from left fixed axis.

5.1.1 Effect of gradation indexes

Influence of the gradation indexes and the axial load intensity on sound power radiated of thick beam under CC end condition is shown in Fig.5.1. For the three different combinations of gradation indexes analyzed, it is observed that with increase in axil load intensity the natural frequency reduces and the resonant peak gets shifted towards the lower frequency side. The decrease in natural frequency is more significant for the fundamental mode as seen in the isotropic beam case. The plot also illustrate that the fundamental frequency is significantly lower when the applied load intensity is around the P_{cr}. It can be observed from the plots that an increase in the gradation index leads to reduction in sound power levels and shifting of resonant peak towards higher frequency side. Fig.5.1(b) & (c) show a significant increase in the peak frequency with increase in the gradation index in the P_z direction. Similarly, from Fig.5.1(a), there is a slight decrease in the peak frequency with increase in the gradation index along the P_x direction. It can be concluded that the variation in gradation indexes significantly influences the sound power radiated in terms of shifting the resonant frequency. From Fig.5.2 it is observed that variation in gradation indexes (P_x) and (P_z) influences the sound power levels of thin (L/h=20) B-FGM beam as well. In the case of variations in both the gradation indexes, the influence is marginal which can be observed clearly in the higher modes. Fig.5.2 also illustrate that as the applied axial load intensity increases, the natural frequency exhibits a decreasing trend. The decreasing trend is more evident in the lower frequency band. From the plots in Fig.5.1(c) and 5.2(c), it is evident that there is a significant variation in the sound power levels when there is a increase in both the gradation indexes (P_x) and (P_z). The variation in the sound power is observed to be less significant whenever there is a variation in any one of the gradation indexes.

5.1.2 Effect of aspect ratio

Fig.5.3 depict that there is a noticeable influence on the sound power response due to the variation in the aspect ratios for CC and SS B-FGM beams. For better comprehension, the sound power levels are plotted for a constant gradation indexes $P_x = 1$ and $P_z = 1$. In some of the frequency ranges, the sound power levels of thin beams are slightly higher compared to those of thick beam. The variation in the sound power levels due to changes in the aspect ratio is significant in higher frequency range. As expected, the sound power radiation is more for

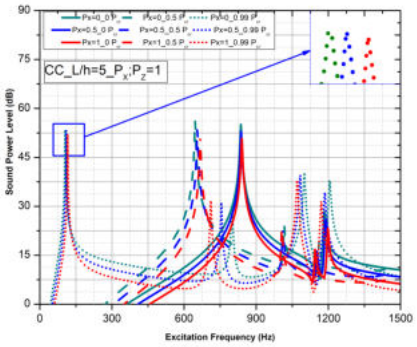

(a) P_z=1; P_x varied

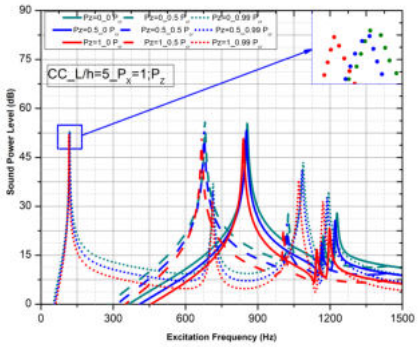

(b) Varying P_x=1; P_z varied

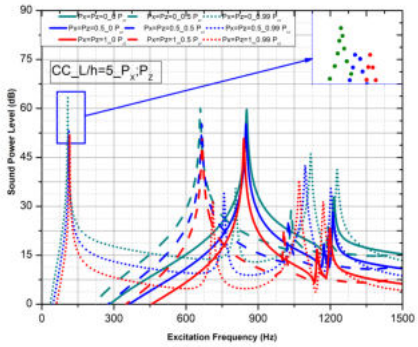

(c) Both P_x and P_z varied

Figure 5.1: Influence of the gradation indexes on sound power level of CC thick ($\frac{L}{h}$=5) CC B-FGM beam

the SS beam compared to the CC beam.

5.1.3 Influence of boundary condition

The influence of end conditions on the sound power level (dB) of bi directional FG beams is represented in Fig.5.4 for the gradation indexes $P_x = 1$ and $P_z = 1$ and for the aspect ratios $\frac{L}{h}$=5 and 20. From the plots, it is evident that the boundary conditions have a remarkable influence on the sound power radiation of B-FGM beams. As expected, the fundamental frequencies increase in the order of CF, SS and CC end conditions due to the increasing stiffness provided support conditions. It is apparent from Fig.5.4, that influence of boundary conditions on sound power levels is more significant for thin beams compared to thick beams. It can be concluded that the influence of end condition is significant on the sound power radiated as observed by several researchers. The radiation efficiency of the

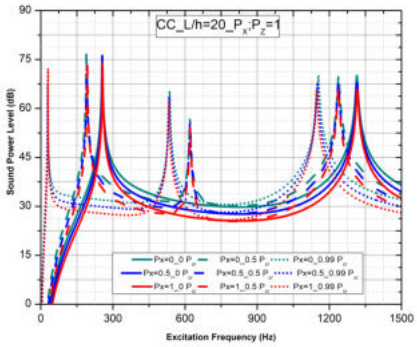

(a) P_z=1;P_x varied

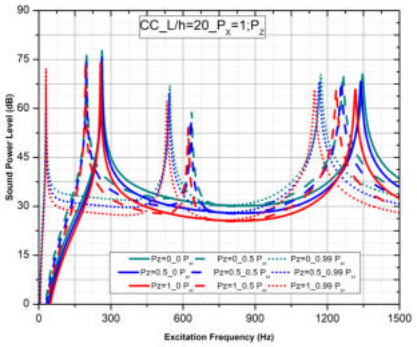

(b) Varying P_x=1; P_z varied

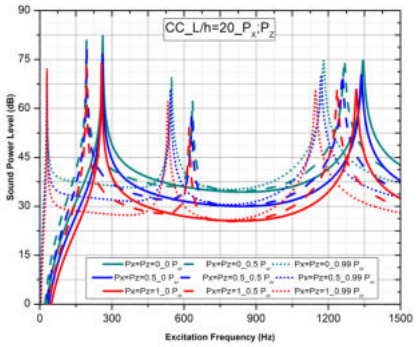

(c) Varying Both P_x and P_z varied

Figure 5.2: Influence of gradation indexes on sound power level of thin ($\frac{L}{h}$=20) CC B-FGM beam

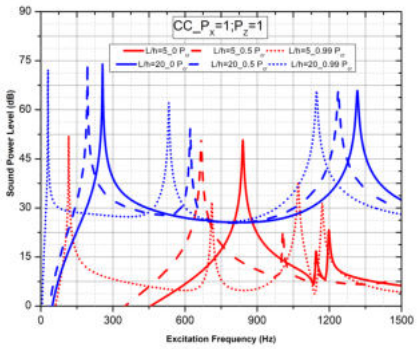

(a) CC B-FGM Beam

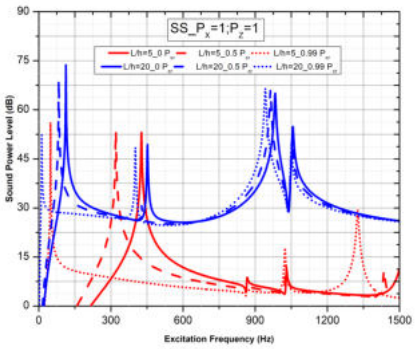

(b) SS B-FGM Beam

Figure 5.3: Significance of aspect ratios on the sound power level of CC and SS B-FGM beams having P_x=P_z=1

B-FGM beams is insensitive to the intensity of the applied axial load as seen in

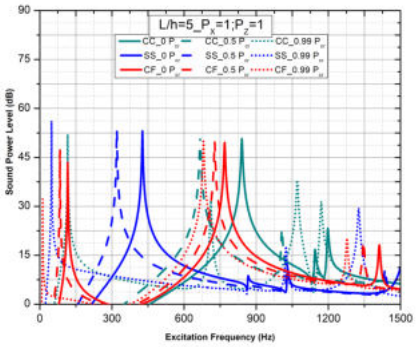

(a) Thick beam $\frac{L}{h}$=5

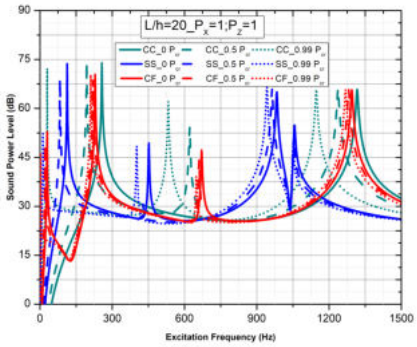

(b) Thin beam $\frac{L}{h}$=20

Figure 5.4: Influence of end conditions on sound power level for B-FGM beam P_x=P_z=1

Fig.5.5. However, there is a marginal variation in the sound radiation efficiency observed between the thick and the thin beams. The marginal change is due to the change in the significant amount of structural stiffness which is effected due to the variation in aspect ratio. Variation of sound power level as a function as

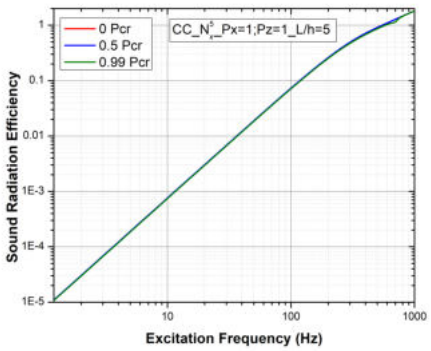

(a) Thick beam $\frac{L}{h}$=5

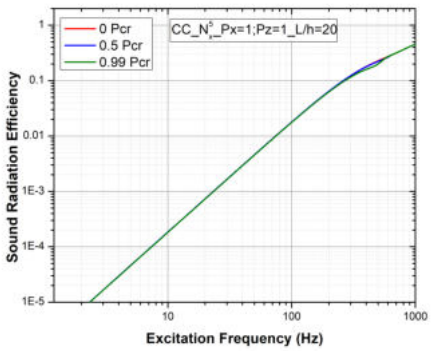

(b) Thin beam $\frac{L}{h}$=20

Figure 5.5: Effect of aspect ratios on radiation efficiency of CC bi directional FGM beams (P_x=P_z=1)

applied axial load intensity in octave bands is shown in Fig.5.6 for thin CC and SS B-FGM beams. It is clear that there is remarkable increase in sound power levels with the applied axial load intensity in the lowest frequency band due to reduction in the structural stiffness which is more when the applied load is equal to the P_{cr}. However, due to the presence of more number of modes and higher sound power levels, the band-wise increase in sound power level is not clearly seen in the higher frequency bands. The overall sound power levels of CC, SS and CF

B-FGM beams for the increment in the buckling load magnitude are presented in Fig.5.6(c). The curve is almost linear for the CF B-FGM beam, decreasing linearly for the SS B-FGM beam and, decreasing quadratically for the CC B-FGM beam. It is apparent that the nature of the decrement is highly sensitive to the boundary stiffness of the B-FGM beams. The higher the boundary stiffness, higher the rate of decrement of overall sound power level with an increase in applied load intensity.

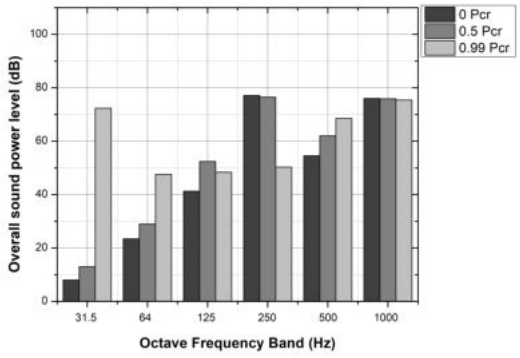

(a) Octave band for CC_L/h=20

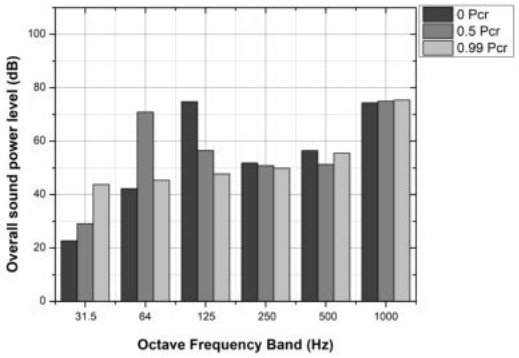

(b) Octave band for SS_L/h=20

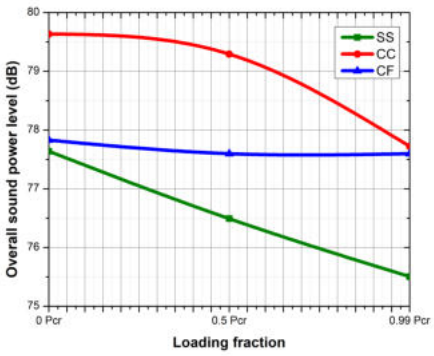

(c) Overall sound power level

Figure 5.6: Octave band and overall sound power level representation of various B-FGM beams

5.1.4 Studies on sound pressure level

It is evident from Fig.5.1 to Fig.5.3 that thick B-FGM beams radiates lesser sound power levels (dB) compared to thin B-FGM beams, as expected. However, the effect of the different parameters associated with the B-FGM beams on sound pressure level, which is function of location at which it is measured is not analyzed.

So, a detailed investigation to analyze the sound pressure level (dB) variation for an increment in the magnitude of buckling load and change in boundary conditions of thick B-FGM beams is carried out in this section. The sound pressure levels (dB) are calculated along the length, up to a height of 1m and, at 0.7 m distance from the fixed support of the B-FGM beams. Table 5.1 and Table

Table 5.1: Contour plots of sound pressure level (dB) variation of the fundamental mode of SS and CF B-FGM beam

P_{cr}	SS	CF
0	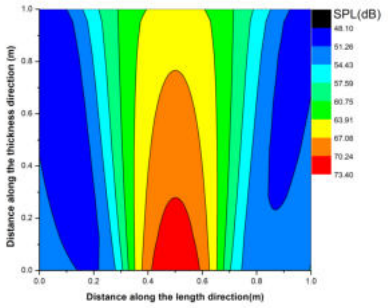	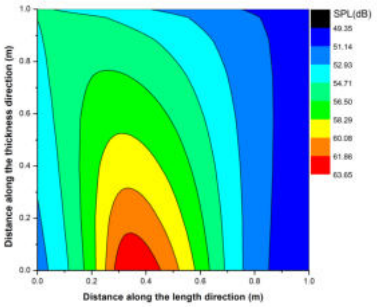
0.5	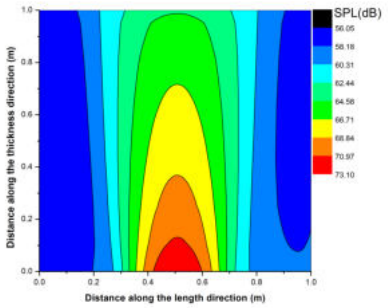	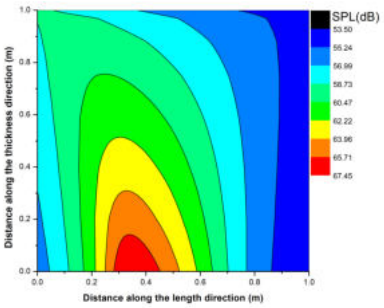
0.99	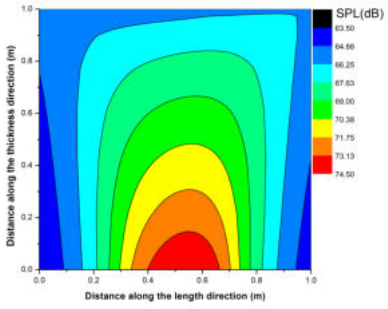	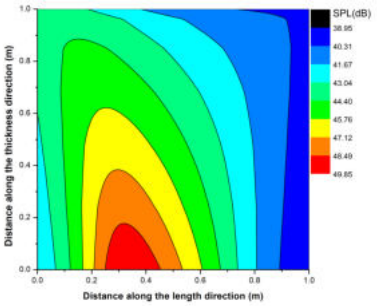

5.2 detail the sound pressure level (dB) variation as contour plots for SS and CF B-FGM beams as a function applied load intensity. At critical buckling load, there

Table 5.2: Contour plots of sound pressure level (dB) variation of first and third mode of CC B-FGM beams

P_{cr}	1^{st}Mode	3^{rd}Mode
0	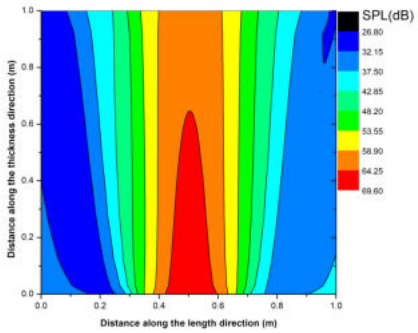	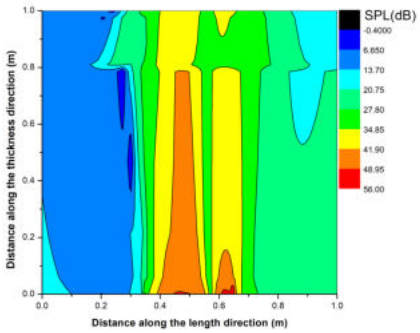
0.5	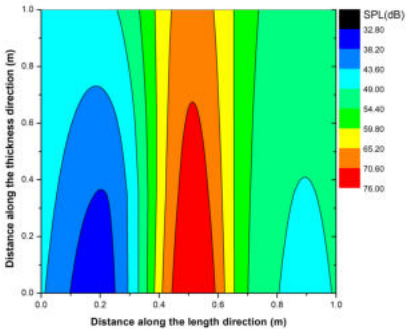	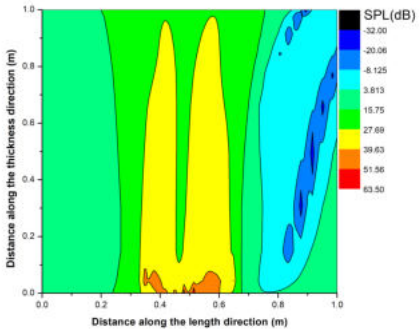
0.99	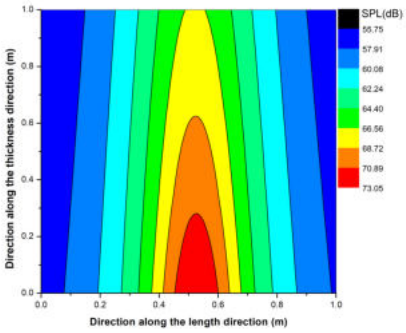	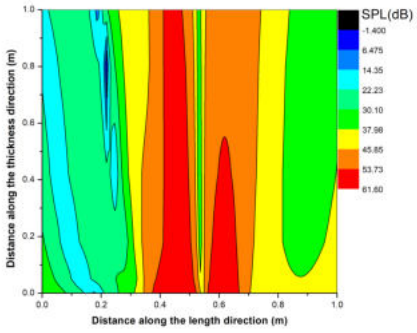

is a shift in the sound pressure radiation towards the right, while for the other two load intensities, the sound pressure is concentrated at the center for the SS B-FGM beam. But, the sound pressure radiation of CF bi-directional functionally graded beam is shifting towards the left. The shift is obvious, as the boundary stiffness will be higher at clamped support. The nature of sound radiation at the

fundamental frequency of CC B-FGM beam in Table 5.2 is concentric about the center. It is due to the equal end stiffness at both ends. The behaviour of sound pressure radiation as contour plots in this section coincides with the behaviour of sound power levels analyzed in the earlier sections. Similar to the contour plot

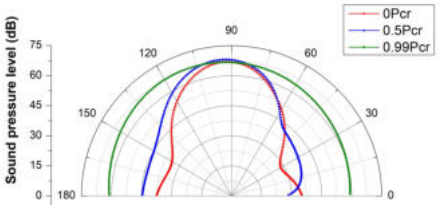

(a) First mode of CC Beam

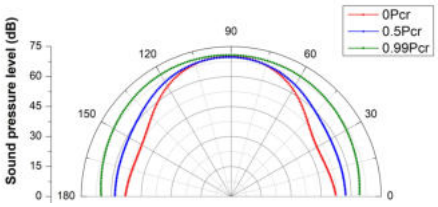

(b) First mode of SS Beam

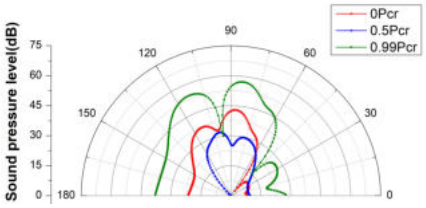

(c) Third mode of CC Beam

Figure 5.7: Directivity pattern representation for first and third modes of various B-FGM beams

representation, the sound pressure level (dB) is presented as a directivity pattern in Fig.5.7 for CC and SS B-FGM beams. The CC B-FGM beam in Fig.10(a) was observed to exhibit a significant variation in the sound pressure directivity compared to the SS B-FGM beam in Fig.5.7(b). Where there is no such variation observed when both the B-FGM beams are subjected to critical buckling load. It can be noted that the influence of structural stiffness along with end stiffness, has a remarkable effect on sound pressure radiation of B-FGM beams. The directivity nature of sound pressure for the third mode of the CC bi directional FG beam presented in Fig.5.7(c) shows an irregular pattern, while also coincides with the typical mode shape of the third mode.

5.2 Closure

This chapter investigated acoustic response characteristics of B-FGM beams subjected to a type of VAL, three boundary conditions, two aspect ratios and for different gradation indexes. Sound power levels are studied within the selected frequency band and presented in terms of individual frequencies and octave band frequencies. Acoustic responses are also investigated in terms of sound radiation efficiency. The sound pressure level variation is analyzed from directivity pattern and contour plot representations. Also, it is observed that the increment in the gradation index increases the sound power levels. The B-FGM beams with higher aspect ratio radiates much higher sound than B-FGM beams with low aspect ratio. Similar to the isotropic beams sound radiation efficiency of B-FGM beam also insensitive to the applied load intensity. The sound pressure level shown in contour plot and directivity pattern representations highly reflecting trends of sound power levels with respect to the different parameters.

Chapter 6

STUDIES ON BIO-INSPIRED COMPOSITE BEAMS

6.1 Introduction

Numerical studies are carried out on non-dimensional buckling loads, natural frequencies and acoustic responses of bio-inspired laminated composite beams are presented in this chapter. The study has been carried out for Glass/Epoxy and Carbon/Epoxy materials, SS,CC and CF boundary conditions, and for($\frac{L}{h}$=5) & ($\frac{L}{h}$=20) aspect ratios. Three types of axially varying loads as shown in Fig.2.2, uniformly distributed (F_x^1), quadratically decreasing (F_x^5) and parabolic varying (F_x^6) types of loads are considered for the analysis. The vibration and acoustics responses are analyzed by varying the magnitude of the VAL from zero to its P_{cr} in fraction. Nine different types of lay up configurations considered for the present study and are presented in the Table 6.1. The nine types of lay-up scheme belonging to five categories which are, uni-directional(UD), crossply-symmetric(CP), Quasi isotropic-symmetric(QI), Helicoidal-symmetric(H) and Helicoidal exponential(HE). All the nine lamination schemes are analyzed for 32 layers. A bio-inspired composite beam having a length of 1m, and square cross section bxh is considered. The beam's thickness is calculated based on the given aspect ratio L/h. Material properties of Glass/Epoxy and Carbon/Epoxy are given in Table 6.2.

Table 6.1: Layup specifications for the selected configurations

S.No	Designation	N_L	Stacking Sequence	Description
1	UD	32	$[0]_{32}$	Unidirectional
2	CP	32	$[0/90]_{8s}$	Crossply-symmetric
3	QI	32	$[45/-45/0/90]_{4s}$	Quasi isotropic-symmetric
4	3H	32	$[0/3.../45]_s$	Helicoidal-symmetric (3^0)
5	6H	32	$[0/6.../90]_s$	Helicoidal-symmetric (6^0)
6	12H	32	$[0/12.../180]_s$	Helicoidal-symmetric (9^0)
7	HE1	32	$[2/4/8/16]_{4s}$	Helicoidal exponential $\delta_\theta = 2$
8	HE2	32	$[2.5/6.3/15.6/39]_{4s}$	Helicoidal exponential $\delta_\theta = 2.5$
9	HE3	32	$[3/9/27/81]_{4s}$	Helicoidal exponential $\delta_\theta = 3$

Table 6.2: Material properties of Glass/Epoxy and Carbon Epoxy composites

Material Property	Glass/Epoxy	Carbon/Epoxy
E_1 (GPa)	37.78	172.9
E_2 (GPa)	10.90	7.2
E_3 (GPa)	10.90	7.2
G_{12} (GPa)	4.91	3.76
G_{23} (GPa)	4.17	3.2
G_{13} (GPa)	4.91	3.76
μ	0.3	0.3
ρ ($\frac{kg}{m^3}$)	1870	1566

6.1.1 Buckling study

This section outlines the significance of different parameters on non dimensional buckling loads (λ) and buckling mode shapes. Table 6.3, elaborates the significance of VALs, aspect ratios, layup schemes and boundary conditions on the non-dimensional buckling loads of Glass/Epoxy bio-inspired composite beams. The non-dimensional buckling loads across the three boundary conditions for the change in the lamination scheme, aspect ratios and VALs indicate similarity in the trend. From the observation on the values of all SS,CC and CF boundary condition, it is noted that with change in the aspect ratio from L/h 5 to 20, there is raise in the non-dimensional buckling loads. The trend for raise in the aspect ratio is presented in Fig.6.1(a) and 6.1(b) of CC Glass/Epoxy bio-inspired composite beams. It can also be noted from Table 6.3, across various

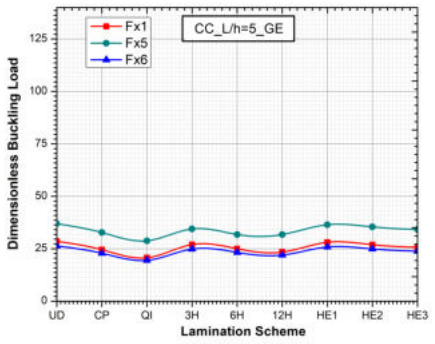

(a) Glass/Epoxy CC Beam for L/h=5

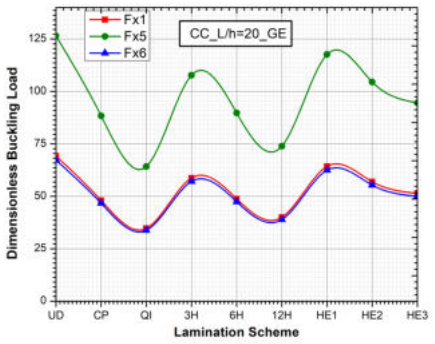

(b) Glass/Epoxy CC Beam for L/h=20

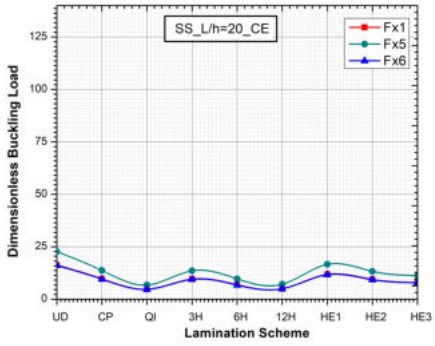

(c) Carbon/Epoxy SS Beam for L/h=20

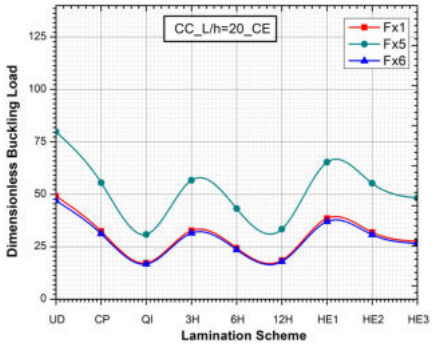

(d) Carbon/Epoxy CC Beam for L/h=20

Figure 6.1: Effect of VALs, layup-scheme on non-dimensional buckling loads of bio-inspired composite Beams

boundary conditions, lamination scheme and aspect ratios, the quadratically decreasing load (F_x^5) yields higher buckling resistance compared to the uniformly distributed load (F_x^1) and parabolic varying load (F_x^6) cases. This variation in non-dimensional buckling loads between F_x^1, $F_x^5$and F_x^6 is following the same trend as reported by earlier researchers. There is a marginal variation in the trends of non-dimensional buckling loads of F_x^1 and F_x^6 of CF bio-inspired composite beams, while the highest buckling strength is reported for F_x^5 loading. The variations in the non-dimensional buckling loads for changes in the aspect ratios, VALs and boundary conditions is due to the influence of stiffness component in the bio-inspired composite beams. Analysing the buckling behaviour across the various layup schemes, one can understand that complexity in the layup scheme is very influential. The beam with UD lay-up is having the highest buckling resistance and beam with QI (45/-45/0/90) layup scheme is having lower buckling resistance compared to the other layup schemes and this change is common ir-

Table 6.3: Influence of axial loads, materials, aspect ratios and boundary conditions on non-dimensional buckling loads of Glass/Epoxy bio-inspired composite beams

		L/h=5			L/h=20		
BC	Lay-up Scheme	$\bar{F}_x^1$	$\bar{F}_x^5$	$\bar{F}_x^6$	$\bar{F}_x^1$	$\bar{F}_x^5$	$\bar{F}_x^6$
SS	UD	13.58	17.79	13.31	18.18	25.98	17.95
	CP	10.03	13.50	9.85	12.39	17.74	12.24
	QI	7.58	10.38	7.45	8.86	12.69	8.75
	3H	11.92	15.82	11.69	15.29	21.86	15.09
	6H	10.18	13.68	9.99	12.60	18.03	12.44
	12H	8.69	11.87	8.55	10.22	14.64	10.09
	HE1	12.82	16.91	12.57	16.79	24.01	16.58
	HE2	11.63	15.49	11.41	14.79	21.16	14.61
	HE3	10.66	14.30	10.47	13.31	19.04	13.14
CC	UD	28.60	36.96	26.33	69.26	126.50	67.25
	CP	24.54	32.73	22.86	48.03	88.38	46.69
	QI	20.68	28.81	19.47	34.70	64.16	33.76
	3H	26.98	34.44	24.85	58.75	107.73	57.09
	6H	25.00	31.78	23.26	48.78	89.72	47.42
	12H	23.41	31.79	22.00	39.98	73.89	38.89
	HE1	28.06	36.44	25.87	64.27	117.62	62.43
	HE2	26.91	35.41	24.91	56.95	104.50	55.34
	HE3	25.65	34.20	23.84	51.45	94.57	50.01
CF	UD	7.07	20.89	7.63	7.79	26.86	8.64
	CP	4.94	15.32	5.38	5.29	18.30	5.87
	QI	3.59	11.50	3.93	3.77	13.06	4.19
	3H	6.02	18.27	6.53	6.54	22.57	7.25
	6H	5.02	15.55	5.46	5.38	18.59	5.97
	12H	4.13	13.19	4.52	4.35	15.07	4.83
	HE1	6.57	19.69	7.11	7.19	24.81	7.98
	HE2	5.84	17.82	6.34	6.32	21.84	7.02
	HE3	5.29	16.31	5.75	5.68	19.64	6.31

respective of boundary condition, material, VALs and aspect ratios. From Table 6.4, it is observed that the variations in non-dimensional buckling loads are similar for Carbon/Epoxy bio-inspired composite beams as well, because, the above

Table 6.4: Influence of axial loads, materials, aspect ratios and boundary conditions on non-dimensional buckling loads of Carbon/Epoxy bio-inspired composite beams

		L/h=5			L/h=20		
BC	Lay-up Scheme	F_x^1	F_x^5	F_x^6	F_x^1	F_x^5	F_x^6
SS	UD	5.27	6.21	5.09	16.30	22.69	16.05
	CP	4.26	5.07	4.13	9.71	13.68	9.57
	QI	2.89	3.54	2.82	4.73	6.73	4.67
	3H	4.50	5.24	4.37	9.57	13.52	9.44
	6H	3.81	4.59	3.71	6.83	9.69	6.74
	12H	3.29	4.12	3.21	4.99	7.11	4.92
	HE1	4.79	5.67	4.64	11.83	16.62	11.65
	HE2	4.37	5.23	4.24	9.40	13.27	9.26
	HE3	4.01	4.84	3.90	7.93	11.23	7.82
CC	UD	7.42	10.44	6.87	49.15	79.86	46.98
	CP	6.34	8.65	5.85	32.40	55.58	31.18
	QI	4.72	6.03	4.33	17.24	30.86	16.69
	3H	6.49	8.28	5.93	32.70	56.72	31.52
	6H	5.66	7.36	5.15	24.37	43.18	23.56
	12H	5.38	6.81	4.92	18.50	33.38	17.93
	HE1	6.99	9.63	6.45	38.54	65.32	37.03
	HE2	6.63	9.02	6.11	31.90	55.20	30.74
	HE3	6.29	8.50	5.80	27.55	48.20	26.58
CF	UD	4.45	8.10	4.34	7.52	24.66	8.26
	CP	3.09	6.54	3.13	4.33	14.53	4.77
	QI	1.72	4.44	1.81	2.05	7.02	2.27
	3H	3.15	6.77	3.22	4.23	14.28	4.67
	6H	2.40	5.81	2.51	2.98	10.14	3.30
	12H	1.86	5.07	1.98	2.15	7.38	2.39
	HE1	3.63	7.36	3.64	5.31	17.74	5.85
	HE2	3.07	6.74	3.14	4.16	14.03	4.60
	HE3	2.68	6.20	2.77	3.49	11.82	3.86

said trends are similar for the changes in layup schemes, boundary conditions and aspect ratios. As expected, buckling strength of CC beams is higher than other SS and CF beams. Effect of lay-up scheme on the buckling mode shape

of different BC is shown in Fig.6.2 The buckling mode shape plots indicate both the aspect ratios and lamination scheme have remarkable influence on buckling mode shape.

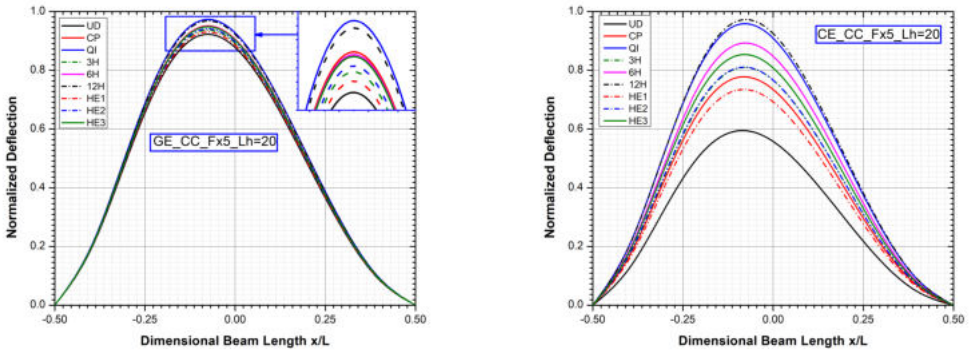

(a) L/h=5 (b) L/h=20

Figure 6.2: Influence of lamination scheme on buckling mode shape of Carbon/Epoxy CC beams for aspect ratio L/h=20 for F_x^5 loading

6.1.2 Free Vibration study

This section details the investigation performed on the free vibration on bio-inspired composite beam vibrations with its mode shape and, damping characteristics. These characteristics are presented for the variation in the material composition, boundary conditions and aspect ratios. Study on fundamental frequency of various bio-inspired composite beams due to the increase in applied VAL intensity is also presented in this section. For better understanding, the said vibrational responses are elaborated for specific cases. Table 6.5 and Table 6.6, presents the first three natural frequencies of Glass/Epoxy and Carbon/Epoxy bio-inspired composite beams receptively, for various layup schemes, aspect ratios and boundary conditions. The values in both the tables, for variation in the boundary conditions clearly depicts the influence of stiffness variations caused by lay-up schemes, aspect ratios, and boundary conditions on the natural frequencies. It is also obvious from the observation that thin beams (L/h=20) vibrating at lower frequencies when compared with thick beams (L/h=5). With the change in the material composition from Glass/Epoxy to Carbon/Epoxy, there is a increase in the values of natural frequencies. This is due to the higher elastic modulus of Carbon/Epoxy beams compared to Glass/Epoxy beams. Similarly, the significance of lay-up schemes on natural frequencies is observed to be follow-

Table 6.5: Influence of axial loads,aspect ratios and boundary conditions on first three natural frequencies (Hz) of Glass/Epoxy bio-inspired composite beams

		L/h=5			L/h=20		
BC	Lay-up Scheme	1st	2nd	3rd	1st	2nd	3rd
SS	UD	355.31	1100.64	1139.17	100.92	392.09	844.14
	CP	301.80	921.57	978.70	83.29	325.88	708.72
	QI	260.54	808.55	876.64	70.39	276.81	606.48
	3H	331.05	911.43	1051.15	92.53	360.91	781.43
	6H	304.49	795.10	988.30	83.99	328.64	714.85
	12H	279.32	812.52	937.32	75.62	297.21	650.71
	HE1	344.24	1079.45	1082.43	97.00	377.59	815.23
	HE2	326.58	996.57	1042.11	91.02	355.26	769.98
	HE3	311.87	936.57	1006.56	86.32	337.49	733.23
CC	UD	594.45	1327.87	2047.51	221.24	587.15	1073.43
	CP	534.17	1221.90	1843.14	184.43	493.82	916.25
	QI	483.24	1131.22	1617.10	156.93	422.95	793.90
	3H	569.66	1287.06	1822.86	203.90	543.82	1002.40
	6H	538.06	1230.02	1590.19	185.89	497.80	923.97
	12H	515.62	1204.22	1625.05	168.43	453.64	850.63
	HE1	584.31	1312.99	2029.29	213.20	567.20	1041.22
	HE2	566.16	1283.76	1991.91	200.77	535.95	989.50
	HE3	548.46	1251.36	1873.15	190.87	510.61	946.10
CF	UD	135.69	642.19	1139.17	36.17	220.57	593.13
	CP	113.65	565.24	921.57	29.82	183.06	496.87
	QI	97.01	502.29	808.55	25.18	155.30	424.42
	3H	125.37	609.10	911.43	33.14	202.83	548.28
	6H	114.53	569.70	795.10	30.06	184.56	501.02
	12H	104.09	536.97	812.52	27.05	166.75	455.41
	HE1	130.93	627.93	1082.43	34.75	212.31	572.42
	HE2	123.52	603.74	996.57	32.59	199.63	540.14
	HE3	117.56	581.77	936.57	30.90	189.58	514.09

ing the similar trend as that of non-dimensional buckling loads. As the least value of natural frequency is observed for QI lay-up and, highest for UD lay-up, while, the other lay-up schemes are following the similar trend as of non-dimensional

Table 6.6: Influence of axial loads,aspect ratios and boundary conditions on first three natural frequencies (Hz) of Carbon/Epoxy bio-inspired composite beams

		L/h=5			L/h=20		
BC	Lay-up Scheme	1st	2nd	3rd	1st	2nd	3rd
	UD	572.23	1366.65	2184.16	225.64	790.38	1512.85
	CP	498.17	1265.04	1902.85	173.28	634.95	1271.32
	QI	394.35	1111.44	1418.99	120.53	459.37	963.60
	3H	511.03	1315.75	1431.72	171.87	636.84	1290.82
SS	6H	459.57	1137.10	1248.06	144.90	547.41	1135.65
	12H	417.16	1214.77	1232.99	123.67	475.16	1007.65
	HE1	534.05	1332.24	2107.15	191.45	694.46	1375.39
	HE2	502.11	1295.87	1811.63	170.35	629.30	1271.39
	HE3	475.90	1257.58	1633.34	156.36	583.44	1192.45
	UD	734.67	1539.88	2392.63	434.19	1043.88	1699.24
	CP	677.65	1428.32	2197.35	352.35	879.02	1480.90
	QI	592.06	1274.36	1941.87	257.48	668.12	1180.15
	3H	699.46	1462.78	2202.22	354.07	892.28	1517.67
CC	6H	662.91	1400.90	2097.04	305.94	786.27	1370.11
	12H	647.89	1401.17	2107.64	266.93	699.09	1251.61
	HE1	713.99	1501.55	2315.25	384.40	950.37	1586.39
	HE2	693.72	1466.29	2252.92	349.87	879.44	1493.92
	HE3	673.17	1429.28	2192.76	325.21	825.43	1418.08
	UD	252.07	895.00	1776.15	82.71	455.34	1098.90
	CP	208.94	796.72	1630.12	62.84	362.04	910.55
	QI	155.89	665.47	1418.99	43.35	259.49	681.20
	3H	210.77	816.71	1431.72	62.17	362.02	920.50
CF	6H	184.15	756.41	1137.10	52.20	309.79	804.80
	12H	162.43	718.88	1232.99	44.40	267.87	710.24
	HE1	226.72	847.37	1719.67	69.59	396.86	988.16
	HE2	208.29	809.33	1667.98	61.67	358.10	908.12
	HE3	194.69	776.81	1617.27	56.48	331.24	849.01

buckling loads. Out of the five designate groups, UD layup is found to be dominant, followed by HE's, CP, H's and least are for QI.

Fig.6.3 presents the study on fundamental frequency variation due to the in-

crease in the VAL intensity. Quadratically decreasing VAL (F_x^5) is chosen for this study. As anticipated, the fundamental frequency drops to its lowest value when the applied load intensity is equal to the critical buckling load. This drop in fundamental frequency for the increase in axial load intensity is observed to be following similar trend for various lamination types, end conditions, aspect ratios and material compositions. The influence of aspect ratio on fundamental frequency is observed to be significant, as one can notice from the plots of Fig.6.3(a) and 6.3(b), that there is a decrease in the fundamental frequency of each layup scheme for the increase in the aspect ratio from L/h=5 to L/h=20. It

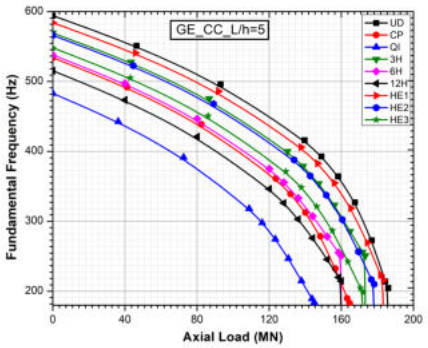

(a) Glass/Epoxy CC Beam for L/h=5

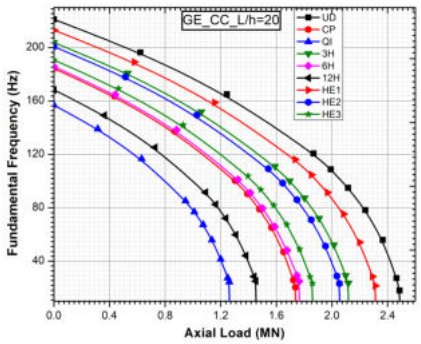

(b) Glass/Epoxy CC Beam for L/h=20

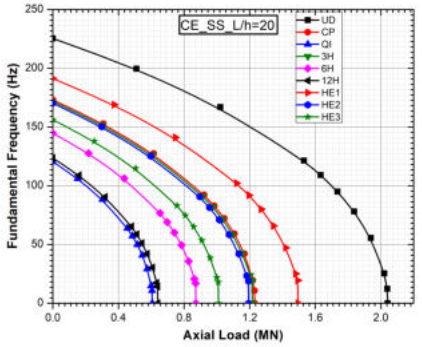

(c) Carbon/Epoxy SS Beam for L/h=20

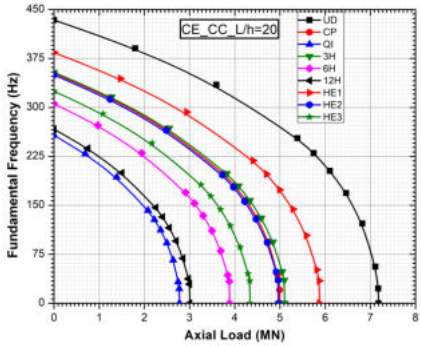

(d) Carbon/Epoxy CC Beam for L/h=20

Figure 6.3: Effect of axial load intensity on fundamental frequency of various bio-inspired composite beams for quadratically decreasing load (F_x^5)

is also observed that the rate of reduction in the frequency is highly correlating to the magnitude of the axial load. The study on the variation of fundamental frequency with increase in the axial load intensity highly supplements the above vibration study. Variation in modal damping of the fundamental mode of the bio-inspired composite beams, is presented in Table 6.7 and Fig.6.4. As antici-

pated, damping values increase with increase in the aspect ratio. It is due to the reduced thickness influencing lower energy dissipation during vibrations. For the change in the material composition from Glass/Epoxy to Carbon/Epoxy, there is a reduction in the modal damping. Similarly from the analysis on the boundary conditions it is observed that the CC beam has less damping values compared to SS beams. In observing the damping of layup schemes, UD and CP layups schemes are showing relatively lower damping values due to the simple layer arrangement of these layups. However, due to complex layer arrangement QI layup scheme exhibiting more damping than the rest of layups. The lamination scheme effects the inter-laminar shear which influences the frictional damping of the layups. From the modal damping values, it can be concluded that higher the stiffness of the bio-inspired composite beams lower will be the modal damping and vice-versa. Effect of different lay up scheme on the fundamental vibration

Table 6.7: Significance of VALs, aspect ratios, material and boundary conditions on fundamental frequency (Hz) and modal damping of bio-inspired composite beams

Material	L/h	BC	Layup								
			UD	CP	QI	3H	6H	12H	HE1	HE2	HE3
Glass/ Epoxy	5	CC	594.45 (0.0021)	534.17 (0.0043)	483.24 (0.0103)	569.66 (0.0044)	538.06 (0.0066)	515.62 (0.009)	584.31 (0.0033)	566.16 (0.0045)	548.46 (0.0053)
Glass/ Epoxy	20	CC	221.24 (0.005)	184.43 (0.0094)	156.93 (0.0189)	203.9 (0.0103)	185.89 (0.014)	168.43 (0.0173)	213.2 (0.0078)	200.77 (0.0103)	190.87 (0.0117)
Carbon/ Epoxy	20	CC	434.19 (0.0013)	352.35 (0.0021)	257.48 (0.0055)	354.07 (0.0077)	305.94 (0.0094)	266.93 (0.0095)	384.4 (0.0061)	349.87 (0.0078)	325.21 (0.0087)
Carbon/ Epoxy	20	SS	225.64 (0.002)	173.28 (0.0029)	120.53 (0.0066)	171.87 (0.0102)	144.9 (0.0117)	123.67 (0.0111)	191.45 (0.0085)	170.35 (0.0103)	156.36 (0.0111)

mode shape of the Carbon/Epoxy beams with aspect ratio L/h=20 is presented in Fig.6.5(a). Similarly, the changed in the third mode of the beam with 6H layup with increase in axial load intensity is shown in Fig.6.5(b). From Fig.6.5(a), it is observed that the patterns of vibration are symmetric for the all the layup schemes and are highly co-relating to the variation of fundamental frequency with respect to lay-up scheme. Similarly, the effect of axial load intensity on the vibration mode shape is significant as seen in Fig 6.5(b).

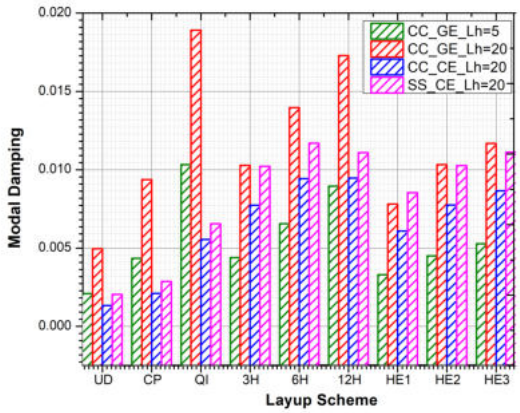

Figure 6.4: Influence of lamination scheme, aspect ratio and material on modal damping of various bio-inspired composite beams

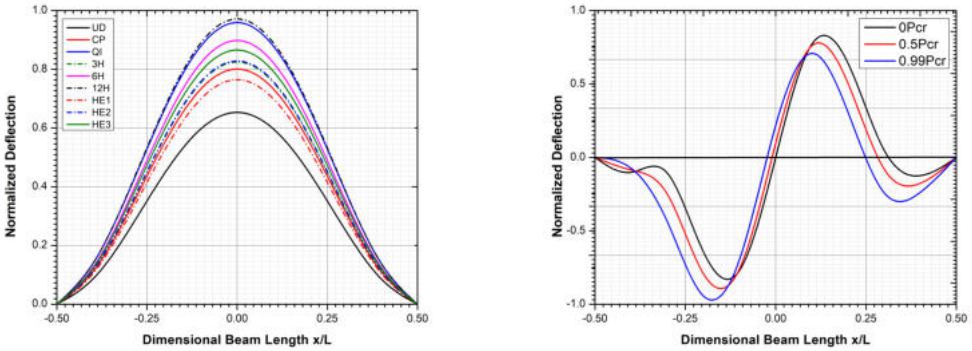

(a) 1^{st} mode of Carbon/Epoxy CC beam for L/h=20

(b) 3^{rd} mode Carbon/Epoxy CC beam for L/h=20 and for layup 6H

Figure 6.5: Variation in the first and third mode shapes of Carbon/Epoxy CC beams with aspect ratio L/h=20 and for F_x^5 loading

6.1.3 Forced vibration study

This section investigates the forced vibration response of various bio-inspired composite CC beams under a quadratically decreasing load (F_x^5) and for an aspect ratio L/h=20. Variation of average rms velocity along the normal direction with respect to excitation frequency is analyzed. The intensity of axial load applied in proportions of 0Pcr, 0.5Pcr and 0.99Pcr, and consequent changes in average rms velocity is studied for a time varying harmonic force (1 N) excitation. From Fig.6.6, it is observed that there is an increase in the average rms velocity of the fundamental mode due to the increase in the buckling load intensity. The

shift in natural frequency to lower values is also observed. This change is similar for the Carbon/Epoxy composite beams as well, as shown in Fig.6.7 (a) to (c). However, it is also observed that high elastic modulus Carbon/Epoxy bio-inspired composite beams depict higher frequencies with lower average rms velocity than the Glass/Epoxy composite beams. A similar observation can be made for QI type composite beam, which is exhibiting highest amplitude compared to other lamination schemes and, coincidently this layup scheme has the least stiffness as discussed in the buckling load and natural frequency studies. The pattern for all the nine lamination schemes in both the plots Fig.9 and Fig.10 highly coincides with the trend observed in the buckling and free vibration studies.

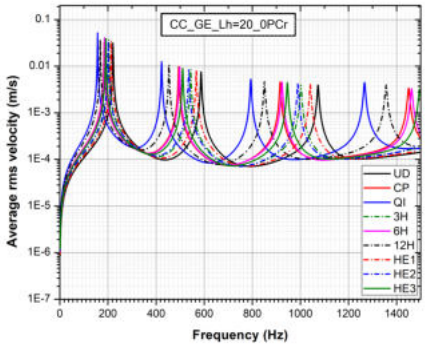

(a) 0Pcr

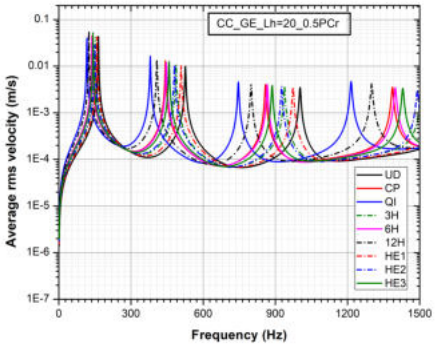

(b) 0.5Pcr

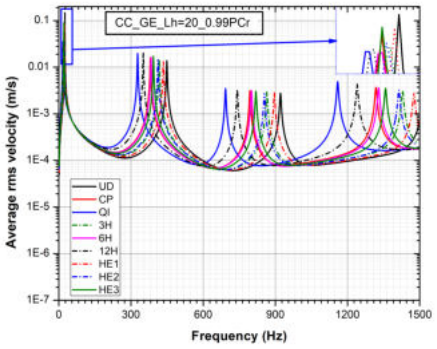

(c) 0.99Pcr

Figure 6.6: Effect of axial load intensity on average rms velocity (m/s) of Glass/Epoxy bio-inspired composite beam with L/h=20 and CC end conditions

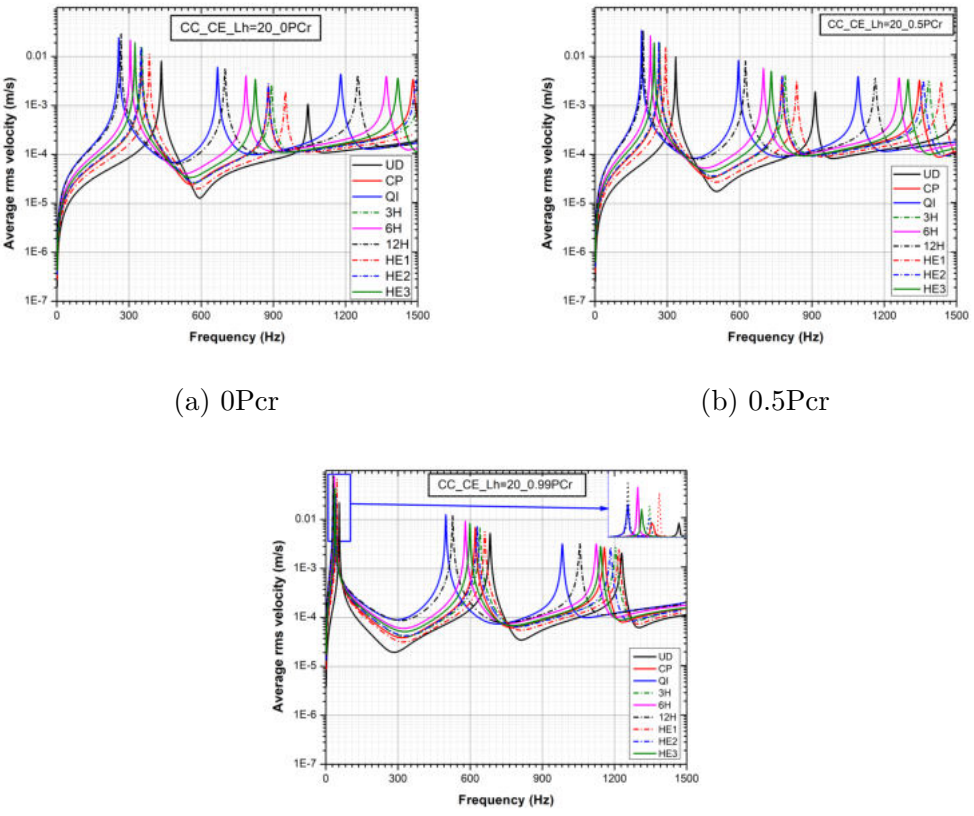

(a) 0Pcr

(b) 0.5Pcr

(c) 0.99Pcr

Figure 6.7: Effect of axial load intensity on average rms velocity (m/s) of Carbon/Epoxy bio-inspired composite beam with L/h=20 and CC end conditions

6.1.4 Acoustic Response

Analysis on the acoustic response characteristics of various bio-inspired composite beams under the influence of VALs is detailed in this section. Fig.6.8 to Fig.6.11 shows the variation of sound power levels (dB) due to the variation in the material composition, aspect ratio and boundary condition of various bio-inspired composite beams. The beam is subjected to F_x^5 type VAL is considered for this study and the effect of axial load intensity on the acoustic response properties is studied by varying its value as 0Pcr, 0.5Pcr and 0.99Pcr. The sound power level (dB) of the fundamental mode is dropping to the minimum values with increase in the axial load intensity from 0 to its critical value as shown from Fig.6.8(a) to Fig.6.8(c). It is due to the influence of axial load intensity on the structural stiffness of the bio-inspired composite beams.

From Fig.6.8 and 6.9, one can notice that the low stiff thin beams (L/h=20)

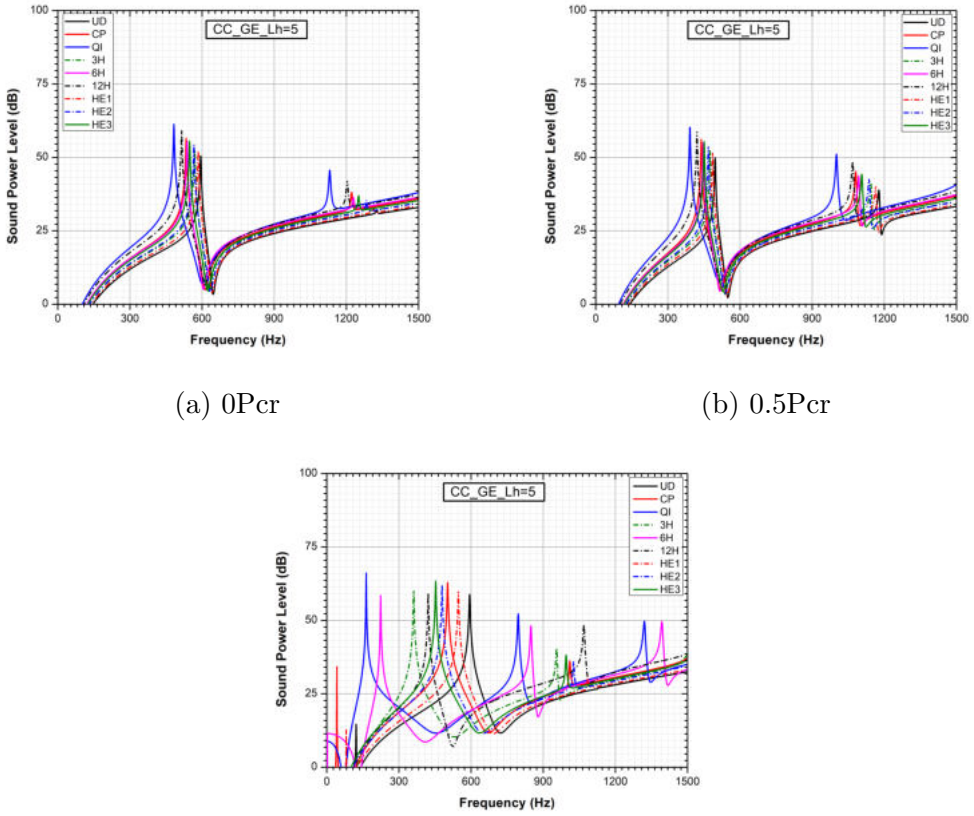

(a) 0Pcr

(b) 0.5Pcr

(c) 0.99Pcr

Figure 6.8: Effect of axial load intensity on sound power levels (dB) of Glass/Epoxy bio-inspired composite beam with L/h=5 and CC end conditions

radiates higher sound power level (dB) than thick beams (L/h=5) as expected. Similar variation can be observed with respect to material property also as seen in Fig.6.9 and 6.10, where, Glass/Epoxy beams have higher sound power levels (dB) compared to Carbon/Epoxy beams. Similar trends can be clearly seen between the SWLs of thin and thick beams shown in Fig.6.9 and Fig.6.10. The acoustic response study findings are coinciding with the findings of buckling and vibration studies with respect to various parameters. Octave bands and overall sound power levels of thick (L/h=20) composite beams and for 6H lamination scheme is presented in Fig.6.12. The octave band plot shown in Fig.6.12 are strongly following the trends observed in the earlier sound power levels plots. This signifies that the buckling strength, vibration frequencies and sound power levels are highly influenced by the stiffness of the bio-inspired composite beams. This also can be clearly seen in the octave band plots shown for change in the material composition Fig.6.12(a) and Fig.(b) and, also for the change in boundary condition

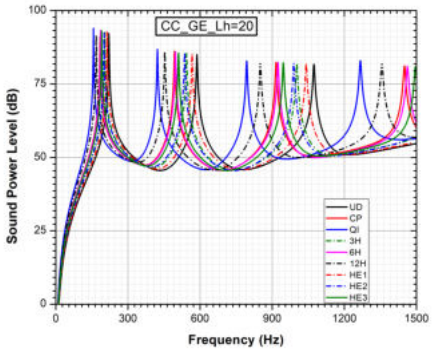

(a) 0Pcr

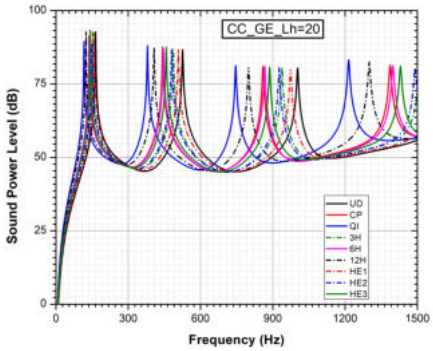

(b) 0.5Pcr

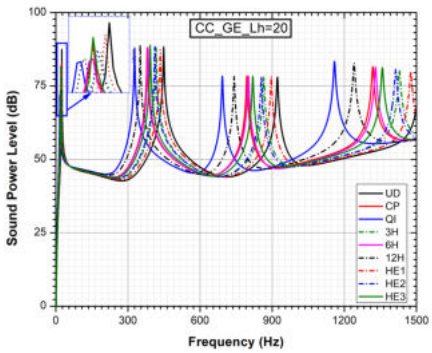

(c) 0.99Pcr

Figure 6.9: Effect of axial load intensity on sound power levels (dB) of Glass/Epoxy bio-inspired composite beam with L/h=20 and CC end conditions

as shown in Fig.6.12(b) and (c) for the variation in the stiffness component. It is also observed that the octave band plots clearly shows higher sound power levels at the critical buckling load in the lower frequency band of various bio-inspired composite beams. This stiffness effect also reflects the overall levels as shown in Fig.6.12(d), with CF boundary conditions exhibiting higher levels compared to SS and CC conditions. Sound radiation efficiency is presented in Fig.6.13(a) and (b) for the two material compositions and for the 6H lamination type CC bio-inspired composite beams with aspect ratio L/h=20. There is no much noticeable variation in the radiation efficiency is observed with the increase in the buckling load intensity. The sound pressure levels (dB) are presented as contour plots in Table 6.8 and 6.9, and as, directivity pattern plots in Fig.6.14 for 6H lamination scheme of Carbon/Epoxy bio-inspired composite beams with aspect ratio L/h=20 for the three boundary conditions. From the contour pressure plots for fundamental mode of SS, CF and CC boundary conditions shown in Table 6.8

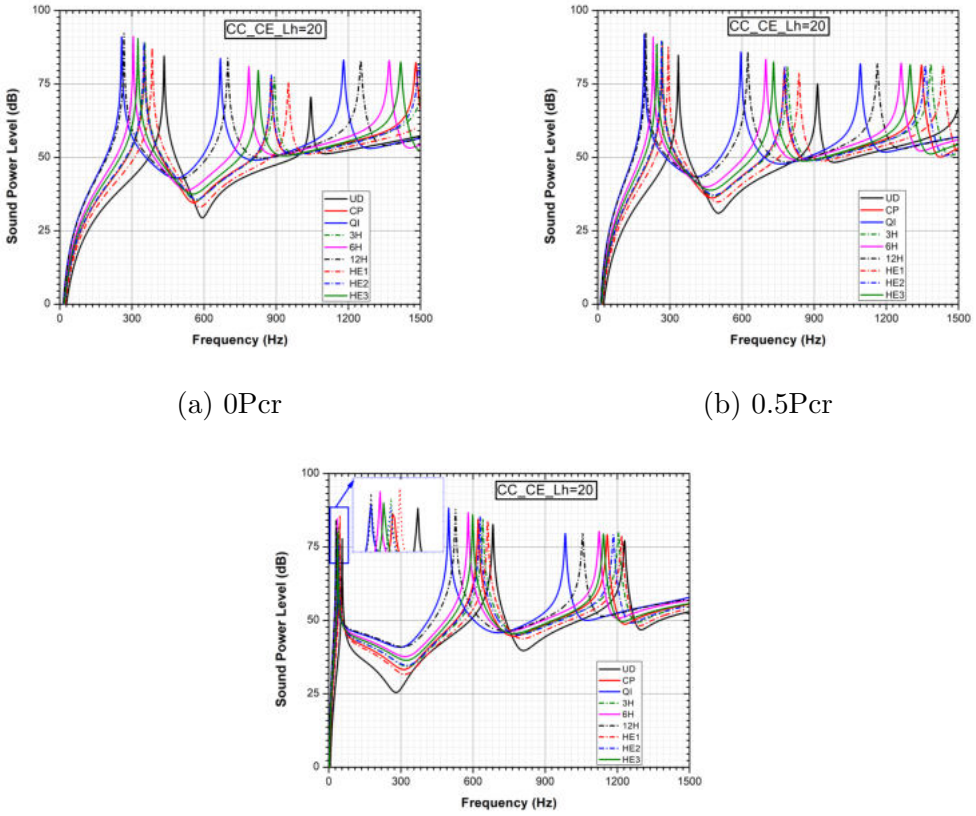

(a) 0Pcr

(b) 0.5Pcr

(c) 0.99Pcr

Figure 6.10: Effect of axial load intensity on sound power levels (dB) of Carbon/Epoxy bio-inspired composite beam with L/h=20 and CC end conditions

and 6.9, it is evident that the sound pressure levels (dB) decrease with increase in the buckling load intensity. It can be noticed that the rate of decrease in the sound pressure levels (dB) from 0.5Pcr to 0.99Pcr buckling load intensity is higher compared to axial load intensity increment from 0Pcr to 0.5Pcr. The third mode of CC bio-inspired composite beams with respect to increase in applied load are seen in third mode contour plots shown in Table 6.9. This can be seen in terms of significant decrease in the sound pressure levels for the variation in the buckling load intensity from 0.5Pcr to 0.99Pcr. The directivity pattern plots for the first mode of SS and CC boundary conditions as shown in Fig.6.14(a) and (b), also indicate that the sound pressure levels are following the first mode shape pattern. The sound pressure levels (dB) are decreasing with increase in the intensity of axial load as observed in the contour plot study. The levels are almost coinciding for third mode of CC bio-inspired composite beam as shown in Fig.6.14(c) while, the pattern is coinciding with the variation of the third mode with the axial load

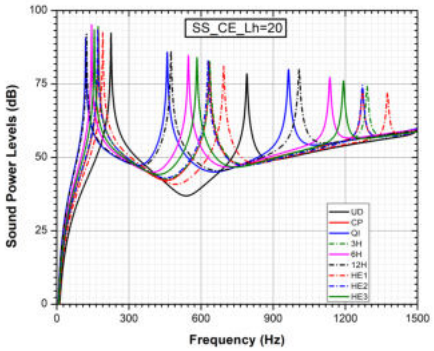

(a) 0Pcr

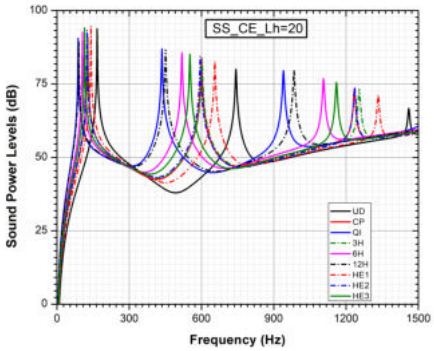

(b) 0.5Pcr

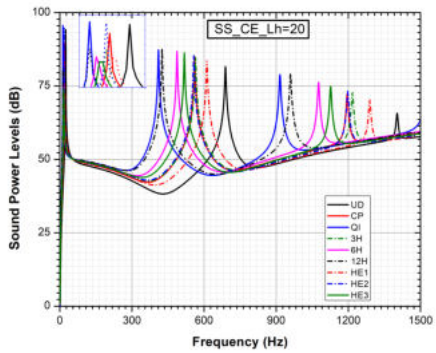

(c) 0.99Pcr

Figure 6.11: Effect of axial load intensity on sound power levels (dB) for various types of Carbon/Epoxy bio-inspired composite beam with L/h=20 and SS end conditions

intensity.

6.2 Closure

This study provides comprehensive insights into the buckling, dynamic, and acoustic responses of bio-inspired beams, shedding light on their unique characteristics and potential applications. The analysis of non-dimensional buckling loads reveals that the buckling behaviour of bio-inspired beams is significantly influenced by various factors, including aspect ratios, layup schemes, and boundary conditions. Furthermore, the free vibration study conducted in this study demonstrates the substantial impact of material composition, aspect ratios, and layup schemes on the natural frequencies and modal damping of bio-inspired beams. While, the forced vibration study strengthened buckling and free vi-

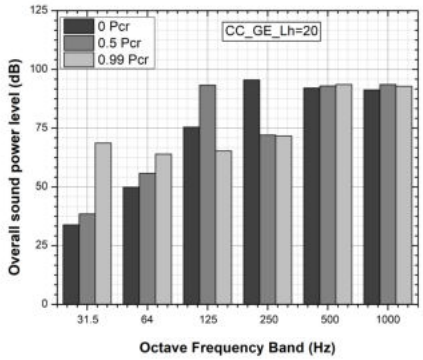

(a) Glass/Epoxy of CC beam

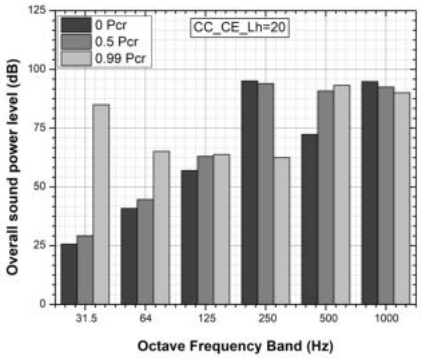

(b) Octave band of CC beam

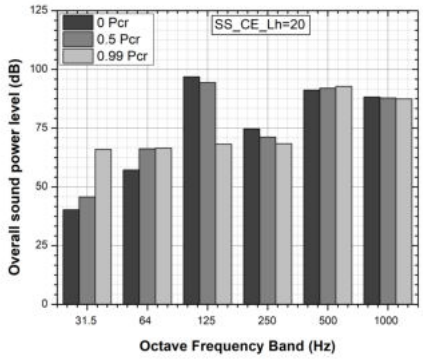

(c) Octave band of SS beam

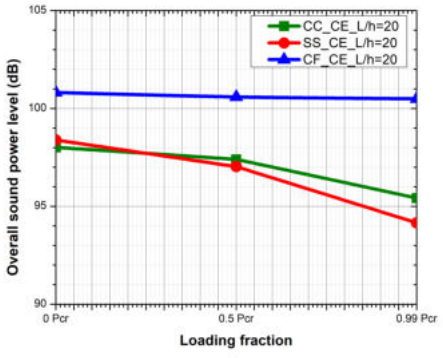

(d) Overall octave band

Figure 6.12: Octave band and overall sound power level representation of bio-inspired composite beams with L/h=20

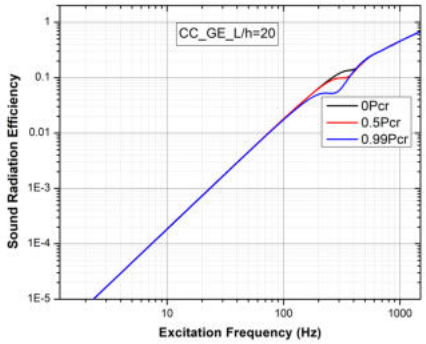

(a) Glass/Epoxy CC beam with $\frac{L}{h}$=20

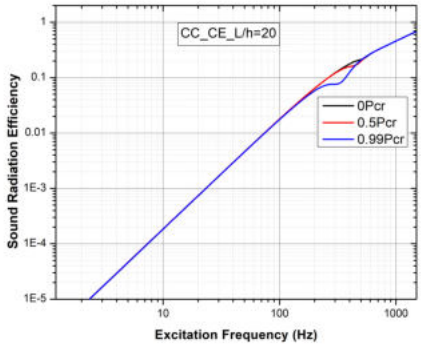

(b) Carbon/Epoxy CC beam with $\frac{L}{h}$=20

Figure 6.13: Effect of material on radiation efficiency of CC bio-inspired composite beams with L/h=20

brational studies . The results indicate that these factors play a crucial role in

Table 6.8: Significance of axial load intensity on the sound pressure levels of SS and CF 0/6.../90 layup bio-inspired composite beams for their first mode

P_{cr}	SS	CF
0	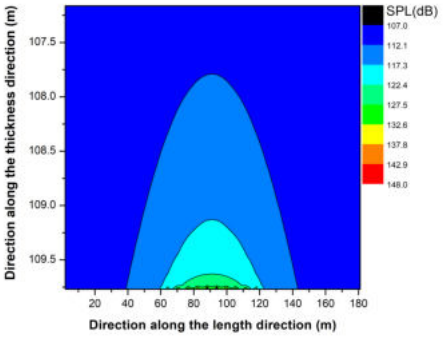	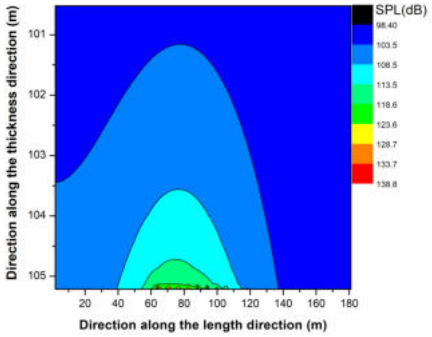
0.5	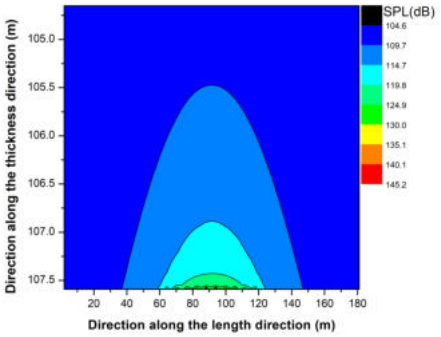	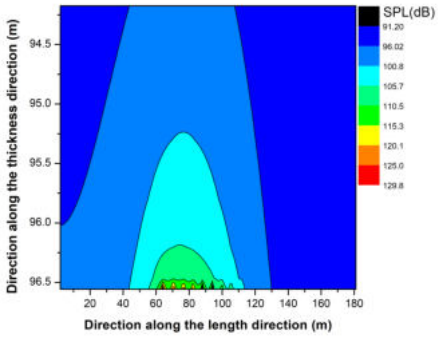
0.99	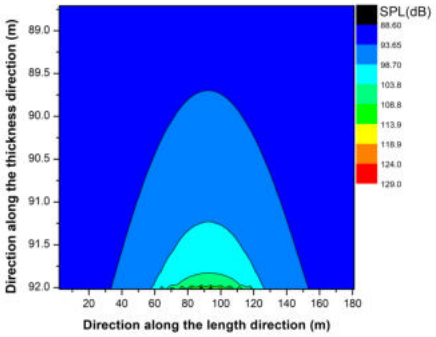	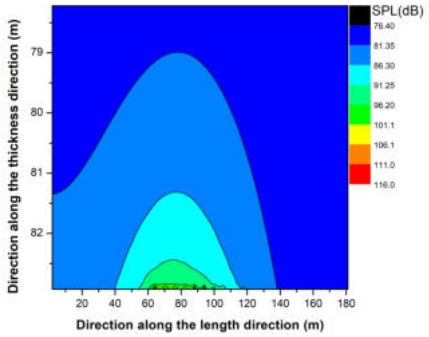

determining the dynamic behaviour and response of such beams. In addition to the dynamic aspects, the investigation of acoustic responses provides valuable insights into the relationship between the beam characteristics of bio-inspired beams and their sound radiation properties. The correlation between sound power levels

Table 6.9: Significance of axial load intensity on the sound pressure levels of CC 0/6.../90 layup bio-inspired composite beams for their first and third mode

P_{cr}	1^{st}Mode	3^{rd}Mode
0	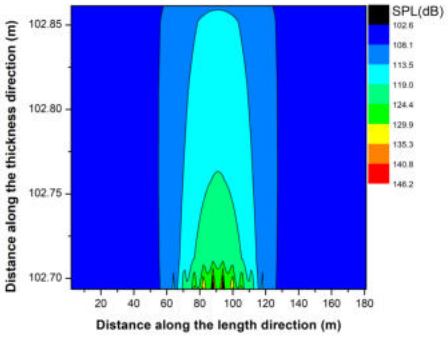	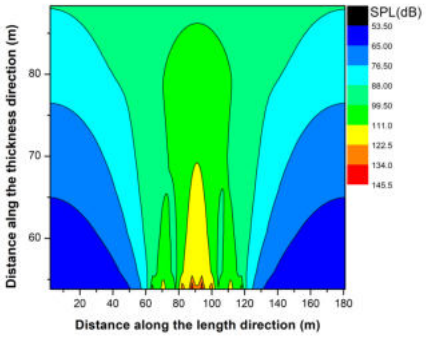
0.5	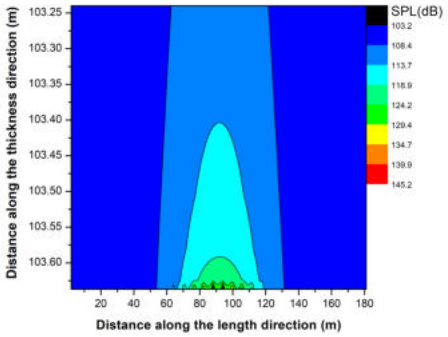	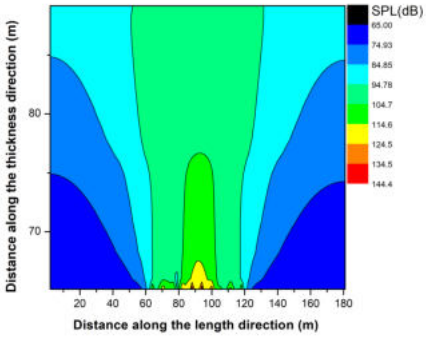
0.99	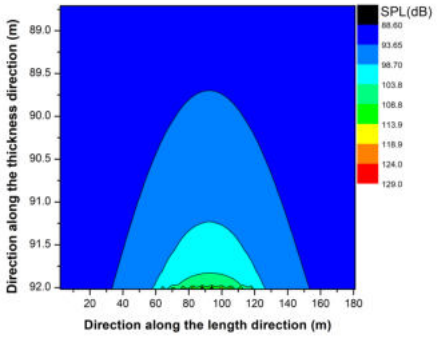	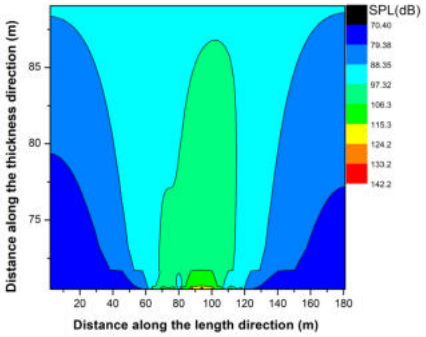

and various structural parameters is highlighted.

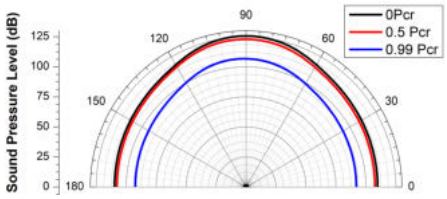

(a) First mode of SS Beam

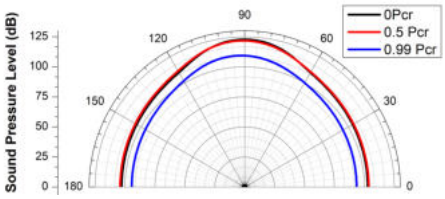

(b) First mode of CC Beam

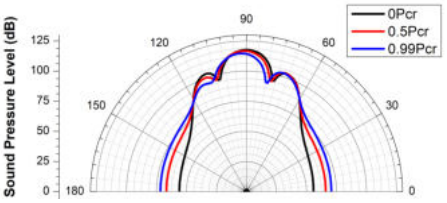

(c) Third mode of CC Beam

Figure 6.14: Directivity pattern representation of bio-inspired composite beams with L/h=20

Chapter 7

SUMMARY AND CONCLUSION

7.1 Summary

A comprehensive numerical investigation is executed to study the buckling, vibration and acoustic responses of isotropic, B-FGM and bio-inspired laminated composite beams subjected to different types of VALs. Ritz method and higher order beam theories are used in the determination of buckling and natural frequencies of isotropic, B-FGM and bio-inspired beams. The forced vibration responses are calculated using the modal super position method and is fed as an input to Rayleigh integral in order to calculate the sound characteristics. In order to validate the current study, a comparative study has been detailed with the results of earlier literature. An elaborative investigation has been carried for analysing the influence of six different types of VALs on the buckling characteristics of isotropic, B-FGM and bio-inspired beams. The buckling study is further extended for beams with various boundary conditions, material composition variation and also for two different aspect ratios. By varying the intensity of buckling load from 0 to its critical value an exclusive study on free vibration characteristics of isotropic, B-FGM beams and bio-inspired has been elucidated. The acoustic response study includes the analysis on sound power levels, sound radiation efficiency and sound pressure levels for buckling load intensities 0 P_{cr}, 0.5 P_{cr} and 0.99 P_{cr}. Sound power level (dB) study was elucidated in individual frequencies and in octave band frequencies within the selected frequency band. Sound pressure levels (dB) are represented as contour plots and directivity pattern.

7.2 Conclusion

7.2.1 Isotropic Beam

From the study of aluminium beam for buckling, vibration and acoustic behaviours the following conclusions are drawn:

• Critical buckling loads are highly sensitive to the type of variation of VAL and boundary conditions.

• Rise in the intensity of VAL leads to significant reduction in natural frequencies and the fundamental frequency approaches zero when the magnitude of the applied load is equal to buckling load.

• Sound power resonant values are influenced by the intensity of VAL and the variation in the resonant amplitude for different intensities of the axial load is clearly seen for the CC beam compared to the SS and CF beams. For instance, this insight can guide the design of aircraft components with specific attention to clamping conditions to optimize noise reduction strategies.

• Significant changes in sound power level are seen in lower frequency bands while there is not much variation in overall sound power level with variation in magnitude of the applied VAL.

7.2.2 B-FGM beam

The numerical investigation is further extended in determining the buckling and natural frequencies and sound radiation characteristics of B-FGM beams. Important observations from the present study are.

• The increment of gradation index along thickness direction is more influential on the dimensionless buckling loads of B-FGM beams compared to lengthwise direction gradation index increment. It has particular relevance in the aerospace context, where optimizing material properties for enhanced structural performance is a critical consideration.

• Quadratically decreasing VAL (F_x^5) yields higher dimensionless BLs compared to the rest of the load cases, while quadratically increasing VAL (F_x^4) showed the least buckling resistance.

• Nature of VALs, gradation indexes, and end conditions are also affecting the buckling mode shapes. This knowledge is very crucial for designing aerospace structures that demand precise control over buckling behaviours.

• Sound power levels (dB) are significantly influenced both the gradation indexes

P_x and P_z.

• As anticipated, thin beams have a great impact on sound power levels compared to thick beams. It holds practical implications for aircraft design, where weight considerations often favour the use of thinner structural elements.

• It is noteworthy that end stiffness has a greater impact on the natural frequencies of the B-FGM beams compared to sound power levels, as marginal variation in the sound power levels is observed for the change in end stiffness.

• The directivity pattern clearly indicates a significant variation in the sound pressure levels with an increase in the axial load intensity. It is valuable for optimizing the acoustic performance of B-FGM beams under different loading conditions.

• With the reduction in the structural stiffness at the critical buckling load, the structures vibrate more critically, resulting in an increase in the acoustic response levels. It highlights the intricate relationship between structural stability and acoustic behaviour,

7.2.3 Bio-Inspired composite beams

Major finding on the buckling, dynamic, and acoustic responses of the bio-inspired composite beam are outlined as follows:

• Buckling loads of the bio-inspired composite beams are influenced by aspect ratios, layup schemes, and boundary conditions.

• Quadratically decreasing type of VAL exhibits higher buckling resistance compared to uniformly distributed and parabolic varying type of VAL.

• Natural frequencies of the bio-inspired composite beams are affected by material composition, aspect ratios, and layup schemes. This aids in tailoring the material selection for bio-inspired components in aerospace designs.

• Carbon/Epoxy beams have higher natural frequencies than Glass/Epoxy beams due to their higher elastic modulus.

• The dominant layup scheme for improved natural frequencies is in the ascending order of uni-directional (UD) layup, followed by the HE's, CP, H's, and QI layup schemes. This hierarchy provides clear guidelines for optimizing the layup configurations of bio-inspired composite beams to achieve specific natural frequency performances.

• Damping values decrease with increasing aspect ratios and are influenced by the end conditions and layup schemes, with UD and CP layups exhibiting lower damping compared to QI layup.

• Glass/Epoxy beams radiate higher sound than Carbon/Epoxy beams.
• Sound pressure levels (dB) and directivity patterns follow the free vibration mode shapes of bio-inspired composite beams with higher sound pressure levels at critical buckling load.

7.3 Scope for Future Research

In the current study buckling, natural frequencies and acoustic responses of isotropic, B-FGM and bio-inspired beams were investigated for variation in the material gradation, in-plane axial loads, boundary conditions and aspect ratios. The study can further be investigated in future for
• The bi-directional functional graded and bio-inspired beams are further investigated for vibro-acoustic responses by treating the beams with porosity.
• The dynamic responses of various composite laminates can also be investigated for dynamic loading.

Appendix A

$K_{11}(i,j) = A\int_{-\frac{L}{2}}^{\frac{L}{2}} \Theta_{i,x}\Theta_{j,x}dx;$

$K_{12}(i,j) = -B\int_{-\frac{L}{2}}^{\frac{L}{2}} \Theta_{i,x}\varphi_{j,xx}dx$

$K_{13}(i,j) = -B_s\int_{-\frac{L}{2}}^{\frac{L}{2}} \Theta_{i,x}\psi_{j,x}dx;$

$K_{22}(i,j) = D\int_{-\frac{L}{2}}^{\frac{L}{2}} \varphi_{i,xx}\varphi_{j,xx}dx$

$K_{23}(i,j) = H\int_{-\frac{L}{2}}^{\frac{L}{2}} \varphi_{i,xx}\varphi_{j,x}dx;$

$K_{33}(i,j) = D_s\int_{-\frac{L}{2}}^{\frac{L}{2}} \varphi_{i,xx}\varphi_{j,xx}dx + A_s\int_{-\frac{L}{2}}^{\frac{L}{2}} \varphi_{i,x}\varphi_{j,x}dx$

$S_{22}(i,j) = \int_{-\frac{L}{2}}^{\frac{L}{2}} P(x)\left(\int_{-\frac{L}{2}}^{x} \varphi_{i,x}\varphi_{j,x}dx\right)dx$

$M_{11}(i,j) = \int_{-\frac{L}{2}}^{\frac{L}{2}} I_0\Theta_i\Theta_j dx;$

$M_{12}(i,j) = -\int_{-\frac{L}{2}}^{\frac{L}{2}} I_1\Theta_i\varphi_{j,x}dx$

$M_{13}(i,j) = \int_{-\frac{L}{2}}^{\frac{L}{2}} J_1\Theta_i\psi_{j,x}dx;$

$M_{22}(i,j) = \int_{-\frac{L}{2}}^{\frac{L}{2}} (I_0\varphi_i\varphi_j + I_2\varphi_{i,x}\varphi_{j,x})dx$

$M_{23}(i,j) = \int_{-\frac{L}{2}}^{\frac{L}{2}} (I_0\varphi_i\varphi_j + J_2\varphi_{i,x}\zeta_{j,x})dx;$

$M_{33}(i,j) = \int_{-\frac{L}{2}}^{\frac{L}{2}} (I_0\zeta_i\zeta_j + K_1\zeta_{i,x}\zeta_{j,x})dx$

Appendix B

$$K_{11}(i,j) = A\int_{-\frac{L}{2}}^{\frac{L}{2}} \Theta_{i,x}\Theta_{j,x}dx,$$

$$K_{12}(i,j) = -B\int_{-\frac{L}{2}}^{\frac{L}{2}} \Theta_{i,x}\varphi_{j,xx}dx,$$

$$K_{13}(i,j) = -B_s\int_{-\frac{L}{2}}^{\frac{L}{2}} \Theta_{i,x}\zeta_{j,xx}dx,$$

$$K_{14}(i,j) = X\int_{-\frac{L}{2}}^{\frac{L}{2}} \Theta_{i,x}\psi_j dx,$$

$$K_{22}(i,j) = D\int_{-\frac{L}{2}}^{\frac{L}{2}} \varphi_{i,xx}\varphi_{j,xx}dx,$$

$$K_{23}(i,j) = H\int_{-\frac{L}{2}}^{\frac{L}{2}} \varphi_{i,xx}\zeta_{j,xx}dx,$$

$$K_{24}(i,j) = -Y\int_{-\frac{L}{2}}^{\frac{L}{2}} \varphi_{i,xx}\psi_j dx,$$

$$K_{33}(i,j) = D_s\int_{-\frac{L}{2}}^{\frac{L}{2}} \zeta_{i,xx}\zeta_{j,xx}dx + A_s\int_{-\frac{L}{2}}^{\frac{L}{2}} \zeta_{i,x}\zeta_{j,x}dx,$$

$$K_{34}(i,j) = -Y_s\int_{-\frac{L}{2}}^{\frac{L}{2}} \zeta_{i,xx}\psi_j dx + A_s\int_{-\frac{L}{2}}^{\frac{L}{2}} \zeta_{i,x}\psi_{j,x}dx,$$

$$K_{44}(i,j) = Z\int_{-\frac{L}{2}}^{\frac{L}{2}} \zeta_i\zeta_j dx + A_s\int_{-\frac{L}{2}}^{\frac{L}{2}} \zeta_{i,x}\zeta_{j,x}dx,$$

$$S_{22}(i,j) = \int_{-\frac{L}{2}}^{\frac{L}{2}} P(x)\left(\int_{-\frac{L}{2}}^{x} \varphi_{i,x}\varphi_{j,x}dx\right)dx$$

$$S_{23}(i,j) = \int_{-\frac{L}{2}}^{\frac{L}{2}} P(x)\left(\int_{-\frac{L}{2}}^{x} \varphi_{i,x}\zeta_{j,x}dx\right)dx$$

$$S_{24}(i,j) = \int_{-\frac{L}{2}}^{\frac{L}{2}} P(x)\left(\int_{-\frac{L}{2}}^{x} \zeta_{i,x}\zeta_{j,x}dx\right)dx$$

$$M_{11}(i,j) = \int_{-\frac{L}{2}}^{\frac{L}{2}} I_0\Theta_i\Theta_j dx$$

$$M_{12}(i,j) = -\int_{-\frac{L}{2}}^{\frac{L}{2}} I_1\Theta_i\varphi_{j,x}dx$$

$$M_{13}(i,j) = \int_{-\frac{L}{2}}^{\frac{L}{2}} J_1\Theta_i\psi_{j,x}dx$$

$$M_{22}(i,j) = \int_{-\frac{L}{2}}^{\frac{L}{2}} (I_0\varphi_i\varphi_j + I_2\varphi_{i,x}\varphi_{j,x})dx$$

$$M_{23}(i,j) = \int_{-\frac{L}{2}}^{\frac{L}{2}} (I_0\varphi_i\zeta_j + J_3\varphi_{i,x}\zeta_{j,x})dx$$

$$M_{24}(i,j) = \int_{-\frac{L}{2}}^{\frac{L}{2}} J_2\varphi_i\psi_j dx$$

$$M_{33}(i,j) = \int_{-\frac{L}{2}}^{\frac{L}{2}} (I_0\zeta_i\zeta_j + K_1\zeta_{i,x}\zeta_{j,x})dx$$

$$M_{34}(i,j) = \int_{-\frac{L}{2}}^{\frac{L}{2}} J_2\zeta_i\psi_j dx$$

$$M_{44}(i,j) = \int_{-\frac{L}{2}}^{\frac{L}{2}} K_2\psi_i\psi_j dx$$

REFERENCES

Abo-bakr R.M., Abo-bakr H.M., Mohamed S.A., Eltaher M.A. (2021). "Optimal weight for buckling of FG beam under variable axial load using Pareto optimality",*Composite Structures*, 258: 113193.

Alshabatat N.T., Naghshineh K. (2014)." Optimization of natural frequencies and sound power of beams using functionally graded material",*Advances in Acoustics and Vibration*, 2014: Article ID 752361.

Alazwari M.A., Mohamed S., Eltaher M. (2022). "Vibration analysis of laminated composite higher order beams under varying axial loads",*Ocean Engineering*, vol. 252, p. 111203.

Almitani K.H., Mohamed N., Alazwari M.A., Mohamed S. A., Eltaher M. A. (2022). "Exact solution of nonlinear behaviours of imperfect bioinspired helicoidal composite beams resting on elastic foundations," *Mathematics*, vol. 10, no. 6, p. 887.

Akgöz B., Civalek O. (2013). "Buckling analysis of functionally graded microbeams based on the strain gradient theory",*Acta Mechanica* 224 (9) 2185–2201.

Arunkumar M., Jagadeesh M., Pitchaimani J., Gangadharan K., Babu M.L. (2014). "Sound radiation and transmission loss characteristics of a honeycomb sandwich panel with composite facings: Effect of inherent material damping",*Journal of Sound and Vibration*, vol. 383, pp. 221232.

Aydogdu M. (2005). "Vibration analysis of cross-ply laminated beams with general boundary conditions by Ritz method" *International Journal of Mechanical Sciences*, 47(11): 1740–1755.

Aydogdu M. (2006). "Buckling analysis of cross-ply laminated beams with general boundary conditions by Ritz method",*Composites Science and Technology*,

66(10): 1248–1255.

Aydogdu M., V. Taskin (2007). "Free vibration analysis of functionally graded beams with simply supported edges",*Materials & design*, vol. 28, no. 5, pp. 1651-1656.

Banerjee J., Ananthapuvirajah A. (2018)." Free vibration of functionally graded beams and frameworks using the dynamic stiffness method",*Journal of Sound and Vibration* 422 34–47.

Barati A., Adeli M.M., Hadi A. (2020)."Static torsion of bi-directional functionally graded microtube based on the couple stress theory under magnetic field", *International Journal of Applied Mechanics* 12 (02) 2050021.

Barati A., Hadi A., Nejad M.Z., Noroozi R. (2022)."On vibration of bi-directional functionally graded nanobeams under magnetic field", *Mechanics Based Design of Structures and Machines* 50 (2) 468–485.

Chakraverty S., Behera L. (2015). "Free vibration of non-uniform nanobeams using Rayleigh-Ritz method",*Physica E: Low-Dimensional Systems and Nanostructures*, 67: 38–46.

Chew E., Liu J., Tay T., Tran L., Tan V. (2021). Improving the mechanical properties of natural fibre reinforced laminates composites through biomimicry," Composite Structures, vol. 258, p. 113208.

Cheng L., Thomas A., Glancey J.L., Karlsson A.M. (2011). "Mechanical behaviour of bio-inspired laminated composites", *Composites Part A: Applied Science and Manufacturing*, vol. 42, no. 2, pp. 211-220.

Chandra R., Singh S., Gupta K. (1999). " Damping studies in fiber-reinforced composites a review",*Composite structures*, vol. 46, no. 1, pp. 4151.

Dash S., Chakraborty S., Dey T., Kumar R. (2022). "Buckling and free vibration analysis of randomly distributed cnt reinforced composite beam under thermomechanical loading",*European Journal of Mechanics-A/Solids*, vol. 96, p. 104749.

Dangi C., Saini S., Lal R., Singh I.V. (2020). "Size dependent FEM model for bi-directional functionally graded nano-beams",*Materials Today: Proceedings* 24 1302–1311.

Denli H., Sun J.Q. (2007). "Structural-acoustic optimization of sandwich structures with cellular cores for minimum sound radiation",*Journal of Sound and Vibration*, 301(1–2): 93–105.

Eltaher M.A., Mohamed S.A.. (2020) "Buckling and stability analysis of sandwich beams subjected to varying axial loads",*Steel and Composite Structures* 34 (2) 241–260.

George, N., Jeyaraj, P. (2018). "Nonuniform heat effects on buckling of laminated composite beam: experimental investigations", *International Journal of Structural Stability and Dynamics*, 18(12), 1850153.

Giunta G., Crisafulli D., Belouettar S., Carrera E. (2011). "Hierarchical theories for the free vibration analysis of functionally graded beams",*Composite Structures* 94 (1) 68–74.

Ghannadpour S.A., Mohammadi B., Fazilati J. (2013). "Bending, buckling and vibration problems of nonlocal Euler beams using Ritz method",*Composite Structures*, 96: 584–589.

Hadi A., Nejad M.Z., Rastgoo A., Hosseini M. (2018). "Buckling analysis of FGM Euler-Bernoulli nano-beams with 3D-varying properties based on consistent couple-stress theory," *Steel and Composite Structures*, 26(6), 663–672.

Hadi A., Nejad M.Z., Hosseini M. (2018). "Vibrations of three-dimensionally graded nanobeams",*International Journal of Engineering Science* 128 12–23.

Harsha B., Jeyaraj P., Lenin B. (2021). "Effect of porosity and profile axial loading on elastic buckling and free vibration of functionally graded porous beam",*[in:] IOP Conference Series: Materials Science and Engineering*, 1128: 012025, IOP Publishing.

Hamed M.A., Abo-bakr R.M., Mohamed S.A., Eltaher M.A.(2020). "Influence of axial load function and optimization on static stability of sandwich functionally graded beams with porous core",*Engineering with Computers*, 36(4): 1929-1946.

Hamed M.A., S.A. Mohamed, M.A. Eltaher (2020). "Buckling analysis of sandwich beam rested on elastic foundation and subjected to varying axial in-plane loads",*Steel and Composite Structures* 34 (1) 75–89.

Heydari A.(2011). "Buckling of functionally graded beams with rectangular and annular sections subjected to axial compression",*Advanced Design and Manufacturing Technology* 5 (1).

Huang, Y., Li X. F. (2010)."A new approach for free vibration of axially functionally graded beams with non-uniform cross-section." *Journal of sound and vibration*, 329(11), 2291-2303.

Huang Y. and Li X.-F (2010)."A new approach for free vibration of axially functionally graded beams with non-uniform cross-section",*Journal of sound and vibration*, vol. 329, no. 11, pp. 2291-2303.

Ilanko S., Monterrubio L., Mochida Y. (2014). "The Rayleigh-Ritz Method for Structural Analysis",*John Wiley & Sons*.

Jaworski J.W., Dowell E.H. (2008). "Free vibration of a cantilevered beam with multiple steps: Comparison of several theoretical methods with experiment",*Journal of Sound and Vibration*, 312(4–5): 713–725.

Kahya, V., Karaca S., Okur F. Y., Altunışık, A. C., Aslan, M. (2019). "Free vibrations of laminated composite beams with multiple edge cracks: Numerical model and experimental validation". *International Journal of Mechanical Sciences*, 159, 30-42.

Kanade S.A., Chinnapandi L.B.M., Jeyaraj P., Subramanian J. (2021). "Buckling and vibration behaviour of composite beam due to axially varying in-plane loads",*in: IOP Conference Series: Materials Science and Engineering*, Vol. 1128, IOP Publishing, 012043.

Kadoli R., Akhtar K., Ganesan N. (2008). "Static analysis of functionally graded beams using higher order shear deformation theory",*Applied Mathematical Modelling* 32 (12) 2509–2525.

Karamanli A. (2018)."Free vibration analysis of two directional functionally graded beams using a third order shear deformation theory", *Composite Structures* 189, 127–136.

Karamanli A., Aydogdu M. (2019a). "On the vibration of size dependent rotating laminated composite and sandwich microbeams via a transverse shearnormal deformation theory",*Composite Structures*, 216: 290–300.

Karamanli A., Aydogdu M. (2019b)."Buckling of laminated composite and sandwich beams due to axially varying in-plane loads",*Composite Structures*, 210: 391–408

Khoram M.M., Hosseini M., Hadi A., Shishehsaz M. (2020). "Bending analysis of bidirectional FGM Timoshenko nanobeam subjected to mechanical and magnetic forces and resting on Winkler–Pasternak foundation", *International Journal of Applied Mechanics* 12 (08) 2050093.

Kumar S. (2022)" Vibration analysis of non-uniform axially functionally graded beam resting on pasternak foundation",*Materials Today: Proceedings*. 62, 619-623.

Larbi L.O, Kaci A., Houari M.S.A., Tounsi A. (2013). "An efficient shear deformation beam theory based on neutral surface position for bending and free vibration of functionally graded beams",*Mechanics Based Design of Structures and Machines* 41 (4) 421–433.

Liao F.S., Su A.C, Hsu T.-C. J. (1994). "Vibration damping of interleaved carbon fiber-epoxy composite beams",*Journal of Composite Materials*, vol. 28, no. 18, pp. 1840-1854.

Li H., Niu Y.,Li Z. ,Xu Z., Han Q. (2020). "Modeling of amplitude-dependent damping characteristics of fiber reinforced composite thin plate",*Applied Mathematical Modelling*, vol. 80, pp. 394-407.

Liu J., Lee H., Tan V. (2018). "Effects of inter-ply angles on the failure mechanisms in bioinspired helicoidal laminates," *Composites Science and Technology*, vol. 165, pp. 282-289.

Li J., Hu X.,Li X. (2016). "Free vibration analyzes of axially loaded laminated composite beams using a unified higher-order shear deformation theory and dynamic stiffness method," *Composite Structures*, 158, 308–322.

Li J., Hu X., Li X. (2016). "Free vibration analyzes of axially loaded laminated composite beams using a unified higher-order shear deformation theory and dynamic stiffness method", *Composite Structures*, 158, 308-322.

Li Q., Yang D. (2020). "Vibro-acoustic performance and design of annular cellular structures with graded auxetic mechanical metamaterials",*Journal of Sound*

and Vibration, 466: 115038.

Leissa A.W. (2005). "The historical bases of the Rayleigh and Ritz methods",*Journal of Sound and Vibration*, 287(4–5): 961–978.

Li X.F., Wang B.L. , Han J.C. (2010). "A higher-order theory for static and dynamic analyzes of functionally graded beams",*Archive of Applied Mechanics* 80 (10) 1197–1212.

Mareishi, S., Rafiee M., He X.Q., Liew K. M. (2014). "Nonlinear free vibration, postbuckling and nonlinear static deflection of piezoelectric fiber-reinforced laminated composite beams", *Composites Part B: Engineering*, 59, 123-132.

Majkut L. (2006). "Acoustical diagnostics of cracks in beam like structures",*Archives of Acoustics*, 31(1): 17–28.

Melaibari A., Wagih A., Basha M., Kabeel A., Lubineau G., Eltaher M. (2021). "Bio-inspired composite laminate design with improved out-of-plane strength and ductility". *Composites Part A: Applied Science and Manufacturing*, vol. 144, p. 106362.

Melaibari A., Abo-bakr R.M. , Mohamed S., Eltaher M. (2020). "Static stability of higher order functionally graded beam under variable axial load",*Alexandria Engineering Journal* 59 (3) 1661–1675.

Melaibari A., Khoshaim A.B., Mohamed S.A., Eltaher M.A. (2020). "Static stability and of symmetric and sigmoid functionally graded beam under variable axial load",*Steel and Composite Structures*, 35(5): 671– 685.

Mohamed, N., Mohamed S. A., Abdelrhmaan A. A., Eltaher M. A. (2023). "Nonlinear stability of bio-inspired composite beams with higher order shear theory." *Steel and Composite Structures*, 46(6), 759.

Mohamed N., Mohamed S. A., Eltaher M. A. (2022)."Nonlinear static stability of imperfect bio-inspired helicoidal composite beams," *Mathematics*, vol. 10, no. 7, p. 1084.

Nguyen N.-D., Nguyen T.-K., Vo T.P., Thai H.-T. (2018). "Ritz-based analytical solutions for bending, buckling and vibration behaviour of laminated composite beams",*International Journal of Structural Stability and Dynamics*, 18(11):

1850130.

Nguyen T.K, Nguyen T.T.P., Vo T.P., Thai H.-T. (2015). "Vibration and buckling analysis of functionally graded sandwich beams by a new higher-order shear deformation theory",*Composites Part B: Engineering* 76 273–285.

Nguyen T.K., Nguyen B.D. (2015). "A new higher-order shear deformation theory for static, buckling and free vibration analysis of functionally graded sandwich beams",*Journal of Sandwich Structures and Materials* 17 (6) 613–631.

Nguyen T.K, Nguyen B.D., Vo T.P., Thai H.T. (2020)."A novel unified model for laminated composite beams",*Composite Structures* 238 111943.

Ni R., Adams R. (1984). "The damping and dynamic moduli of symmetric laminated composite beams—theoretical and experimental results",*Journal of Composite Materials*, vol. 18, no. 2, pp. 104-121.

Noroozi R., Barati A., Kazemi A., Norouzi S., Hadi A. (2020). "Torsional vibration analysis of bi-directional functionally graded nano-cone with arbitrary cross-section based on nonlocal strain gradient elasticity", *Advanced Nano Research* 8 (1) 13–24.

Nejad M.Z., Hadi A. (2016). "Non-local analysis of free vibration of bi-directional functionally graded Euler–Bernoulli nano-beams", *International Journal of Engineering Science* 105, 1–11.

Nejad M.Z., Hadi A., Farajpour A.(2017). "Consistent couple-stress theory for free vibration analysis of Euler-Bernoulli nano-beams made of arbitrary bi-directional functionally graded materials", *Structural engineering and mechanics: An international journal* 63 (2) 161–169.

Nejad M.Z., Hadi A., Omidvari A., Rastgoo A. (2018). "Bending analysis of bi-directional functionally graded Euler-Bernoulli nano-beams using integral form of Eringen's non-local elasticity theory", *Structural engineering and mechanics: An international journal* 67 (4) 417–425.

Nejad M.Z., Hadi A., Rastgoo A. (2016). "Buckling analysis of arbitrary two-directional functionally graded Euler–Bernoulli nano-beams based on nonlocal elasticity theory", *International Journal of Engineering Science*, 103, 1–10.

Omidi Soroor A., Asgari M., Haddadpour H.(2021). "Effect of axially graded constraining layer on the free vibration properties of three layered sandwich beams with magnetorheological fluid core",*Composite Structures*, 255: 112899.

Ozer M.S, Koruk H., Sanliturk K. Y.(2020). "Development of an equivalent shell finite element for modelling damped multi-layered composite structures",*Composite Structures*, vol. 254, p. 112828.

Patil, H. H., Pitchaimani J., Eltaher M. A. (2023). "Buckling and vibration of beams using Ritz method: Effects of axial grading of GPL and axially varying load",*Mechanics of Advanced Materials and Structures*, 1-14.

Pradhan P., Sutar M.K., Pattnaik S. (2019). A state of the art in functionally graded materials and their analysis, Mater. Today Proc. 18 3931–3936.

Pradhan K.K, Chakraverty S. (2014). "Effects of different shear deformation theories on free vibration of functionally graded beams",*International Journal of Mechanical Sciences* 82 (2014) 149–160.

Priyanka R., Pitchaimani J. (2022). Static stability and free vibration characteristics of a micro laminated beam under varying axial load using modified couple stress theory and ritz method",*Composite Structures*, vol. 281, p. 115028.

Ruzzene M. (2004). "Vibration and sound radiation of sandwich beams with honeycomb truss core",*Journal of Sound and Vibration*, 277(4–5): 741–763.

Selmi A., Mustafa A.A. (2021)."Dynamic analysis of bi-dimensional functionally graded beams", *Mater. Today Proc.* 46 8675–8680.

Sayyad A.S. and Ghugal Y. M. (2017). "Bending, buckling and free vibration of laminated composite and sandwich beams: A critical review of literature," *Composite Structures*, vol. 171, pp. 486-504.

Sherafatnia K., Farrahi G., Faghidian S. A. (2014). "Analytic approach to free vibration and buckling analysis of functionally graded beams with edge cracks using four engineering beam theories," *International Journal of Engineering*, vol. 27, no. 6, pp. 979-990.

Şimşek M. (2010). "Fundamental frequency analysis of functionally graded beams by using different higher-order beam theories",*Nuclear Engineering and Design*

240 (4) 697–705.

Şimşek M., Kocatürk T. (2009). "Free and forced vibration of a functionally graded beam subjected to a concentrated moving harmonic load",*Composite Structures*. 90 (4) 465–473.

Sharma P., Gautam M., Chaturvedi M. (2022). "Effects of material grading and geometry on natural frequency of functionally graded beam",*Materials Today: Proceedings,* 62, 4222-4224.

Sharma P., Singh R. (2021). "A numerical study on free vibration analysis of axial FGM beam", *Materials Today: Proceedings* 44 1664–1668.

Sabah, S. A., Kueh A. B. H., Al-Fasih M. Y. (2017)."Comparative low-velocity impact behaviour of bio-inspired and conventional sandwich composite beams", *Composites Science and Technology*, 149, 64-74.

Spadoni A., Ruzzene M. (2006). "Structural and acoustic behaviour of chiral truss-core beams",*Journal of Vibration and Acoustics, Transactions of the ASME*, 128(5): 616–626.

Sina S., Navazi H., Haddadpour H. (2009)." An analytical method for free vibration analysis of functionally graded beams",*Materials Design*, vol. 30, no. 3, pp. 741-747.

Thai H.T, Vo T.P. (2012). "Bending and free vibration of functionally graded beams using various higher-order shear deformation beam theories",*International Journal of Mechanical Sciences* 62 (1) 57–66.

Talekar N., Kotambkar M. (2020). "Free vibration analysis of generally layered composite beam with various lay-up and boundary conditions". *Materials Today Proceedings*, 21, 1283-1292.

Tang H.B., Xu B.G. (2017). "Vibroacoustic modeling of an elastic beam in low subsonic flows with mean velocities", *European Journal of Mechanics and Solids,* 66: 322–328.

Torres-Romero J., Cardenas W., Carbajo J., Segovia Eulogio E.-G., Ramis-Soriano J. (2018). "An experimental approach to vibro-acoustic study of beam-type structures", *Archives of Acoustics*, 43(2): 283–295.

Vosoughi, A. R., Malekzadeh, P., Banan, M. R., Banan, M. R. (2012). Thermal buckling and postbuckling of laminated composite beams with temperature-dependent properties. International Journal of Non-Linear Mechanics, 47(3), 96-102.

Vo T.P., Thai H.-T., Aydogdu M. (2017). "Free vibration of axially loaded composite beams using a four-unknown shear and normal deformation theory," *Composite Structures*, 178, 406–414.

Vo T.P., Thai H.-T. , Nguyen T.-K., Inam F. (2014)." Static and vibration analysis of functionally graded beams using refined shear deformation theory",*Meccanica* 49 (1) 155–168.

Wattanasakulpong N., Prusty B.G. , Kelly D.W., Hoffman M. (2012)." Free vibration analysis of layered functionally graded beams with experimental validation",*Materials and Design* (1980-2015) 36 182–190.

Waddar, S., Pitchaimani J., Doddamani M. (2018). "Experimental investigation on stability and dynamic behaviour of laminated composite beam". In *AIP Conference Proceedings* Vol. 1943, No. 1.

Waddar, S., Pitchaimani, J., Doddamani, M., & Barbero, E. (2019). "Buckling and vibration behaviour of syntactic foam core sandwich beam with natural fiber composite facings under axial compressive loads". *Composites Part B: Engineering*, 175, 107133.

Wang, X., Zhu X., & Hu P. (2015). "Isogeometric finite element method for buckling analysis of generally laminated composite beams with different boundary conditions", *International Journal of Mechanical Sciences*, 104, 190-199.

Wang Z.H., X.-h. Wang, G.-d. Xu, S. Cheng, T. Zeng (2016). "Free vibration of two-directional functionally graded beams", *Composite Structures* 135, 191–198.

Zhang L., Huang H., Zhao B., Peng X. (2020). "Effect of gradient on the deflection of functionally graded rectangular microcantilever induced by surface stress",*Materials Today Communication* 25 101598.

Zhang W., Xu J.,Yu T. (2022). "Dynamic behaviours of bio-inspired structures: Design, mechanisms, and models," *Engineering Structures*, vol. 265, p. 114490.

Zheng H., Cai C. (2004). "Minimization of sound radiation from based beams through optimization of partial constrained layer damping treatment",*Applied Acoustics*, 65(5): 501–520.

Zhu T.L. (2011). "The vibrations of pre-twisted rotating Timoshenko beams by the Rayleigh-Ritz method",*Computational Mechanics*, 47(4): 395–408.

LIST OF PUBLICATIONS

INTERNATIONAL JOURNALS

1 B. Somi Naidu, Jeyaraj Pitchaimani, Lenin Babu Mailan Chinnapandi, Ch V S N Reddi, "Acoustic Response Of An Isotropic Beam Under Axially Variable Loads Using Ritz And Rayleigh Integral Methods",Archives of Acoustics (2022), pp. 97-112 (SCIE,IF=1.24)

2 B. Somi Naidu, Jeyaraj Pitchaimani "Stability and Dynamic Behaviour of Bi-Directional Functionally Graded Beam Subjected to Variable Axial Load", Materials Today Communications Vol 32, (2022), 104043 (SCIE, IF=3.38)

3 B. Somi Naidu, Jeyaraj Pitchaimani, Lenin Babu Mailan Chinnapandi "Acoustic Response of Bi-directional Functionally Graded Beam under Axially Varying Load", Noise & Vibration Worldwide, (Accepted, SCOPUS, IF=1.29)

CURRICULUM VITAE

1.	Name:	**Naidu Balireddy S**
2.	Date of Birth:	20/12/1983
3.	Permanent Address:	D-No:13-123, Ramalayam Street, R R V Puram, Visakhapatnam, Andhra Pradesh-530029, India.
4.	Mobile Number:	7382193034
5.	Email ID:	bnaidus.177me502@nitk.edu.in /bnaidus@gmail.com
6.	Educational Qualification:	
2005	**Bachelor of Technology**	
	Institution:	VITAM College of Engineering, Affiliated to JNTUH Hyderabad, Vizianagaram Andhra Pradesh, India
2013	**Master of Technology**	
	Institution:	MVGR College of Engineering, Affiliated to JNTUK Kakinada, Vizianagaram Andhra Pradesh, India
2023	**Doctor of Philosophy**	
	Institution:	National Institute of Technology Karnataka, Surathkal, Mangalore, Karnataka, India
	Registration Date:	12/07/2017
	Thesis Submission Date:	04/08/2023
	Viva-Voice Date:	09/03/2024